HER⬤N

Contents

THE STATIC BEHAVIOUR OF AXIALLY LOADED
UNIPLANAR AND MULTIPLANAR TUBULAR
X-JOINTS

G.J. van der Vegte
Faculty of Civil Engineering
Delft University of Technology
The Netherlands

The Static Behaviour of Axially Loaded Uniplanar and Multiplanar Tubular X-Joints

1. Introduction

1.1 *Structural applications of hollow sections*

In nature, many applications of hollow sections as a structural element can be observed. Besides excellent properties with regard to resisting compression, tension, bending and torsion forces, hollow sections offer the possibility for architecturally attractive designs.

In particular, circular hollow sections have proved to be suitable structural elements. Due to their shape, circular hollow sections have relatively low drag coefficients and are therefore the most favourite choice for elements subjected to wind and wave loading. In addition, the surface area of structures made of circular hollow sections, is much smaller than for comparable structures made of open structures. This, in combination with the smooth circular shape, requires lower costs for protection against corrosion and maintenance of circular members.

Therefore, circular hollow sections are applied in a wide range of onshore and offshore structures e.g. buildings, barriers, towers, bridges, offshore platforms etc.

Since all of these structures are three dimensional, it is obvious that in many cases multiplanar connections are present at the intersection of several circular members.

1.2 *Current design of multiplanar joints*

During the last 30 years, extensive series of experiments have been carried out on tubular joints involving the static and fatigue strength of simple uniplanar joints. Most of the tests concern axially loaded joints. Only a few tests have been performed on joints loaded by bending. Regression analyses and other curve fitting methods have been used to establish design formulae for these simple uniplanar joints.

Until a few years ago, no experimental test results on multiplanar joints were available. Of the existing design codes, only A.W.S. D1.1-92 (1992) and Eurocode 3 (1992) take multiplanar effects into account for joints made of circular hollow sections. However, the A.W.S. code is only based on elastic considerations and not on experimental results. A detailed description of the A.W.S. recommendations is given by Marshall (1991). The design recommendations of Eurocode 3 for multiplanar joints are based on test results. However, this code only considers a few types of multiplanar joints.

Most of the other design codes treat multiplanar joints as being uniplanar, thereby ignoring the interaction between the different planes (A.P.I. (1991)). Depending on the geometry and the loading of the multiplanar joints, this may result in conservative or unsafe actual strengths. For multiplanar joints loaded by bending, no recommendations are given at all.

In summary, it can be stated that the basis for the design of multiplanar joints is still insufficient.

1.3 *Joint classification*

The joint types which are discussed in the present work, consist of uniplanar and multiplanar connections between circular hollow section members, directly welded together without the use of gussets or stiffener plates. A uniplanar joint is a type of joint where the braces are located in the same plane along the chord axis, while for a multiplanar joint, the braces lie in different planes along the chord axis.

Several basic types of uniplanar and multiplanar joints, including their classification, are shown in Table 1.1. Axial loads have been applied to the braces for illustration.

The geometry of joints can be described by the geometrical dimensions d_0, t_0 etc. However, a more common way to describe the geometry of joints is by non-dimensional geometrical parameters. The most important non-dimensional geometrical parameters of joints made of circular hollow sections, are defined in Fig. 1.1.

$$\alpha = 2l_0/d_0$$
$$\beta = d_1/d_0$$
$$2\gamma = d_0/t_0$$
$$\tau = t_1/t_0$$
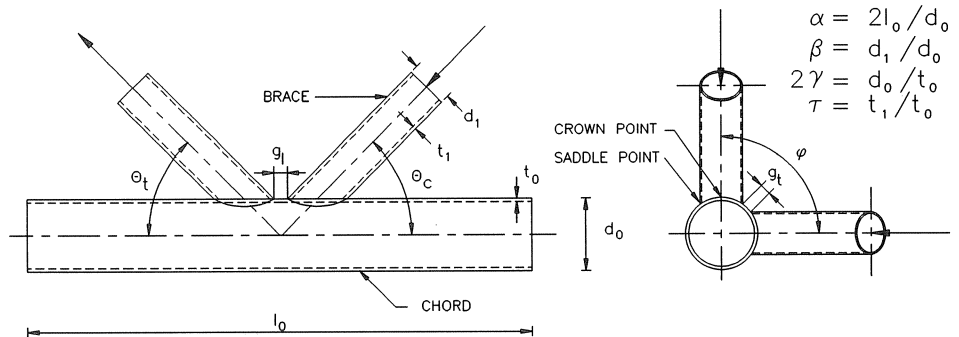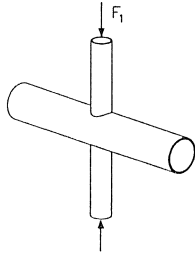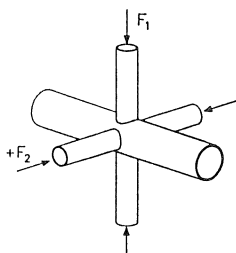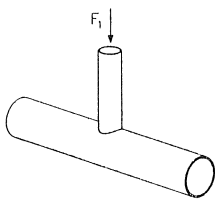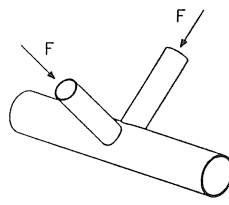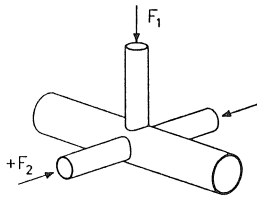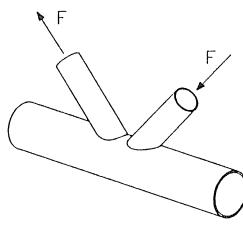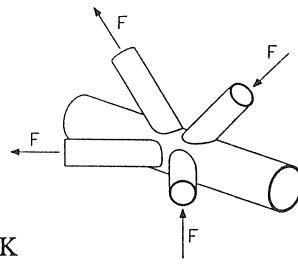
Fig. 1.1 : Dimensions and non-dimensional geometrical parameters of tubular joints.

1.4 *Aims of the present research*

As mentioned in section 1.2, the basis for the design of multiplanar is still insufficient. Therefore, the present research is focused on the extension of experimental and numerical data with regard to the static strength of uniplanar X- and multiplanar XX-joints made of circular hollow sections.
Numerical parametric studies have been carried out on axially loaded uniplanar X- and multiplanar XX-joints, based on numerical models which have been calibrated against the available experimental evidence (see Table 4.1 for a summary of the numerical studies). In addition, analytical models have been developed based on the plasticity theory (i.e. in line with Togo's ring model approach (Togo, 1967)).

Table 1.1 : Classification of tubular joints

	Uniplanar joints	Multiplanar joints
X-joints	X	XX
T-joints	T	TT
		TX
K-joints	K	KK

Remark :
In addition to the numerical analyses reported in the present work, extensive numerical studies have been performed on uniplanar T- and X-joints and multiplanar XX- TX- and TT-joints subjected to different types of loading (e.g. axial loading, in-plane bending or out-of-plane bending). Furthermore numerical studies have been carried out for axially loaded uniplanar X- and multiplanar XX-joints reinforced by a can to determine the influence of the can length on the strength of the joints. The results of these studies have been described in detail by van der Vegte (1995).

These analytically derived formulae provide a theoretical description of the joint strength and are used as a basis for the ultimate strength equations of axially loaded uniplanar X- and multiplanar XX-joints.

The objective of the present research is to combine the results of the numerical analyses of uniplanar and multiplanar X-joints with the analytically derived strength expressions in order to establish (basic) strength formulae which form the basis for future design recommendations. Simplifications of the basic ultimate strength equations to design rules in combination with the available experimental results, is not included in the present work.

The strategy to comply with the aims of the present research can be summarized as follows :

- 1.4.1 General FE aspects and numerical calibration (chapters 2, 3 and 4)
- 1.4.2 Numerical research on uniplanar X-joints (chapter 5)
- 1.4.3 Numerical research on multiplanar XX-joints (chapter 6)
- 1.4.4 Some general remarks with respect to the simplification of the basic ultimate strength formulae (chapter 7)
- 1.4.5 Conclusions and summary of the basic ultimate capacity equations (chapter 8)
- 1.4.6 Survey of relevant literature

1.4.1 General FE aspects and numerical calibration

General aspects with respect to finite element analyses are discussed in chapter 2. Experimental results of uniplanar X- and multiplanar XX-joints have been used for calibration of the numerical models. The experiments have been described in detail by van der Vegte (1990, 1991). Therefore, in chapter 3 of the present work, only the experimental research programme has been summarized without a detailed description. In addition, the numerical simulations of the experiments have been reported (chapter 3).

Due to the good agreement between the experimental and numerical load-deformation curves for the axially loaded joints, numerical parametric studies have been set up for axially loaded uniplanar X- and multiplanar XX-joints. The general features of these numerical studies are presented in chapter 4. Table 4.1 gives an overview of the various numerical studies.

1.4.2 Numerical research on uniplanar X-joints

Before a good understanding of the static behaviour of multiplanar joints can be obtained, it is necessary to gain accurate insight into the behaviour of the relative simple uniplanar joints. Therefore, the following numerical parametric studies have been performed on axially loaded uniplanar X-joints.

- In chapter 5, the results are presented of non-linear finite element analyses carried out on uniplanar X-joints. Although many test results exist for axially loaded uniplanar X-

joints, numerical simulations have been made for 16 axially loaded uniplanar X-joints in order to exclude the effects due to loading conditions, which often vary for different series of experiments. The results can be found in section 5.1.

- In the past, many questions arose regarding the influence of the chord length on the joint strength. In order to investigate the influence of the chord length on the static strength of axially loaded uniplanar X-joints, non-linear finite element analyses have been performed. The results of the chord length analyses are presented in section 5.2.

1.4.3 Numerical research on multiplanar XX-joints

- Extensive numerical parametric studies have been performed on multiplanar XX-joints (section 6.1), where axial loading has been applied to the in-plane braces. The load applied to the out-of-plane braces varied from tension to compression. In these analyses, the geometrical parameters β and 2γ as well as the ratio between the in-plane to out-of-plane loading have been varied over a wide range.

- In section 6.2, the influence of the chord length on the strength of axially loaded multiplanar XX-joints has been determined for various load ratios.

1.4.4 Some general remarks with respect to the simplification of the basic ultimate strength formulae

The basic ultimate strength formulae which have been established in chapters 5 and 6 may be too complex to be used for design purposes. Therefore, simplifications of the formulae may be required. Although simplification of the ultimate strength equations is not included in the present work, some general remarks have been made in chapter 7.

1.4.5 Conclusions and summary of the basic ultimate capacity equations

As mentioned earlier, the objective of the present research is to establish basic ultimate strength equations for axially loaded uniplanar and multiplanar X-joints, based on the results of the FE analyses in combination with analytically derived strength formulae. The basic ultimate strength formulae as well as the conclusions of the numerical simulations of the experiments are summarized in chapter 8.

1.4.6 Survey of relevant literature

Van der Vegte (1995) gives a detailed description of the relevant literature with respect to the static strength of multiplanar connections between circular hollow sections. Both references related to experimental as well as numerical work are included. In addition, a

complete overview of literature which addresses the static strength of circular hollow section joints, is presented. This bibliography only includes references after 1982, since an extensive summary of publications before this year can be found in Hollow Section Joints by Wardenier (1982).

2. General aspects regarding finite element analyses on tubular joints

2.1 *Introduction*

Current design codes and recommendations for the design of tubular joints are mainly based on regression analyses of a large number of experiments on simple uniplanar joints. In order to extend the current data base for more complex joints, the finite element (FE) method has proven to be a very suitable tool. During the last ten years, the FE method has been developed extensively. Coupled with the development in the numerical methods, is the introduction of more powerful computer systems. Due to still decreasing computer costs and the abilities to easily model complex joint geometries, material and geometrical non-linearities, loading and boundary conditions, FE analyses have gained much popularity in tubular joint research.

Therefore, in this section, a description will be given of the numerical models that have been set up and the calibration of these models against experimental evidence. Furthermore, some important influences, e.g. modelling of the weld geometry and choice of the finite element type, are discussed. In the next chapter, numerical simulations are made of experiments on uniplanar X- and multiplanar XX-joints. The numerical models are used as a basis for subsequent numerical parametric studies, which are described in detail in the following chapters.
In the next sections, the following features of the FE strategy will be discussed :

- 2.2 FE programs and hardware used
- 2.3 Main characteristics of the FE work with regard to tubular joints
- 2.4 Effects of the type of finite element
- 2.5 Effects of modelling of weld geometry
- 2.6 Effects of material post-yield property

2.2 *Finite element programs and hardware used*

All FE models have been generated using the pre- and post-processing package SDRC-IDEAS (level IV and V) (1990) and run on SUN SPARC Workstations. The numerical analyses have been performed using the general purpose finite element program MARC (k4.2 and k5). Converting IDEAS files to MARC files and vice versa has been carried out by MENTAT (version 5.4), MARC's pre-and post processor. Both MARC and MENTAT have been run on a CONVEX Super Computer or on an IBM RS/6000-350 Workstation.

2.3 *Main characteristics of the FE work with regard to tubular joints*

For all tubular joints, which have been analyzed numerically, a description is given of the main FE characteristics, denoted by : <u>FE characteristics.</u> In this section, each of these aspects is discussed. However, two main influences namely the choice of finite element type and modelling of weld geometry, are described extensively in sections 2.4 and 2.5 respectively and are only mentioned in this section (2.3) for completeness.

2.3.1 Finite element meshes and boundary conditions

For all joints modelled, a proper mesh grading has been pursued. Therefore, the size of the elements in the vicinity of the intersection of the braces with the chord and between the braces in the out-of-plane gap is relatively small as compared to the element size in other regions. Due to symmetry in loading and geometry, for all joints analyzed, only a part of the joints has been modelled in order to reduce the number of elements and nodes. Depending on the loading type and the joint type, the modelled part varies from an eighth to a half of the complete joint, thus creating planes of symmetry. As a result, boundary conditions have to be applied to the nodes which lie on these planes of symmetry to ensure that the model behaves the same as it would do in a complete joint.

The following boundary conditions have been simulated for each node on a plane of symmetry (of course only valid if the degree of freedom is available for the particular node, which depends on the element type) :
- nodal displacements perpendicular to the plane of symmetry are restrained. The two remaining translational degrees of freedom are free.
- nodal rotations around the axis perpendicular to the plane of symmetry are allowed. The two remaining rotational degrees of freedom are restrained.

Furthermore, boundary conditions have to be applied to prevent rigid body displacements and rotations of a complete joint.

2.3.2 Finite element type

An extensive description of the proper choice of element type which should be used for the analyses of tubular joints, is given in section 2.4.

2.3.3 Loading of the joints

Generally, there are two methods available for applying loads during the analyses : load-control and displacement control. The load control method implies that the load is applied directly to one or more nodes in a number of steps. In the displacement control method, the displacement growth of one or more nodes is prescribed. The displacement control method

results in nodal reaction forces at the nodes where the displacements are prescribed. Summation of these reaction forces gives the applied external load. When there is no preference for each of the loading types from a physical point of view, the displacement control method is to be preferred for the following reasons (de Borst (1991a)) :
- the tangent stiffness matrix is better conditioned for displacement control than for load control, which will result in a faster convergence behaviour of the iterative procedure.
- under load control, the stiffness matrix becomes singular at a limit point in the load-deformation diagram, not only when global failure occurs but also for a local maximum along this curve. For displacement control, the tangent stiffness matrix does not come become singular.

Therefore, where possible in the numerical analyses, the load has been applied by displacement control.

2.3.4 Modelling of the post-yield material property

In case geometrical non-linear numerical analyses are performed, the option LARGE DISP and UPDATE should be used in the MARC input file. When using the MARC option LARGE DISP, strains will include non-linear displacement terms. The option UPDATE activates the updated Lagrangian approach, which defines a new frame of reference at the beginning of each increment.

Furthermore, in all MARC analyses, the FINITE option has been activated, which takes care of conservation of volume. For shell elements, this results in updating the thickness of the elements as soon as the elements deform. Due to the activation of both UPDATE and FINITE, the MARC program uses true stresses and deformation rates. Integration of the deformation rate in a uniaxial tensile specimen furnishes logarithmic strains. Therefore, the MARC input of material properties requires true stress - logarithmic strain curves.

In all numerical analyses, the true stress - true strain curve is modelled as a multilinear relationship. These multilinear relationships have been obtained after converting an engineering stress - strain curve for a material into a true stress - strain curve. The engineering stress - strain curves have been determined experimentally by tensile tests.
Converting engineering stresses and strains to true stresses and strains can be described as follows :

$$\varepsilon = \ln (1 + e)$$

$$\sigma = S . (1 + e)$$

(2.1)

in which :
   e : engineering strain
   S : engineering stress
   ε : true strain
   σ : true stress

10

The true stress - strain relationship can be described by Ramberg - Osgood's power law (Ramberg (1943)) :

$$\frac{\varepsilon}{\varepsilon_0} = a . (\frac{\sigma}{\sigma_0})^N \qquad (2.2)$$

in which :
  ε_0 and σ_0 are the reference strain and reference stress
  a and N are constants which should be determined from the experimentally determined engineering stress - strain curve

In Fig. 2.1, an example is given in which way an engineering stress - strain curve is converted to a true stress - true strain curve.
Furthermore in all numerical analyses, the Von Mises yield criterion and isotropic strain hardening are used.
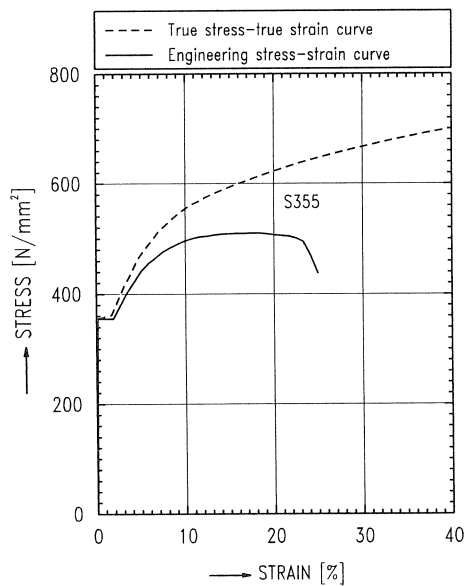
Fig. 2.1 : Engineering and true stress - strain curves.

2.3.5 Iteration procedure and convergence criteria

In geometrical and material non-linear analyses, it is recommended to impose the total load in a number of small loading steps, the so-called increments. Within each increment, a number of recycles or iterations is carried out until the user prescribed convergence tolerances are fulfilled.
MARC (1991a) offers various methods to perform iterations within an increment. In this research work, full Newton-Raphson iterations have been applied. This method is

11

characterized by its (fast) quadratic convergence, which is based on the assembly and decomposition of the stiffness matrix for every recycle (= iteration).

Also for the method of convergence testing, MARC offers various methods. In all numerical analyses of the present research work, the procedure for convergence criteria is based on checking of relative residual errors. This implies that if the ratio of maximum residual forces and moments to the maximum reaction forces and moments exceeds a certain (small) tolerance, recycling is continued within an increment. The convergence tolerances, both for forces and moments, have been set to 1 %.

2.3.6 Numerical modelling of the weld geometry

A detailed description of the modelling of welds is given in section 2.5, accompanied by examples.

2.4 *Effects of the type of finite element*

2.4.1 Available types of elements

The FE program MARC (1991b) offers various elements to model tubular joints. The following elements can be considered :

Solid elements :
- twenty noded solid elements (MARC element type 21). Quadratic interpolation functions have been used for coordinates and displacements. Each node has three translational degrees of freedom. The elements are integrated numerically using 27 Gauss points.

- twenty noded solid elements (MARC element type 57), including reduced integration. Quadratic interpolation functions have been used for coordinates and displacements. Each node has three translational degrees of freedom. The elements are integrated numerically using 8 Gauss points.

Shell elements :
- eight noded thick shell elements (MARC element type 22), including reduced integration. For these elements quadratic interpolation functions have been used for coordinates, displacements and rotations. Both the corner nodes and the midside nodes have six degrees of freedom : three translational and three rotational degrees of freedom. 4 Gauss points are used for numerical integration. Seven layers of integration points are used for integration through the thickness of the shell elements. Transverse strains are taken into account.

- eight noded thin shell elements (MARC element type 72). Bilinear interpolation functions have been used for coordinates and displacements. Global rotations are interpolated

quadratically from the rotation vector at the centroid and at the mid-side nodes. Each of the four corner nodes has three translational degrees of freedom. Each midside node only has one rotational degree of freedom about the edge. 4 Gauss points are used for numerical integration. Transverse strains are not taken into account. Seven layers of integration points are used for integration through the thickness of the shell elements. Use of such thin shell elements is advisable, only when the chord diameter to wall thickness ratio 2γ is equal to 20 or above. Below this value, thick shell elements should be used.

-   four noded thick shell elements (MARC element type 75). For these elements, bilinear interpolation functions have been used for coordinates, displacements and rotations. Each of the four nodes has six degrees of freedom. 4 Gauss points are used for numerical integration. Seven layers of integration points are used for integration through the thickness of the shell elements. Transverse strains are taken into account.

Transition elements :
-   twenty noded solid elements (MARC no. 21) offer the possibility to reduce any plane (but only one plane for each element) to a line. These so-called "collapsed" elements can be used as transition elements i.e. a FE mesh can be generated which consists of twenty noded solid elements (MARC no. 21) and eight noded thick shell elements (MARC no. 22) whereas these two types of elements are connected by the transition elements.
    In modelling of tubular joint geometries, these elements can be used to provide the transition between the (solid) elements to model the weld at the intersection of the braces with the chord and the (shell) elements to model the remaining parts of the joints.

2.4.2 Quantitative and qualitative comparison of different types of elements

Before choosing the most suitable element for the analyses of tubular joints, a quantitative and qualitative comparison is made between the available types of elements.
In geometrical and material non-linear analyses, the loading process is performed by a number of small load steps, the so-called increments. Within each increment, a number of recycles is carried out until the user prescribed convergence tolerances are fulfilled. After each load increment, MARC offers the possibility to suspend the FE analyses and to write the available data to a RESTART tape. The loading process can be continued after reading the stored RESTART tape. These files, however, require a considerable amount of disk storage which does not only depends on the size of the numerical model but also on the element type used.

In order to obtain insight in differences between required CPU times and disk space for different types of element, a very simple structure has been modelled, namely a supported plate subjected to a force perpendicular to the plate surface. The following types of elements have been used to model the plate (for each element type, the plate has been modelled by 10 elements) :

- a combination of 6 thick shell elements and 2 solid elements using 2 transition elements (in total 10 elements).
- twenty noded solid elements.
- eight noded thick shell elements.
- eight noded thin shell elements.
- four noded thick shell elements.

The element meshes used for the models are shown in Fig. 2.2 (the element configuration for the meshes with shell elements only, are similar). In this simple example, for each element type, the required CPU time for one recycle and the disk space needed for the storage of the restart file including one increment, have been determined and made relative to the results for the eight noded thick shell elements (for this simple structure, the absolute figures are not relevant). The results are summarized in Table 2.1.

As can be observed in Table 2.1, the presence of both solid elements and thick shell elements connected by transition elements dramatically increases the required CPU time and disk storage, which is mainly due to the increasing bandwidth of the stiffness matrix (each type of element has a different number of degrees of freedom).

The plate modelled with solid elements only, also shows an increase for both quantities as compared to the model with eight noded thick shells. Furthermore, the use of twenty noded solid elements and transition elements may lead to the following unwanted effects :

- as mentioned in section 2.4.1, for the twenty noded solid elements, three Gauss points are used through the thickness of the elements. For a satisfactory description of non-linearity through the thickness, this number is insufficient. As a result, the numerical solution overestimates the real behaviour. To solve this problem, at least two layers of solids are required for a representative description of the stress distribution through the thickness. However, this results in a doubling of the number of elements and nodes and subsequently in another large increase in required CPU time (about 4 times) and disk storage.

- solving non-linear problems with numerical models that include twenty noded solid elements (with 27 Gauss points), may result in solutions which overestimate the real strength, due to incompressibility of the elements (de Borst, 1991b). The use of twenty noded solid elements with reduced integration (8 Gauss points) (MARC no. 57) may overcome this problem. However, also for this type of element, two layers of elements are required through the thickness.

Based on the above mentioned disadvantages, and the fact that these elements are modelled in the areas of most interest (intersection between chord and braces), use of solid elements is not recommended.

14
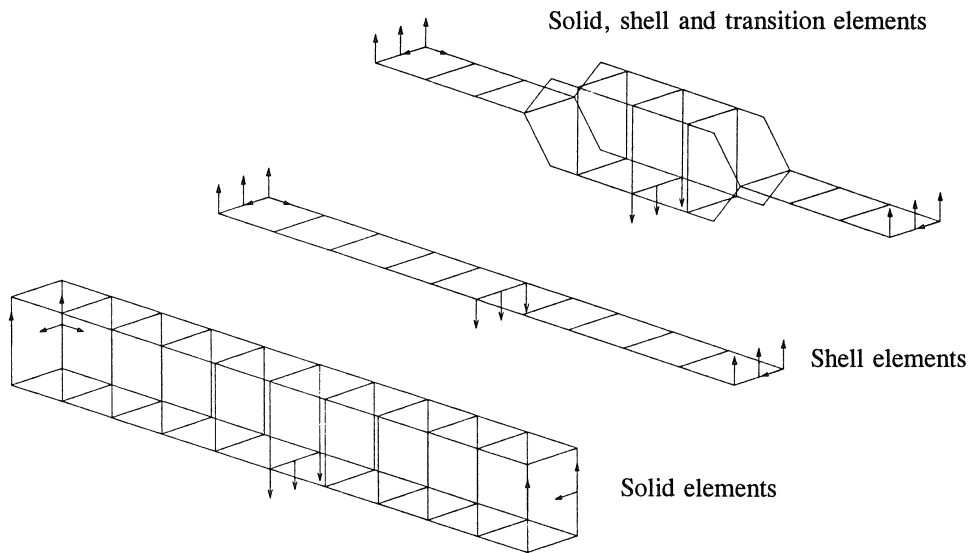
Fig. 2.2 : Finite element meshes for a simply supported beam.

Table 2.1 : FE performance of different types of elements.

	Number of elements :	Number of nodes :	Relative size restart file :	Relative CPU-time per recycle :
20 noded solid and 8 noded thick shell elem. incl. transition elements	10	76	6.14	6.35
20 noded solid elements	10	128	1.26	3.75
8 noded thick shell elem.	10	53	1.00	1.00
8 noded thin shell elements	10	53	0.67	0.55
4 noded thick shell elem.	10	22	0.90	0.66

After comparing the results of the shell elements in Table 2.1, it appears that the eight noded thin shell elements and the four noded thick shell elements show the best performance as far as required CPU time and disk storage are concerned. However, the accuracy of these four noded thick and eight noded thin shell elements is less than for the eight noded thick shell elements, since for the eight noded thick shell elements quadratic interpolation functions have been used for coordinates, displacements and rotations instead of the less accurate bi-linear interpolation functions used for the two other types of shell

15

elements.

Based on these theoretical considerations, the use of eight noded thick shell elements is recommended. In practice, however, for very large numerical models (more than 700 eight noded thick shell elements), the CPU time required for a complete non-linear analysis is beyond reasonable limits. Therefore, in the next section, additional numerical analyses on tubular joints will be described, in order to show the differences in load-deformation behaviour for the various types of shell elements.

BOUNDARY CONDITIONS			
Degree of freedom	Nodes on plane X = 0.0	Nodes on plane Y = 0.0	Nodes on plane Z = 0.0
u_x	0.	free	free
u_y	free	0.	free
u_z	free	free	0.
ϕ_x	free	0.	0.
ϕ_y	0.	free	0.
ϕ_z	0.	0.	free

Fig. 2.3 : FE mesh and boundary conditions for axially loaded uniplanar joint X1.

16

2.4.3 The effects of the finite element type on the strength of tubular joints

In order to determine the effects of the type of elements on the load-displacement behaviour of axially loaded tubular joints, one X-joint has been analyzed three times, each time using another type of shell element.
As mentioned in the preceding section, the joint has been modelled with the following types of elements :
- eight noded thick shell elements.
- eight noded thin shell elements.
- four noded thick shell elements.

Example : An axially loaded uniplanar X-joint

FE characteristics :
- the dimensions of the joint are similar to the measured dimensions of uniplanar X-joint X1 of the experimental and numerical research programme (see Table 3.1).
- one eighth of the joint has been modelled.
- 220 elements are used to model the joint. The FE mesh and the boundary conditions are presented in Fig. 2.3.
- no additional boundary conditions were needed to prevent rigid body movements.
- the load has been applied at the brace tip by displacement control.
- the material properties used for the analysis, have been obtained from the experimentally determined engineering stress - strain curves for uniplanar X-joint X1 with $f_{y,0,L}$ = 331 N/mm^2.
- the geometry of the weld has been modelled in accordance with the measured dimensions of the weld of uniplanar X-joint X1 (see section 2.5 for more details).

The numerically determined static behaviour of the axially loaded uniplanar joint has been presented in non-dimensionalized load-displacement curves (Fig. 2.4).
A summary of the numerical results for the different types of shell elements, is presented in Table 2.2.

Table 2.2 : Numerical results of axially loaded uniplanar X-joint X1.

	No. of elements :	No. of nodes :	Relative CPU time per recycle :	Ultimate load F_u [kN] :	Strength ratio :
8 noded thick shell elements	200	654	1.00	466.0	1.000
8 noded thin shell elements	200	654	0.41	474.0	1.017
4 noded thick shell elements	200	227	0.50	511.4	1.097

As expected, the curve obtained using the eight thick shell elements gives the lowest solution. As can be observed from Table 2.2, for eight noded thin shell elements, the ultimate load is only 1.7 % higher than for the eight noded thick shell elements. The required CPU time, however, is almost 60 % lower. For the four noded thick shell elements, the difference in ultimate load is much larger (up to 9.7 %), while the required CPU time is less favourable than for eight noded thin shell elements.
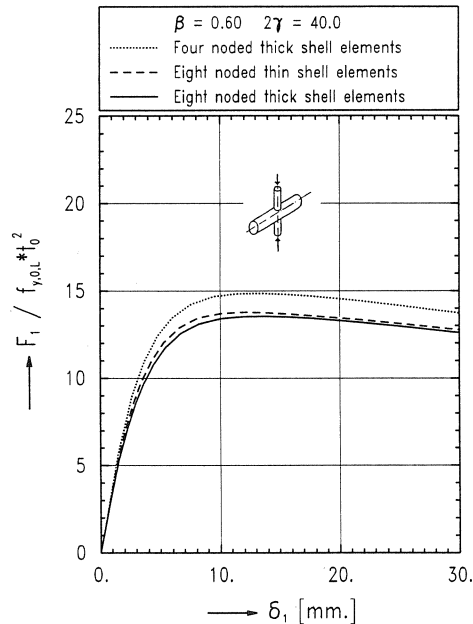
Fig. 2.4 : The effects of the finite element type on the load-displacement behaviour of axially loaded uniplanar joint X1.

2.4.4 Recommended finite element type

Based upon the above mentioned considerations, it is recommended to use, where possible, eight noded thick shell elements for the modelling of tubular joints. In case of very large numerical models, the use of eight noded thick shell elements requires too much CPU time. For these numerical models (and provided that $2\gamma > 20$), use of thin shell elements might be considered. However, a warning should be made. In loading cases where relatively large transverse shear stresses occur (e.g. equal compression loading on all braces of a multiplanar XX-joint), the differences in ultimate load, when using either eight noded thick or thin shell elements, may be larger than the differences observed in the last example.

2.5 *Effects of modelling of weld geometry*

As shown in this section, it appears that without modelling of the welds, the numerically determined load-displacement (e.g. axially loaded multiplanar joint XX4) or moment-

18

rotation curves (e.g. uniplanar joint X5 loaded by in-plane bending, see Table 3.1) lie far below the experimental ones (even 20 % or more). Therefore, the welds have been modelled in accordance with the measured weld sizes in the following way :

Shell elements have been used to model the welds, as shown in Fig. 2.5. The dashed lines indicate the mid-planes of the assumed shell elements. The wall thickness of the elements AC and A'C', used to model the fillet DEF and D'E'F' of the butt weld is taken as the fillet thickness of the butt weld after averaging at the crown point (t_w) and the saddle point (t'_w). The dotted lines AD, CF, A'D' and C'F' indicate how the fillet of the butt weld has been moved from the outer surfaces to the mid-planes of the circular members.
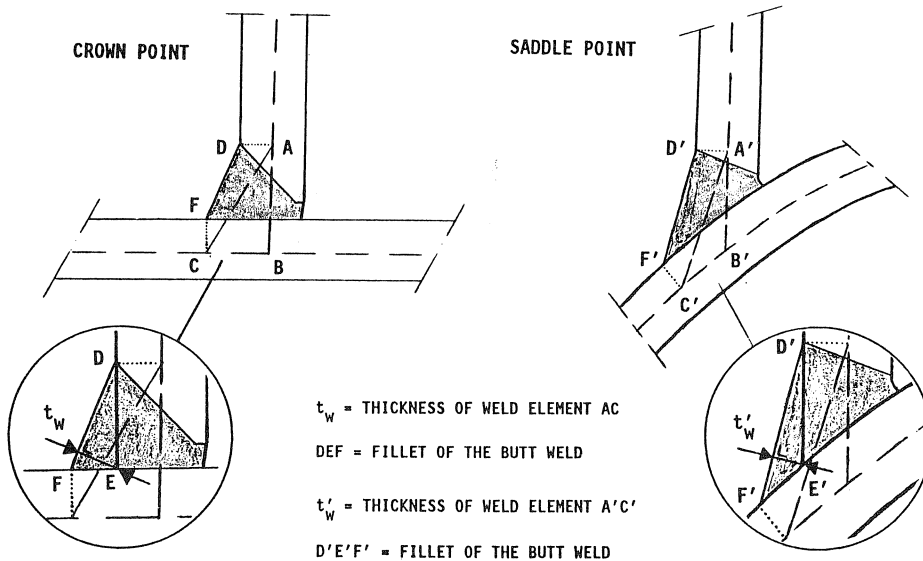
Fig. 2.5 : Numerical modelling of the weld geometry.

In order to show the influence of weld modelling on the load-displacement behaviour, multiplanar joint XX4 of the experimental research programme (Table 3.1) has been modelled two times : once including and once excluding the weld geometry. For both joints, the FE analyses can be summarized as follows :

FE characteristics :
- the dimensions of the joints are similar to the measured dimensions of multiplanar XX-joint XX4 of the experimental research programme (see Table 3.1).
- one eighth of the joint has been modelled.
- eight noded thick shell elements are used to model the joint.
- 371 elements are used to model the joint including the weld geometry and 330 elements for the joint without the weld geometry. Only 16 of these 41 additional elements have been used to model the weld geometry : the other extra elements have been located on the brace in order to pursue a smoother mesh grading on the brace. The FE mesh for the joint including the weld geometry is shown in Fig. 2.6.

19
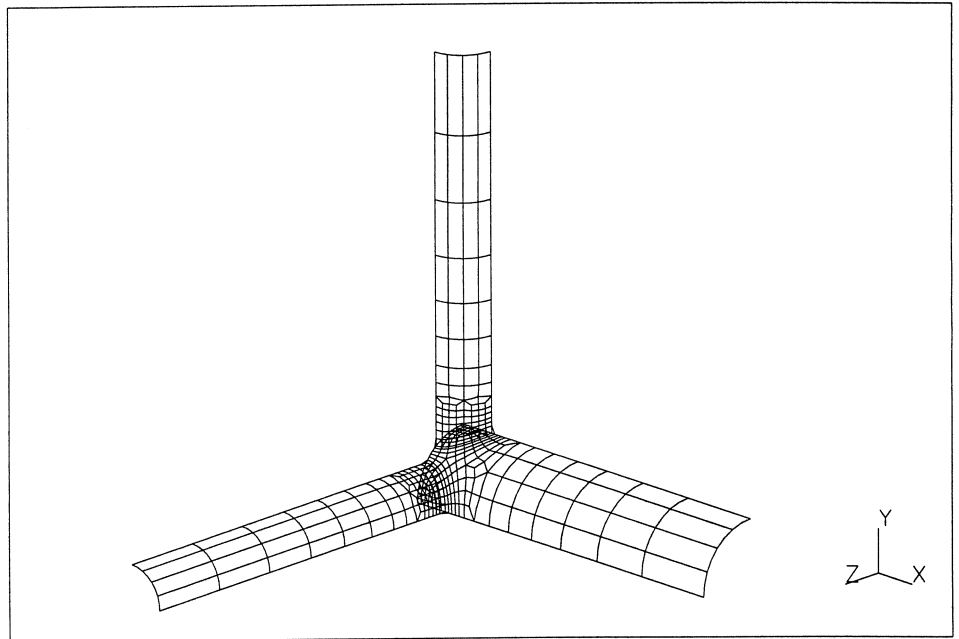
Fig. 2.6 : Finite element mesh for axially loaded multiplanar XX-joint XX4.

The boundary conditions are similar to those for axially loaded uniplanar X-joint X1 (see Fig. 2.3).
- no additional boundary conditions were needed to prevent rigid body movements.
- in agreement with the experiments, the out-of-plane brace has been preloaded by an axial tensile force (see section 3.1). This load has been applied to the out-of-plane brace tip, using the load control method. Subsequently, the axial compression load has been applied to the in-plane brace tip by displacement control.
- the material properties used for the analysis, have been obtained from the experimentally determined engineering stress - strain curves for XX-joint XX4 with $f_{y,0,L} = 318$ N/mm^2.

Table 2.3 : Experimental and numerical results of multiplanar XX-joint XX4 with and without modelling of the weld geometry.

	Number of elements :	Number of nodes :	Ultimate load [kN] :	Relative ultimate load :
Experiment			422.0	1.000
Weld geometry not modelled	330	1073	334.8	0.793
Weld geometry modelled	371	1196	414.1	0.981

20

In Fig. 2.7, the experimental load-displacement curve as well as the two numerical load-displacement curves (with and without modelling of the welds) are shown for multiplanar joint XX4. The results are summarized in Table 2.3. From Fig. 2.7, it can be seen that modelling of the welds gives satisfactory results.
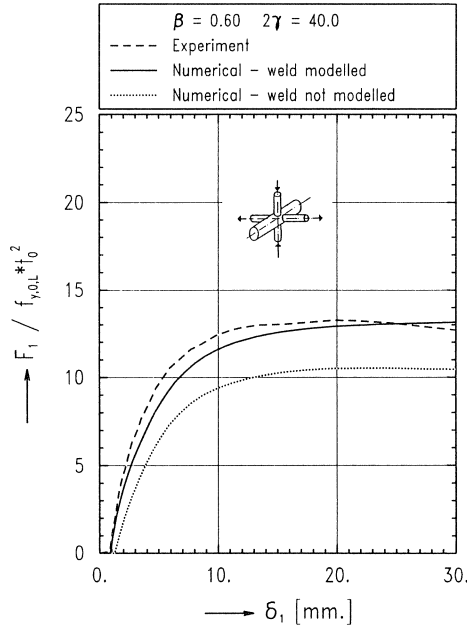
Fig. 2.7 : The effects of the weld modelling on the load-displacement behaviour of axially loaded multiplanar XX-joint XX4.

2.6 *Effects of material post-yield property*

In order to show the effects of the material post-yield property on the ultimate load of tubular joints, a uniplanar X-joint has been analyzed using two different material post-yield properties. The two material types that have been considered are shown in Fig. 2.8. Material type 2 does not include strain hardening and has a simple linear-elastic, perfectly plastic stress-strain relationship. For each of the material types, the yield strength is $f_{y,0} = 355$ N/mm^2. The FE features can be summarized as follows :

FE characteristics :
- the joints have the following dimensions :
  chord : $d_0 = 406.4$ mm. $t_0 = 16.0$ mm. $l_0 = 3251.2$ mm.
  braces : $d_1 = 244.5$ mm. $t_1 = 16.0$ mm.
  which results in the following non-dimensional parameters : $\alpha = 16.0$, $\beta = 0.60$, $2\gamma = 25.4$ and $\tau = 1.0$
- one eighth of the joint has been modelled.
- eight noded thick shell elements are used to model the joint.

21

- 240 elements are used to model the joint. The FE mesh and boundary conditions are similar to those shown in Fig. 2.3.
- no additional boundary conditions were needed to prevent rigid body movements.
- the load has been applied at the brace tip by displacement control.
- the geometry of the weld has been modelled in agreement with the method as has been described in section 2.5.
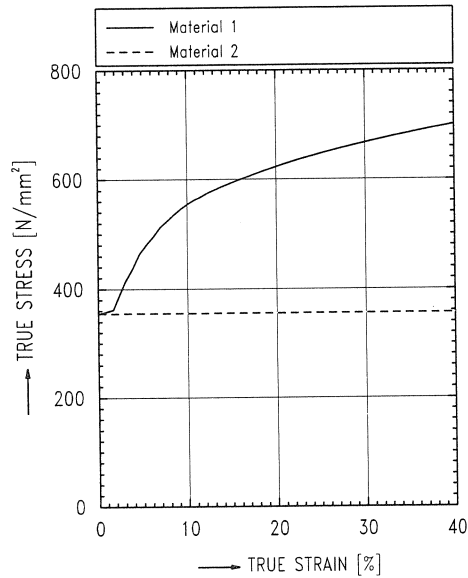
Fig. 2.8 : Two different material post-yield properties.

The load-deflection curves for the uniplanar joint analyzed with two different material types are shown in Fig. 2.9. The ultimate loads are summarized in Table 2.4.

As expected, the curve for material type 2 lies below the curve for material type 1. However, the differences are small, due to the fact that plasticity occurs in a localized area, thereby not influencing the overall load-deflection relationship too much.

Table 2.4 : Numerical results of a uniplanar X-joint with different material post yield properties.

	Number of elements :	Number of nodes :	Ultimate load [kN] :	Relative ultimate load :
Material type 1	240	786	1194.8	1.000
Material type 2	240	786	1139.0	0.953

22
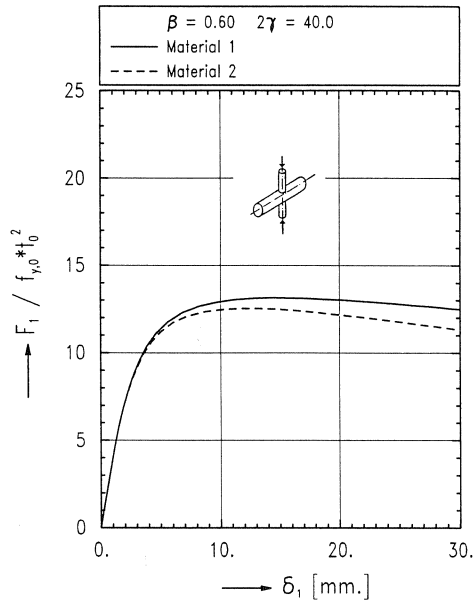
Fig. 2.9 : The effects of the post-yield properties on the load-displacement behaviour of an axially loaded uniplanar X-joint.

3. Numerical simulation of the experiments on uniplanar X- and multiplanar XX-joints
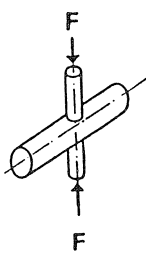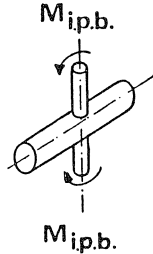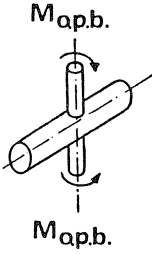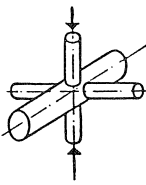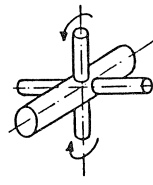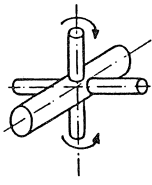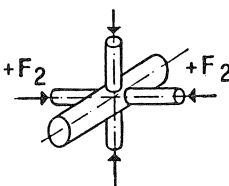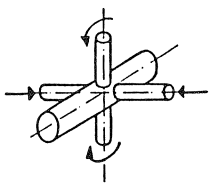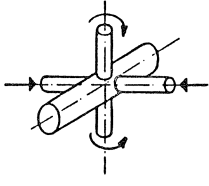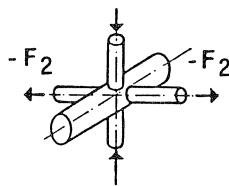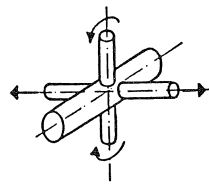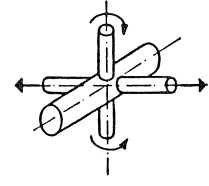
In this chapter, numerical simulations are presented of the experiments on uniplanar X- and multiplanar XX-joints (van der Vegte (1990, 1991)), based on the numerical models which have been derived in chapter 2. The following subdivision is made :

- 3.1 Research programme
- 3.2 General FE aspects
- 3.3 Axially loaded X-joints X1 to XX4
- 3.4 X-joints loaded by in-plane bending X5 to XX8
- 3.5 X-joints loaded by out-of-plane bending X9 to XX12
- 3.6 Comparison between the experimental and numerical results

3.1 Research programme

The numerical research programme is identical to the experimental one and summarized in Table 3.1. The geometry is limited to joints with a diameter ratio $\beta = 0.6$ and a chord radius to thickness ratio $2\gamma = 40$. To prevent (in-plane bending) failure of the brace before joint failure, the wall thickness ratio τ is taken as 1.0. The geometric chord length parameter α is taken as 12.0 (the nominal dimensions of the joints are : $d_0 = 406.4$ mm, $t_0 = 10.0$ mm, $d_1 = 244.5$ mm, $t_1 = 10.0$ mm, $l_0 = 2438$ mm).

23

Table 3.1 : Research programme for uniplanar X- and multiplanar XX-joints.

Joint	Loading conditions		
	Axial	Bending in plane	Bending out of plane
Uniplanar	F / F — X 1	$M_{i.p.b.}$ / $M_{i.p.b.}$ — X 5	$M_{o.p.b.}$ / $M_{o.p.b.}$ — X 9
Multiplanar	XX 2	XX 6	XX 10
Multiplanar	$+F_2$ / $+F_2$ — XX 3	XX 7	XX 11
Multiplanar	$-F_2$ / $-F_2$ — XX 4	XX 8	XX 12

The test series consists of three sets of four specimens. Each set consists of three multiplanar XX-joints and one uniplanar X-joint for reference.

The following loading conditions have been applied to the in-plane braces :
- compression forces for X1, XX2, XX3 and XX4
- in-plane bending moments for X5, XX6, XX7 and XX8 (as a result of in-plane forces perpendicular to the brace axis)
- out-of-plane bending moments for X9, XX10, XX11 and XX12 (as a result of out-of-plane forces perpendicular to the brace axis)

The following loading conditions were applied to the out-of-plane braces :
- unloaded (XX2, XX6, XX10)
- compressive forces equal to 60% of the calculated ultimate strength of a uniplanar joint under compression load, using the mean strength formula of Kurobane (1980) for axially compression loaded uniplanar X-joints :

$$F_{1,u} = \frac{7.46}{1 - 0.812\beta} (2\gamma)^{-0.05} \cdot (\frac{f_{u,0}}{f_{y,0}})^{0.173} \cdot f_{y,0} \cdot t_0^2 \tag{3.1}$$

These forces were applied prior to loading the in-plane braces and maintained constant throughout the test (XX3, XX7, XX11).
- tensile forces equal to 60% of the calculated ultimate strength of a uniplanar X-joint under compression load (Eq. 3.1). These forces were also applied prior to loading the in-plane braces and maintained constant throughout the test (XX4, XX8, XX12).

The specimens are fabricated of hot finished circular seamless hollow sections with steel grade Fe 360 (Euronorm 25-72) (= S235 according to the current European standard : EN 10210-1). The measured dimensions and material properties of the chord i.e. the yield stress and ultimate stress, have been determined in longitudinal direction and are presented in Table 3.2 for the axially loaded joints, in Table 3.3 for the joints loaded by in-plane bending and in Table 3.4 for the joints loaded by out-of-plane bending. Detailed information about the actual dimensions of the chord, the braces and the welds and the measured mechanical properties of all tubular members are referenced by van der Vegte (1990).

3.2 *General FE aspects*

For all joints which have been analyzed numerically, the following remarks hold (see chapter 2 for additional information) :

- the numerical analyses have been performed using the FE program MARC.
- the joints are modelled in agreement with the actual dimensions of the tested joints.
- the sizes of the weld elements are in accordance with the measured dimensions of the welds (see also section 2.5).
- the experimentally determined engineering stress - strain curves have been converted to

true stress - true strain relationships which have been represented as multi-linear relationships. These step-wise functions have been used to model the material post-yield properties (see also 2.3.4).
- the Von Mises yield criterion and isotropic strain hardening are used.
- the relative convergence tolerances (maximum residual forces and moments divided by the maximum reaction forces and moments respectively) are both set to 1%.
- full Newton-Raphson iterations have been applied.

3.3 *Axially loaded X-joints X1 to XX4*

The general FE characteristics have been described in section 3.2. For the axially loaded joints, the following additional FE features should be mentioned :

FE characteristics :
- one eighth of each joint has been modelled.
- eight noded thick shell elements are used to model the joints.
- 200 elements are used to model uniplanar joint X1 and 371 elements for multiplanar joints XX2 to XX4. The FE meshes and boundary conditions for uniplanar joint X1 and multiplanar joints XX2 to XX4 are shown in Fig. 3.1.
- no additional boundary conditions are needed to prevent rigid body movements.
- for the joints X1 and XX2 the load has been applied to the in-plane brace tip by displacement control. Similar to the experimental loading conditions, for the joints XX3 and XX4, the out-of-plane braces have been preloaded by an axial force. This load has been applied to the out-of-plane braces using the load control method. Subsequently, the axial load has been applied to the in-plane brace tip by displacement control.

For each of the axially loaded joints, the experimental and numerical load-displacement curves are given in Fig. 3.2. The non-dimensionalized load $F_1/f_{y,0,L} \cdot t_0^2$ has been plotted against the deflections of the crown points of the in-plane braces. The experimentally and numerically determined failure loads are summarized in Table 3.2. The horizontal shift of the curves for multiplanar XX-joints XX3 and XX4 is caused by the loading of the out-of-plane braces, prior to the loading of the in-plane braces.

3.4 *X-joints loaded by in-plane bending X5 to XX8*

The general FE characteristics are described in section 3.2. For the joints loaded by in-plane bending, the following additional FE features should be described :

FE characteristics :
- one quarter of each joint has been modelled.
- eight noded thick shell elements are used to model uniplanar joint X5. However, the cheaper eight noded thin shell elements have been used to model multiplanar joints XX6, XX7 and XX8, due to the large number of elements (see also section 2.4.4).

26

BOUNDARY CONDITIONS			
Degree of freedom	Nodes on plane X = 0.0	Nodes on plane Y = 0.0	Nodes on plane Z = 0.0
u_x	0.	free	free
u_y	free	0.	free
u_z	free	free	0.
ϕ_x	free	0.	0.
ϕ_y	0.	free	0.
ϕ_z	0.	0.	free

BOUNDARY CONDITIONS			
Degree of freedom	Nodes on plane X = 0.0	Nodes on plane Y = 0.0	Nodes on plane Z = 0.0
u_x	0.	free	free
u_y	free	0.	free
u_z	free	free	0.
ϕ_x	free	0.	0.
ϕ_y	0.	free	0.
ϕ_z	0.	0.	free

Fig. 3.1 : Finite element meshes and boundary conditions for the axially loaded X-joints (X1 to XX4).

27
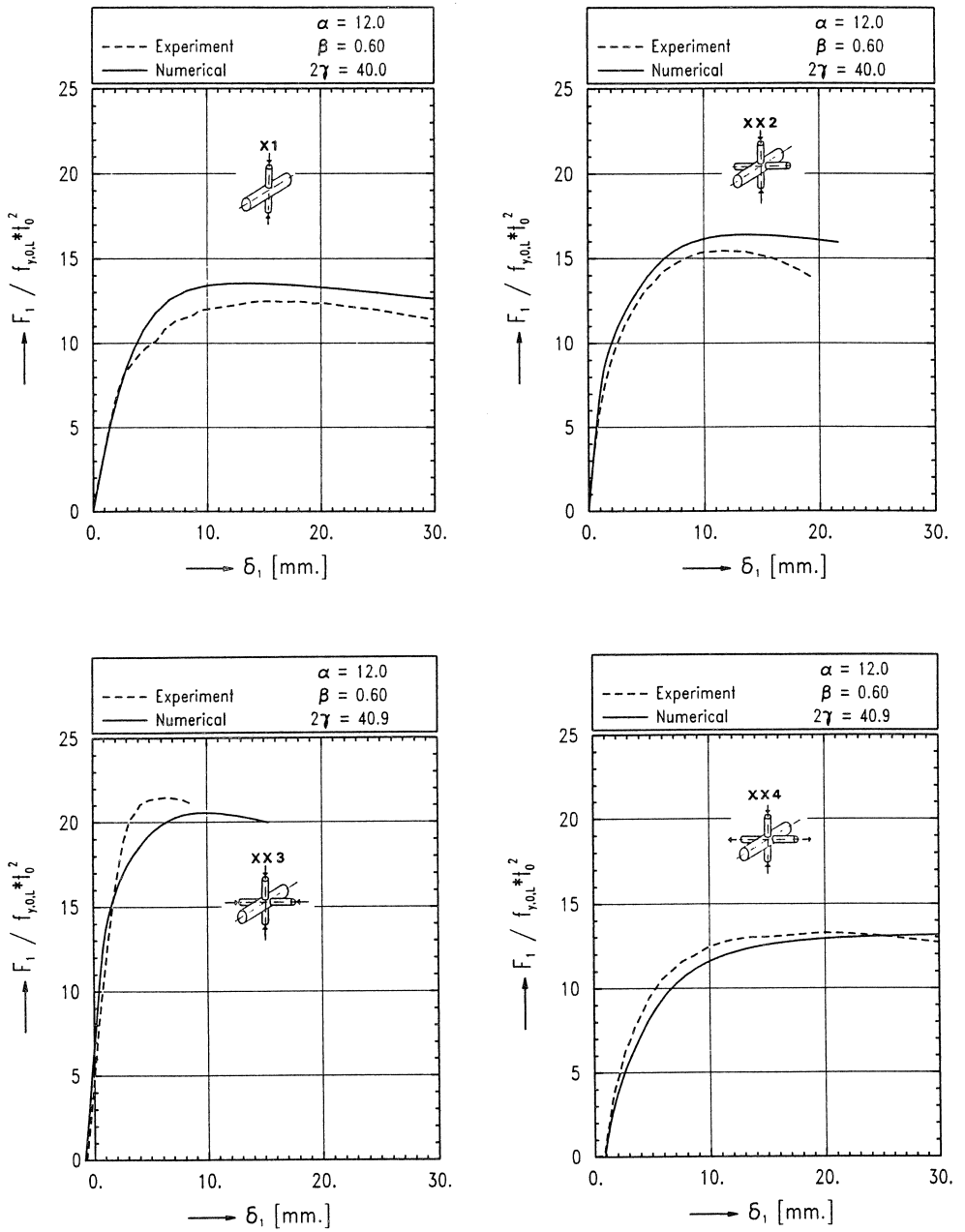
Fig. 3.2 : Load-deformation curves of the axially loaded X-joints.

28

Table 3.2 : Numerical results of the axially loaded X-joints

					Axially loaded joints					Test results		$F_{1,u,num}$	$\dfrac{F_{1,u,test}}{F_{1,u,num}}$
Joint	No. of elements	No. of nodes	Element type (1)	Required CPU seconds (2)	d_0 mm.	t_0 mm.	β	2γ	$f_{y,0,L}$ N/mm²	$F_{1,u}$ kN	Failure mode (3)	kN	
X1	200	654	22	7,250	408.0	10.2	0.6	40.0	331.	430.	1	466.	1.08
XX2	371	1196	22	13,700	408.0	10.2	0.6	40.0	331.	532.	2	565.	1.06
XX3	371	1196	22	14,800	408.5	10.0	0.6	40.9	318.	683.	2	654.	0.96
XX4	371	1196	22	17,250	408.5	10.0	0.6	40.9	318.	422.	2	414.	0.98

(1) : Element type : 22 = Eight noded thick shell elements

(2) : All numerical analyses have been carried out on a CONVEX C240, which has four processors. Each of these processors has a peak performance of 50 Megaflops.

(3) : Modes of failure :
1 - Plastic deformation leading to failure of chord cross section.
2 - Plastic deformation leading to failure of chord cross section + initiation of cracks at the weld toe(s).

29

- 400 shell elements are used to model uniplanar joint X5 and 742 shell elements for multiplanar joints XX6 to XX8. The FE meshes and boundary conditions for uniplanar joint X5 and multiplanar joints XX6, XX7 and XX8 are shown in Fig. 3.3.
- similar to the experimental circumstances, boundary conditions have been applied to the chord end to react the external load applied to the in-plane brace tip.
- for the joints X5 and XX6, the load has been applied to the in-plane brace tip by lateral displacements, perpendicular to the original brace axis (displacement control). At the in-plane brace tip, beam elements are modelled in order to ensure that the brace tip remains prismatic.
- Similar to the experimental loading conditions, for the joints XX7 and XX8, the out-of-plane braces have been preloaded by axial forces. These axial forces have been applied to the out-of-plane brace tip, using the load control method. Subsequently, lateral displacements have been applied to the in-plane brace tip in order to simulate the loading process (displacement control).

For each of the joints where the in-plane braces are loaded by in-plane bending, the experimentally and numerically determined behaviour is presented in moment-rotation curves (Fig. 3.4). The non-dimensionalized moment $M_{1,ipb}/f_{y,0,L} \cdot t_0^2 \cdot d_1$ has been plotted against the rotations of the in-plane braces. The in-plane bending moments are given at the chord surface at the crown point of the brace.

The moments and rotations have been corrected for the second order effects to obtain the real joint behaviour. The ultimate loads, given in Table 3.3 are based on the maximum loads obtained from the tests. However, the ultimate loads based on Yura's deformation limit (described in section 4.2), are also given in Table 3.3.

3.5 *X-joints loaded by out-of-plane bending X9 to XX12*

The general FE characteristics are described in section 3.2. For the joints loaded by out-of-plane bending, the specific FE aspects are the same as for the joints loaded by in-plane bending (see section 3.4, for the joints under out-of-plane loading, X5, XX6, XX7 and XX8 should be substituted by X9, XX10, XX11 and XX12 respectively) :

FE characteristics :
- the FE meshes for uniplanar joint X9 and multiplanar joints XX10, XX11 and XX12 are shown in Fig. 3.5.
- similar to the experimental circumstances, boundary conditions have been applied to one node at the chord end, necessary to react the external load applied to the in-plane brace tip. At this chord end, beam elements were modelled to remain the chord prismatic.

For each joint, the behaviour of uniplanar joint X9 and the multiplanar XX-joints XX10, XX11 and XX12, where the in-plane braces are loaded by out-of-plane bending, is presented in moment-rotation curves (Fig. 3.6).

30

BOUNDARY CONDITIONS

Degree of freedom	Corner nodes on plane X = 0.5 l_0	Corner nodes on plane Y = 0.0	Corner nodes on plane Z = 0.0	Mid-side nodes on planes X = 0.5 l_0, Y = 0.0 and Z = 0.0
u_x	0.	free	free	-
u_y	0.	0.	free	-
u_z	0.	free	0.	-
ϕ_{edge} *	-	-	0.	0.

* - ϕ_{edge} : rotation about the edge itself

BOUNDARY CONDITIONS

Degree of freedom	Nodes on plane X = 0.5 l_0	Nodes on plane Y = 0.0	Nodes on plane Z = 0.0
u_x	0.	free	free
u_y	0.	0.	free
u_z	0.	free	0.
ϕ_x	0.	0.	0.
ϕ_y	0.	free	0.
ϕ_z	0.	0.	free

Fig. 3.3 : Finite element meshes and boundary conditions for the X-joints loaded by in-plane bending (X5 to XX8).

31

Fig. 3.4 : Moment-rotation curves of the X-joints loaded by in-plane bending.

Table 3.3 : Numerical results of the X-joints loaded by in-plane bending.

					Joints loaded by in-plane bending									
										Test results (3)			$M_{1,Yura,num}$ kNm	$\dfrac{M_{1,Yura,num}}{M_{1,Yura,test}}$
Joint	No. of elem	No. of nodes	Elem type (1)	CPU sec. (2)	d_0 mm.	t_0 mm.	β	2γ	$f_{y,0,L}$ N/mm^2	$M_{1,u}$ kNm	$M_{1,Yura}$ kNm	Fail. mode (4)		
X5	400	1254	22	14,400	408.5	10.0	0.6	40.9	318.	113.	112.	2	107.	0.96
XX6	742	2293	72	11,000	408.0	10.2	0.6	40.0	331.	123.	123.	2	119.	0.97
XX7	742	2293	72	17,200	408.5	10.0	0.6	40.9	318.	137.	136.	2 + 4	128.	0.94
XX8	742	2293	72	15,800	408.5	10.1	0.6	40.4	268.	94.	92.	2	89.	0.95

(1) : Element type : 22 = Eight noded thick shell elements
72 = Eight noded thin shell elements

(2) : All numerical analyses have been carried out on a CONVEX C240, which has four processors. Each of these processors has a peak performance of 50 Megaflops.

(3) : All moments have been calculated at the crown intersection of the chord and brace.
M_{Yura} = moment at Yura's deformation limit.

(4) : Modes of failure :
1 - Plastic deformation leading to failure of chord cross section.
2 - Plastic deformation leading to failure of chord cross section + initiation of cracks at the weld toe(s).
3 - Plastic deformation leading to failure of chord cross section + through cracks at the weld toe(s)
4 - Full plastic moment of the brace(s).

33

The non-dimensionalized load $M_{1,opb}/f_{y,0,L} \cdot t_0^2 \cdot d_1$ has been plotted against the rotations of the in-plane braces.

The moments and rotations have been corrected for second order effects to obtain the real joint behaviour. The out-of-plane bending moments are given at the chord surface at the crown point of the brace. The ultimate strength values and the values based on Yura's deformation limit are presented in Table 3.4.

3.6 *Comparison between the experimental and numerical results*

Considering the load-deformation and the moment-deformation diagrams in Figs. 3.2, 3.4 and 3.6, the following observations can be made.

- residual stresses that may occur in the welded joints could be expected to increase the flexibility in load-displacement behaviour (i.e. the experimental curves). However, this influence is not noticeable for the joints considered here. The influence of residual stresses on the ultimate load is usually negligible.

- the load-displacement curves for the axially loaded joints show that the numerically and experimentally determined curves are in good agreement. The numerically determined ultimate loads vary between 4 % below and 8 % above the experimental values.

- for the joints loaded by in-plane bending, the moment-rotation curves show that the numerically determined moments at Yura's deformation limit and the experimental results are in very good agreement. The numerically determined results lie between 4 and 6 % below the experimental values.

- for the joints loaded by out-of-plane bending, the moment-rotation curves show that the numerically determined moments at Yura's deformation limit vary between 5 % below and 14 % above the experimental values. Since material cracking has not been modelled in the numerical analyses, the numerically determined curves do not reflect the drop in load observed experimentally beyond the occurrence of cracks (XX10, XX11 and XX12). A fracture failure approach has not been included in the present modelling because of the high complexity and expense of such a procedure.

Due to the good agreement between the experimental and numerical results, parametric studies have been set up for axially loaded joints and joints loaded by in-plane bending. In the present research, only the results of the axially loaded uniplanar X- and multiplanar XX-joints have been reported (chapters 5 and 6). The results of uniplanar and multiplanar joints loaded by in-plane bending are described in detail by van der Vegte (1995).

For the joints loaded by out-of-plane bending, only uniplanar joints have been considered. For accurate numerical simulations of the out-of-plane bending behaviour of multiplanar XX-joints, a fracture failure approach should be considered which is outside the scope of the present research.

34

BOUNDARY CONDITIONS

Degree of freedom	Node on plane X = 0.5 l_0 with Z = 0.5 d_0	Corner nodes on plane X = 0.0	Corner nodes on plane Y = 0.0	Mid-side nodes on planes X = 0.0 and Y = 0.0
u_x	free	0.	free	-
u_y	0.	free	0.	-
u_z	0.	free	free	-
ϕ_{edge}*	-	-	-	0.

* - ϕ_{edge} : rotation about the edge itself
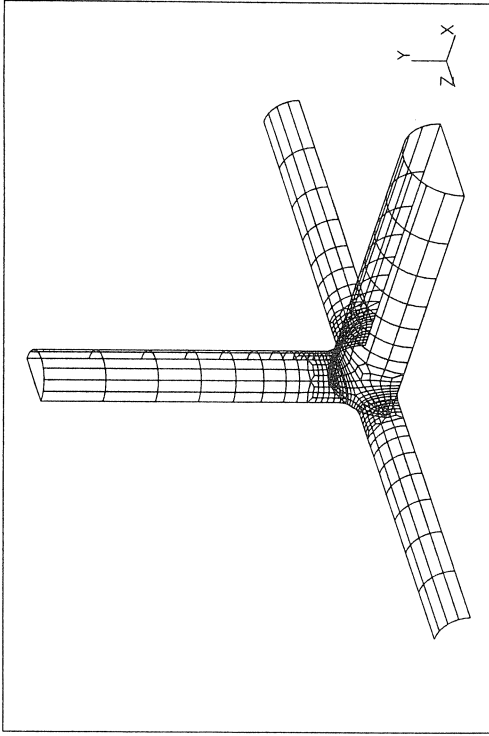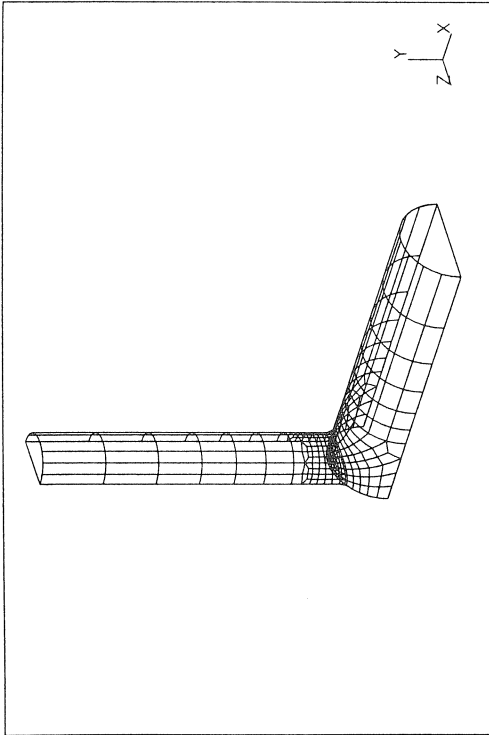
BOUNDARY CONDITIONS

Degree of freedom	Node on plane X = 0.5 l_0 with Z = 0.5 d_0	Nodes on plane X = 0.0	Nodes on plane Y = 0.0
u_x	free	0.	free
u_y	0.	free	0.
u_z	0.	free	free
ϕ_x	0.	free	0.
ϕ_y	free	0.	free
ϕ_z	0.	0.	0.

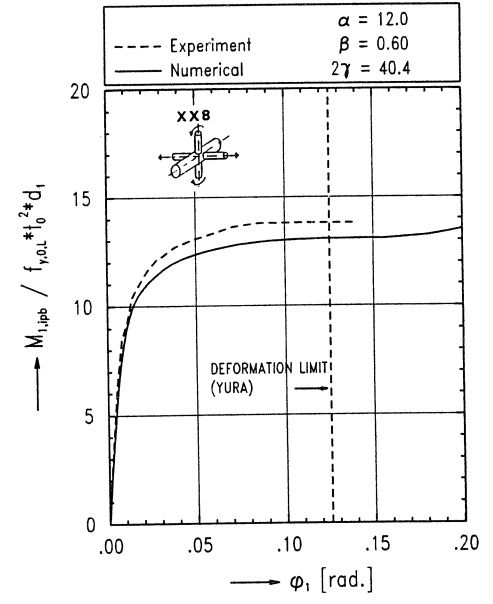Fig. 3.5 : Finite element meshes and boundary conditions for the X-joints loaded by out-of-plane bending (XX9 to XX12).
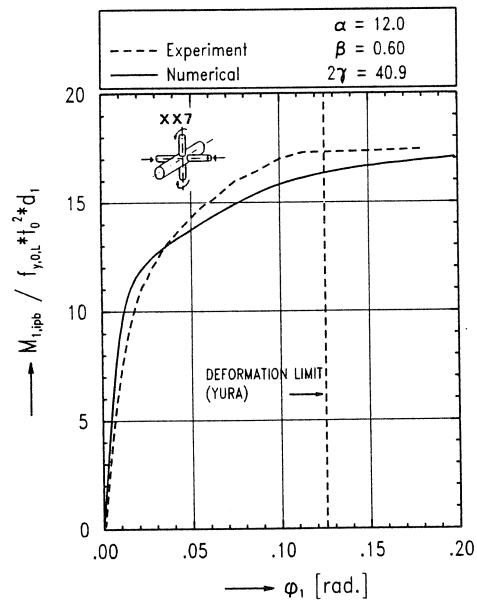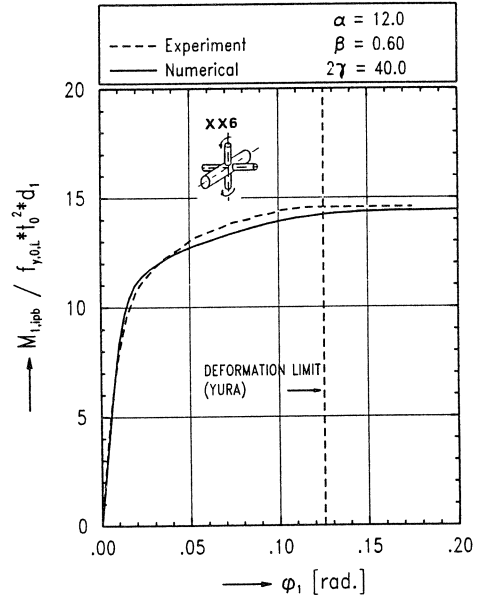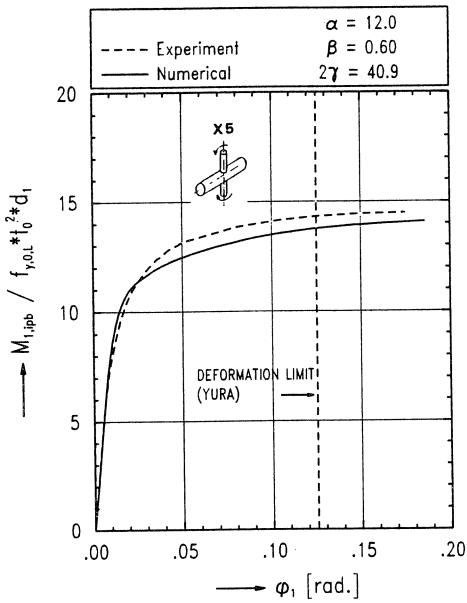
35
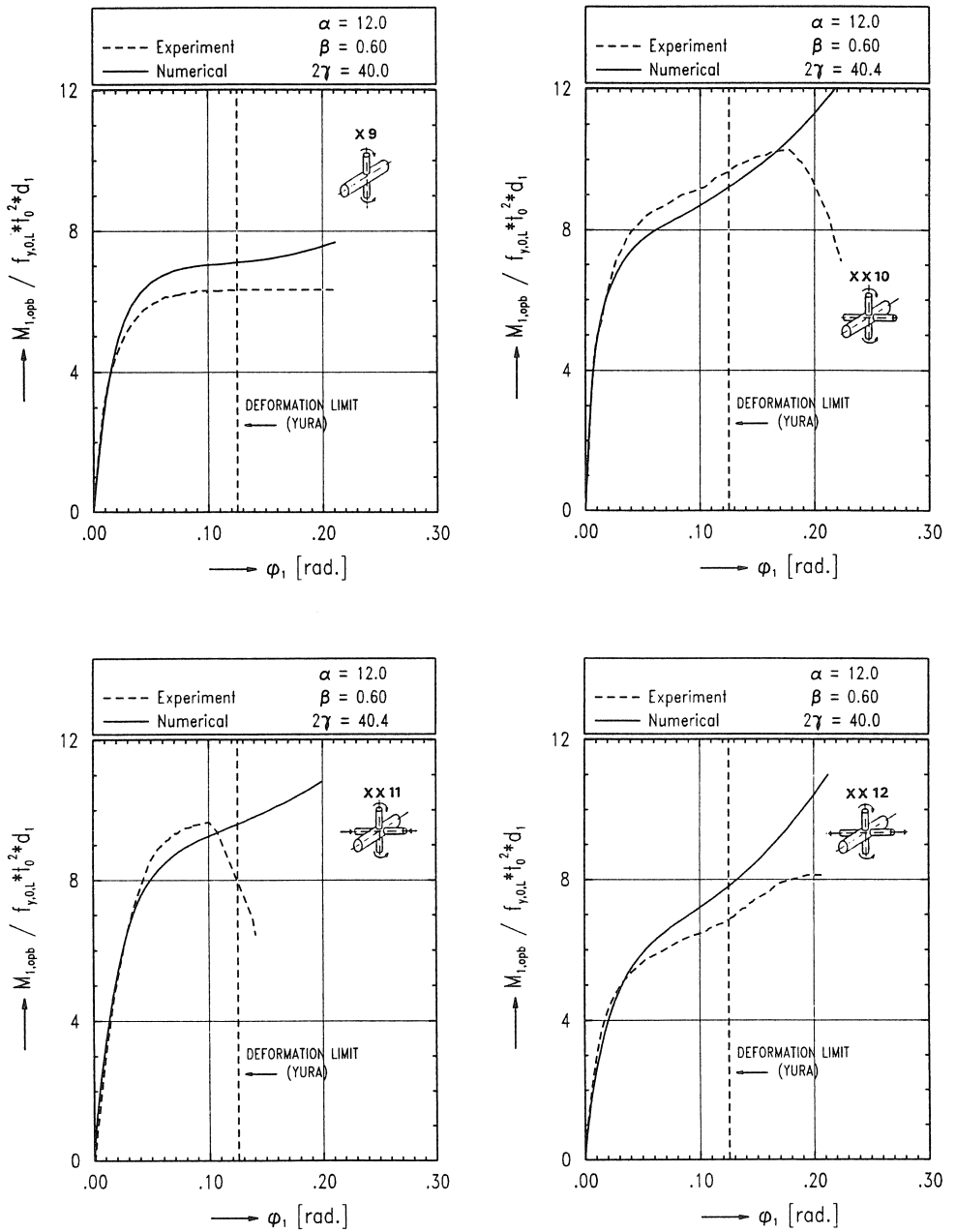
Fig. 3.6 : Moment-rotation curves of the X-joints loaded by out-of-plane bending.

Table 3.4 : Numerical results of the X-joints loaded by out-of-plane bending.

| | | | | | | | | | | Joints loaded by out-of-plane bending | | | | |
| | | | | | | | | | | | Test results (3) | | | |
Joint	No. of elem	No. of nodes	Elem type (1)	CPU sec. (2)	d_0 mm.	t_0 mm.	β	2γ	$f_{y,0,L}$ N/mm^2	$M_{1,u}$ kNm	$M_{1,Yura}$ kNm	Fail. mode (4)	$M_{1,Yura,num}$ kNm	$\dfrac{M_{1,Yura,num}}{M_{1,Yura,test}}$
X9	400	1242	22	13,400	408.0	10.2	0.6	40.0	331.	54.	53.	2	60.	1.13
XX10	742	2322	72	19,800	408.5	10.1	0.6	40.4	268.	70.	65.	3	62.	0.96
XX11	742	2322	72	18,100	408.5	10.1	0.6	40.4	268.	65.	-	3	64. (5)	0.98 (5)
XX12	742	2322	72	18,100	408.0	10.2	0.6	40.0	331.	69.	58.	3	66.	1.14

(1) : Element type : 22 = Eight noded thick shell elements
72 = Eight noded thin shell elements

(2) : All numerical analyses have been carried out on a CONVEX C240, which has four processors. Each of these processors has a peak performance of 50 Megaflops.

(3) : All moments have been calculated at the crown intersection of the chord and brace.
M_{Yura} = moment at Yura's deformation limit.

(4) : Modes of failure :
1 - Plastic deformation leading to failure of chord cross section.
2 - Plastic deformation leading to failure of chord cross section + initiation of cracks at the weld toe(s).
3 - Plastic deformation leading to failure of chord cross section + through cracks at the weld toe(s).

(5) : For XX11, $M_{1,u,test}$ has been taken instead of $M_{1,Yura,test}$.

37

4. General aspects with respect to the numerical parametric studies

4.1 *Assumptions for the numerical models*

In the two preceding chapters, the main features of the FE analyses on tubular joints have been described and discussed in detail. In these calibration studies, the actual measured values have been used for :
- the dimensions of the joints (e.g. d_0, t_0, etc.)
- the weld sizes
- the yield strength and material post-yield properties

Due to the good agreement between the results of the experiments and the numerical models, numerical parametric studies have been set up. For these numerical studies, the following assumptions are made with respect to the joint dimensions, the weld sizes and the material properties. The choice of the loading process (displacement or load control loading) has been described in section 4.1.4.

4.1.1 The dimensions of the joints

The non-dimensional geometrical parameters which have been considered are summarized in Table 4.1. For all joints, the diameter of the chord is taken as $d_0 = 406.4$ mm.
Although at first sight it may seem that the chord length parameter α differs considerably between the various studies, the following remarks should be made :
- for the axially loaded uniplanar X-joints, α has been taken as 11.5.
- from the analyses of uniplanar X-joints with variable chord length (section 5.2), it appeared that the chord length still had some influence on the strength of the X-joints. Based on these results, it has been decided to take $\alpha = 16.0$ in the studies of axially loaded multiplanar XX-joints (chapter 6). In chapter 8, the correction functions which account for the influence of the chord length, have been given for axially loaded uniplanar X- and multiplanar XX-joints.

In each of the appropriate numerical studies, the non-dimensional joint parameters (α, β, 2γ, etc.) have been presented, as well as the resulting joint dimensions (d_1, t_0, etc.).

4.1.2 Modelling of the welds

As mentioned in section 2.5, the geometry of the weld should be taken into account for accurate predictions of tubular joint behaviour. In chapter 3, the welds have been modelled in accordance with the measured weld dimensions. Since for the numerical parametric studies no weld sizes are available, the welds are modelled in accordance with the weld dimensions as recommended by A.W.S.

Table 4.1 : Summary of the non-dimensional parameters considered in the numerical parametric studies.

		α	β	2γ
uniplanar X-joints (chapter 5)	axial loading (5.1)	11.5	0.25 - 1.0	14.5 - 50.8
	chord length (5.2)	3.0 - 18.0	id.	25.4
multiplanar XX-joints (chapter 6)	axial loading (6.1)	16.0	0.22 - 0.60	14.5 - 50.8
	chord length (6.2)	3.0 - 16.0	id.	25.4 and 50.8

Remark :
the numbers between brackets refer to the appropriate sections.

The following two approximations to model the geometry of the welds have been considered :

- method 1 is shown in Fig. 4.1. In this method, the weld toe at the saddle point is vertically moved from the chord surface to the chord wall centerline. Furthermore, the thickness of the weld elements AC and A'C' is taken as $0.4\ t_1$.

- method 2 is based on the same A.W.S. weld size assumptions as method 1, but is in line with the method used for the calibration of the numerical models as described in section 2.5 (see Fig. 4.2). For this reason, method 2 is used for the parametric studies regarding multiplanar XX-joints and corresponding uniplanar joints (chapter 6).

The main differences between these approaches can be summarized as follows :

- a first difference between both approaches involves the thickness of the weld elements AC and A'C'. In method 2, the thickness of these elements is taken as the fillet thickness of the butt weld after averaging at the crown point and saddle point (see also section 2.5). However, it appears that for β ratios less than 0.7, the averaged thickness of the weld elements AC and A'C' is close to $0.4\ t_1$. Therefore, in method 1, the thickness of the weld elements AC and A'C' is taken as $0.4\ t_1$.

- a second difference can be found at the saddle point. As stated, in method 1, the weld toe is vertically moved from the chord surface to the chord wall centerline. In method 2, the weld toe has been moved perpendicular from the chord surface to the chord wall centerline. For large β ratios, however, method 2 gives very small element sizes for the weld elements B'C' at the saddle point and will therefore result in underestimations of the ultimate loads of these joints. For this reason, method 1 is used for the parametric studies which consider uniplanar X-joints only (chapter 5).
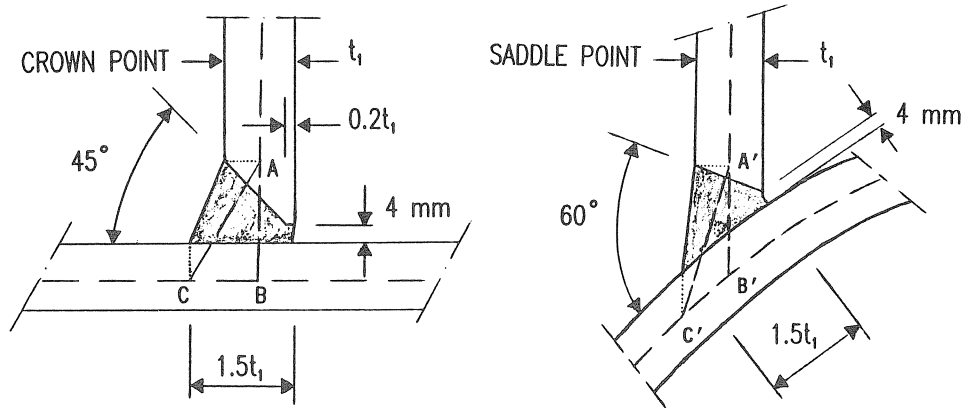
Fig. 4.1 : Numerical modelling of welds - method 1.

t_w = THICKNESS OF WELD ELEMENT AC

DEF = FILLET OF THE BUTT WELD

t_w' = THICKNESS OF WELD ELEMENT A'C'

D'E'F' = FILLET OF THE BUTT WELD
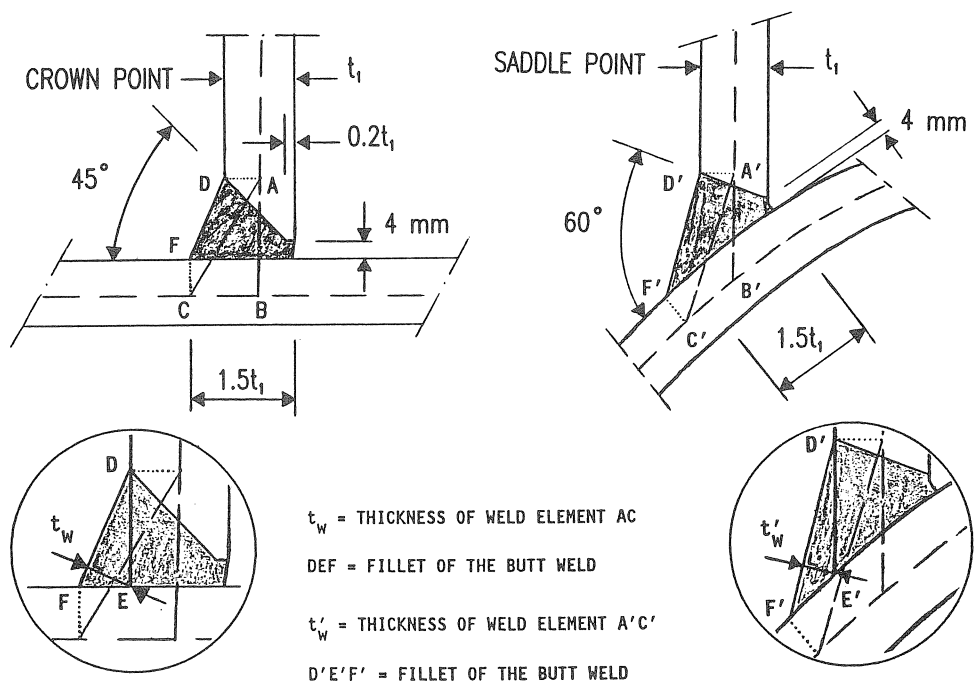
Fig. 4.2 : Numerical modelling of welds - method 2.

4.1.3 Yield strength and material post-yield properties

The steel grade used for almost all tubular members is S355 with f_y = 355 N/mm^2 and f_u = 510 N/mm^2. The experimentally determined engineering stress - strain curve for S355 has been converted to a true stress - true strain curve, which is defined by the Ramberg-Osgood relationship. In section 2.3.4, a detailed description is given of these conversions. Both the engineering stress - strain curve and the logarithmic stress - strain curves are modelled as step-wise linear relationships and shown in Fig. 4.3.

For some tubular (brace) members, however, steel grades with a higher yield strength have been applied to prevent brace failures before joint failures. For these cases, steel grade StE 690 has been used. Both the engineering stress - strain and the true stress - true strain curve for StE 690 are shown in Fig. 4.3. Furthermore, the Von Mises yield criterion and isotropic strain hardening are used in all numerical analyses.
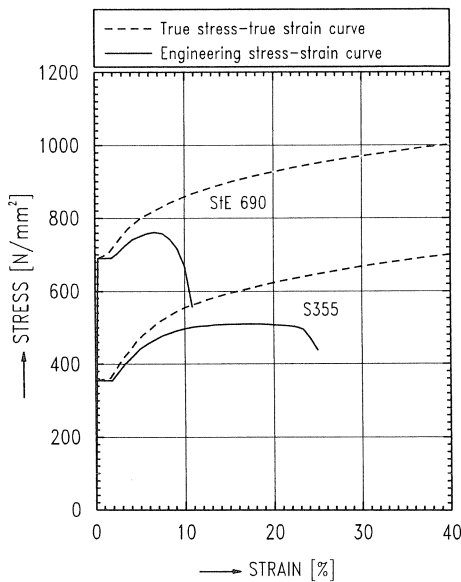
Fig. 4.3 : Engineering and true stress - true strain curves of S355 and StE 690.

4.1.4 Load controlled analyses versus displacement controlled analyses

As mentioned in section 2.3.3, when there is no preference from a physical point of view, the displacement control method is to be preferred to the load control method. Therefore, where possible in the numerical studies, displacement control has been used. However, for those joints where a constant (load) ratio has to be obtained between the applied loads, the load control method has been used since the displacement control method cannot realize these constant load ratios.

4.2 Deformation limits suggested by Yura

For almost all axially loaded joints, a pronounced peak load is observed in the load-displacement curves. This maximum load is considered to be the ultimate load. However, for certain axially loaded joints i.e. joints with low 2γ values, and joints loaded by in-plane or out-of-plane bending, no maximum in load or moment is obtained in the load-displacement or moment-rotation curves for increasing deformations. For these cases, "ultimate load" is considered to be reached if the displacement or rotation exceeds a certain deformation limit. For joints made of circular hollow sections, the practical deformation limits suggested by Yura (1980) are commonly used. Yura's deformation limits, both for axially loaded joints and joints loaded by bending, can be summarized as follows.

For axially loaded joints, the practical deformation limit is assumed to be reached when the strain along a brace member with a length of 30 d_1 is four times its yield strain. Furthermore, Yura assumes that the local joint deformation at each brace end is half of the displacement which results from this strain value. Thus, for axially loaded joints, the deformation limit is expressed as 60 $f_y.d_1/E$.

For joints loaded by bending, the rotation at the end of a simply supported beam (brace) with a span of 30 d_1 is determined for a uniformly distributed loading which causes first yield in the middle of the beam. Yura suggests that the practical deformation limit is reached if the rotation of a brace is four times the beam end rotation which results from the distributed load. Thus, for joints loaded by bending, the deformation limit is given by 80 f_y/E.

4.3 Program used for the regression analyses

As stated in the introduction, the numerical studies are performed in order to come to strength formulae which are based on analytical approaches. However, due to several simplifications in the analytical approaches, some terms in the analytically derived expressions need to be modified by a correction factor. For the determination of these factors (regression constants), regression analyses are performed using the results of the numerical studies.

In each of the numerical studies, non-linear regression analyses are carried out with the program NONLIN, developed at the Stevin Laboratory for Steel Structures of the Delft University of Technology. The non-linear equation solver-part of the program consists of routines developed at the Argonne National Laboratory, USA, in the framework of the MINPACK project and is based on a modified Levenberg-Marquant algorithm.

5. Uniplanar X-joints

5.1 *Axially loaded uniplanar X-joints*

5.1.1 Introduction

During the last three decades, many series of tests have been carried out on uniplanar tubular steel X-joints subjected to axial loading. Semi-empirical approaches through such test data are used to develop design formulae for these joints. However, in the past, major differences in approach in the various design codes have led to inconsistent formulae for the calculation of the axial strength of uniplanar X-joints.

In order to investigate the individual influence of β and 2γ, which are the most important parameters with respect to the static strength of uniplanar X-joints, non-linear FE analyses have been performed on tubular X-joints, subjected to axial compressive loading. Furthermore, analytical expressions for the strength of uniplanar X-joints have been derived. Based on the FE results and the analytical approach, a strength equation has been established for axially loaded uniplanar X-joints.

5.1.2 Research programme

The configuration of axially loaded uniplanar X-joints is shown in Fig. 5.1, while the dimensions and the non-dimensional geometrical parameters are presented in Fig. 5.2.
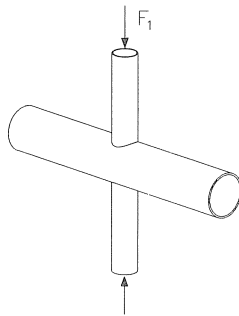
Fig. 5.1 : Configuration of axially loaded uniplanar X-joints.

The research programme is summarized in Table 5.1. The study consists of a total of 16 finite element analyses on tubular X-joints subjected to compressive brace loading. Four β values and four 2γ values have been considered (β = 0.25, 0.48, 0.73, 1.0 and 2γ = 14.5, 25.4, 36.9, 50.8), whereas d_0 = 406.4 mm. For all joints, the chord length parameter α is set to 11.5. For the joints with β = 0.25 and 0.48, the wall thickness ratio τ is set to 0.5, for the joints with β = 0.73 and 1.0, τ is taken as 1.0. The nominal dimensions of the joints are given in Table 5.2.

43

The steel grade of all tubular members is S355 with $f_y = 355$ N/mm^2 and $f_u = 510$ N/mm^2. However, to prevent brace failure before joint failure, the yield strength of the braces of joint XA1 has been increased to 745 N/mm^2

$$\alpha = 2l_0/d_0$$
$$\beta = d_1/d_0$$
$$2\gamma = d_0/t_0$$
$$\tau = t_1/t_0$$
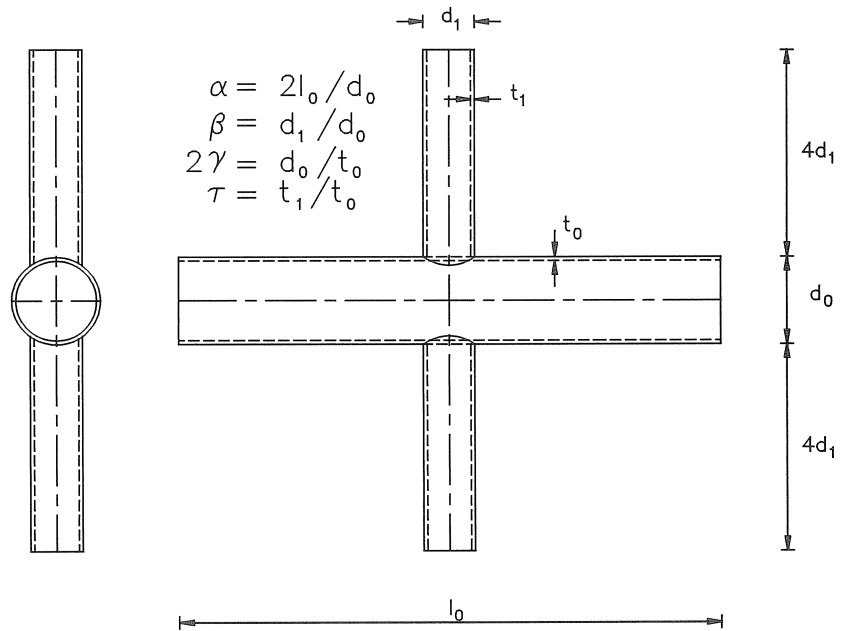
Fig. 5.2 : Dimensions and non-dimensional geometrical parameters of uniplanar X-joints.

Table 5.1 : Research programme of axially loaded uniplanar X-joints.

	2γ			
	14.5	25.4	36.9	50.8
$\beta = 0.25$	XA1	XA2 *	XA3	XA4
$\beta = 0.48$	XA5 *	XA6 *	XA7 *	XA8 *
$\beta = 0.73$	XA9	XA10 *	XA11	XA12
$\beta = 1.00$	XA13 **	XA14 **	XA15 **	XA16 **

Remark :
* : also modelled without a weld
** : modelled without a weld

44

Table 5.2 : Nominal dimensions and numerical results of the axially loaded uniplanar X-joints.

| | Nominal dimensions | | | | | Numerical results | |
| | chord | | | brace | | | |
joint	d_0 mm	t_0 mm	l_0 mm	d_1 mm	t_1 mm	$F_{1,u}$ kN	$\dfrac{F_{1,u}}{f_{y,0} \cdot t_0^2}$
XA1	406.4	28.0	2342.	101.6	14.2	1803. **	6.48 **
XA2	406.4	16.0	2342.	101.6	8.0	621.	6.84
XA2 *	406.4	16.0	2342.	101.6	8.0	580.	6.38
XA3	406.4	11.0	2342.	101.6	5.6	305.	7.09
XA4	406.4	8.0	2342.	101.6	4.0	164.	7.22
XA5	406.4	28.0	2342.	193.7	14.2	2620.	9.41
XA5 *	406.4	28.0	2342.	193.7	14.2	2478.	8.90
XA6	406.4	16.0	2342.	193.7	8.0	959.	10.56
XA6 *	406.4	16.0	2342.	193.7	8.0	934.	10.28
XA7	406.4	11.0	2342.	193.7	5.4	477.	11.10
XA7 *	406.4	11.0	2342.	193.7	5.4	470.	10.93
XA8	406.4	8.0	2342.	193.7	4.0	265.	11.65
XA8 *	406.4	8.0	2342.	193.7	4.0	262.	11.52
XA9	406.4	28.0	2342.	298.5	28.0	4100.	14.73
XA10	406.4	16.0	2342.	298.5	16.0	1406.	15.47
XA10 *	406.4	16.0	2342.	298.5	16.0	1350.	14.85
XA11	406.4	11.0	2342.	298.5	11.0	685.	15.94
XA12	406.4	8.0	2342.	298.5	8.0	377.	16.58
XA13 *	406.4	28.0	2342.	406.4	28.0	8586.	30.85
XA14 *	406.4	16.0	2342.	406.4	16.0	3386.	37.26
XA15 *	406.4	11.0	2342.	406.4	11.0	1761.	40.99
XA16 *	406.4	8.0	2342.	406.4	8.0	1042.	45.87

Remarks :
*   : modelled without a weld
**   : strength at Yura's deformation limit

5.1.3 Finite element analyses

The general characteristics of the FE analyses are summarized in chapters 2 and 3. The specific details of the FE analyses of uniplanar X-joints are as follows :

FE characteristics :
- the nominal dimensions of the joints, summarized in Table 5.2, are used to model the joints.
- one eighth of each joint has been modelled.
- eight noded thick shell elements are used to model the joints.
- the number of elements used to model the joints is about 220. The FE mesh used for the joints with $\beta = 0.48$ is shown in Fig. 5.3. The boundary conditions are similar to those of the axially loaded uniplanar X-joint shown in Fig. 3.1.
- no additional boundary conditions are needed to prevent rigid body movements.
- the load has been applied at the brace tip by displacement control.
- the geometry of the weld has been modelled in accordance with method 1 as described in section 4.1.2. However, some of the joints are also modelled without a weld (the joints with $2\gamma = 25.4$: XA2, XA6 and XA10 and the joints with $\beta = 0.48$: XA5, XA6, XA7 and XA8). For $\beta = 1.0$, no welds have been modelled.
- the material properties used for all tubular members are shown in Fig. 4.3 (S355). The Von Mises yield criterion and isotropic strain hardening have been used.
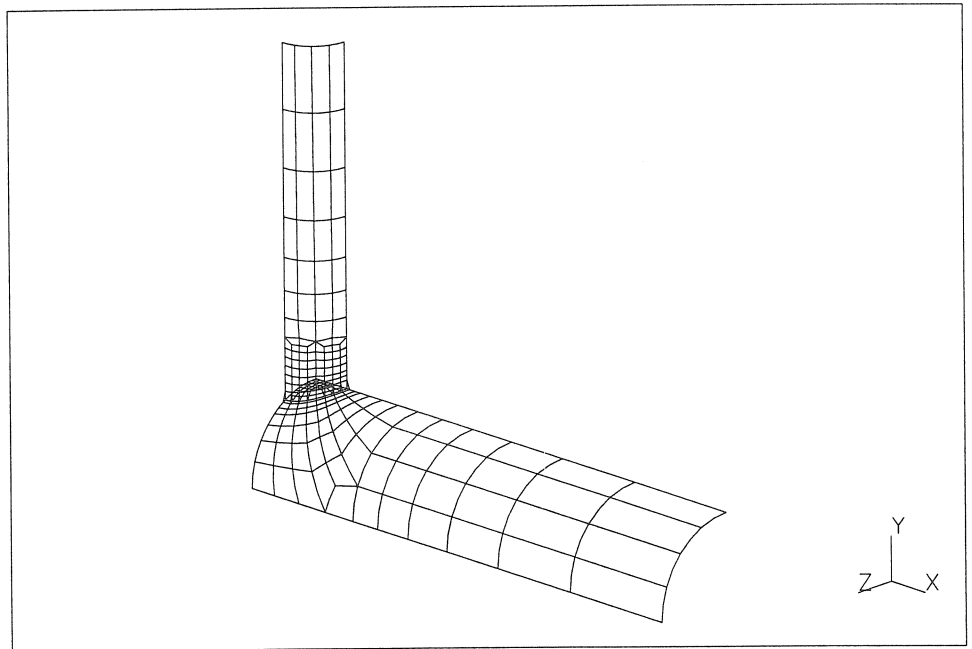
Fig. 5.3 : Finite element mesh for the axially loaded uniplanar X-joints with $\beta = 0.48$.

5.1.4 Numerical results

In Fig. 5.4, the load-displacement curves are separately given for each group of X-joints with the same β value. The non-dimensionalized axial load $F_1/f_{y,0}.t_0^2$ has been plotted against the non-dimensionalized crown point displacement δ_1/d_0. Yura's deformation limit has been shown in those figures which consider X-joints where no maximum in load is observed before Yura's deformation limit. The non-dimensionalized ultimate strength values are summarized in Table 5.2 and presented in Fig. 5.6 as function of β.

Considering the load-deformation diagrams in Fig. 5.4 and the ultimate capacities of the X-joints as a function of β in Fig. 5.6, the following observations can be made.
For all X-joints, it appears that an increasing value of 2γ results in an increasing non-dimensional ultimate load. This effect is most pronounced for $\beta = 1.0$, since for this β value, the load transfer through the joint mainly leads to membrane stresses in the chord wall while for lower β values the load transfer causes considerable bending moments in the chord wall. The observed 2γ influence on the joint capacity has also been noticed by Yura (1980).

For X-joints with $\beta = 1.0$, the deformation capacity decreases with increasing values of 2γ. For the other joints it appears that for each group of X-joints with the same β value the deformation capacity is almost the same.

As expected, modelling of the geometry of the weld increases the ultimate load of tubular X-joints. However, as can be observed from Table 5.2, the differences between the results of analyses with or without modelling of welds are very small for axially loaded uniplanar X-joints, especially for large 2γ values.

5.1.5 Analytical approach for axially loaded uniplanar X-joints : ring model

Analytical yield line models for connections between tubular members are extremely difficult to derive. A more simple model, also based on plasticity theory, has been established for connections between circular tubular members by Togo (1967), Mäkeläinen (1988) and Paul (1992). In literature, this model is referred to as "ring model". The expressions which are derived from this "ring model" are used as a basis for the strength equations.
In the "ring model" the three dimensional connection of the chord is represented by a two dimensional model with the shape of a ring. The connection characteristics in axial direction are not included in the model. The forces in the brace are represented as line loads which act over an effective length B_e of the chord at the theoretical saddle points. The effective ring length and the exact positions of the line loads can only be obtained by using the results of experiments or finite element analyses.
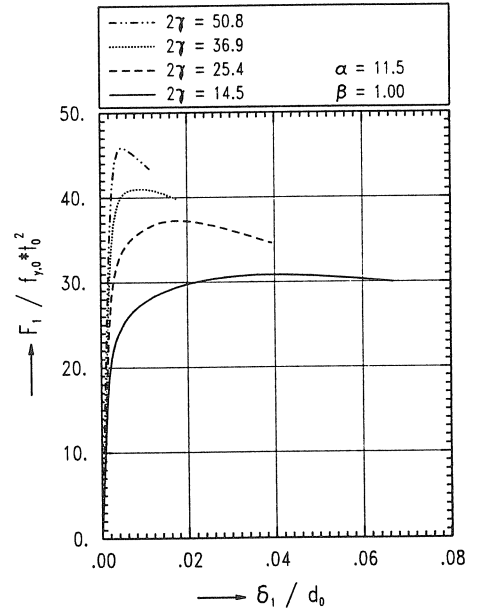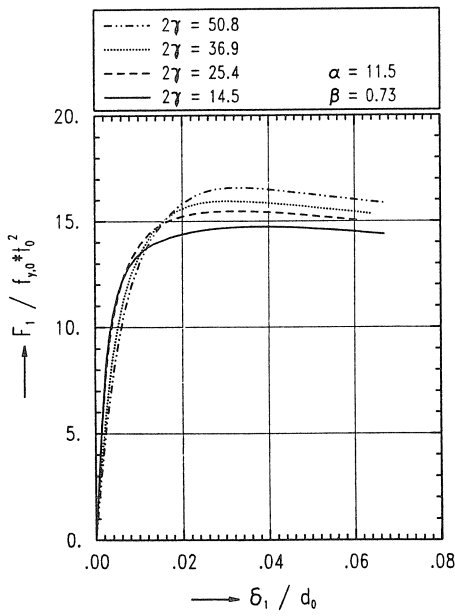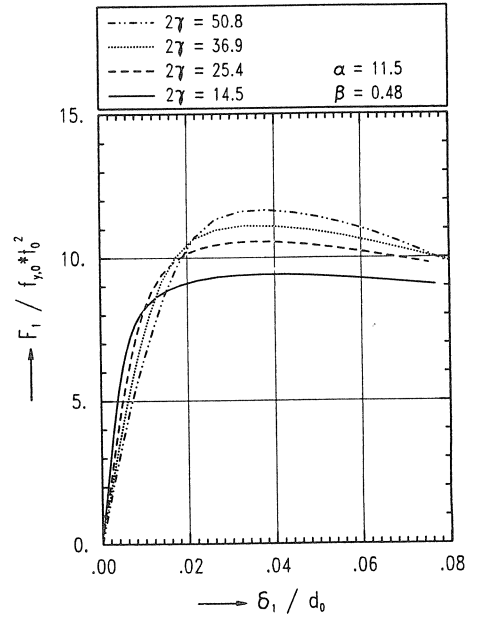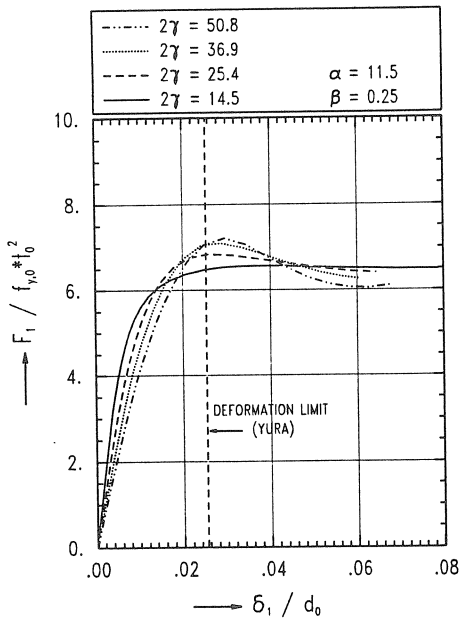
Fig. 5.4 : Numerical load-displacement curves of axially loaded uniplanar X-joints.

48

5.1.5.1 Simple ring model approach

In literature, most of the derivations of the ring model strength formulae are based on a simple approach, thus neglecting the interaction between axial force (N), shear force (V) and bending moment (M). The simplest derivation of the ring model strength formulae for X-joints under axial load, is obtained by taking bending moments into account only.

For uniplanar X-joints, the chord is represented by a ring with a length B_e, whereas the brace load is represented by a force F, acting in the saddle point. See Fig. 5.5, in which one quarter of the model (= chord cross section) has been shown. Yield hinges are assumed to occur in the following two points :
- point 1, the saddle point of the in-plane brace (ψ_1 = arcsin β)
- point 2 ($\psi_2 = \pi/2$)
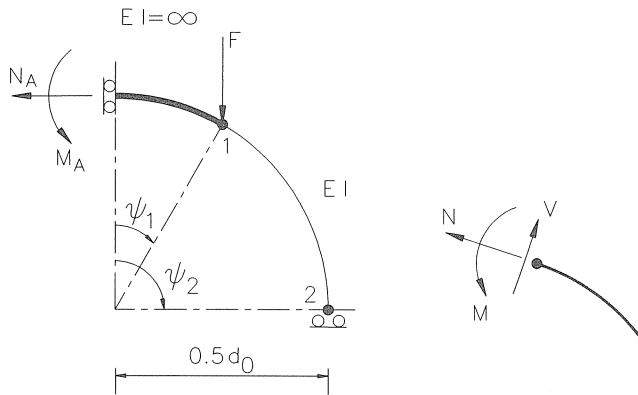
Fig. 5.5 : Analytical "ring model" approach for axially loaded uniplanar X-joints.

The following expressions hold for the bending moments in the yield hinges 1 and 2 :

$$-M(\psi_1) = M_A + N_A \frac{d_0}{2}(1 - \cos \psi_1) \tag{5.1}$$

$$+M(\psi_2) = M_A + N_A \frac{d_0}{2}(1 - \cos \frac{\pi}{2}) + F \frac{d_0}{2}(1 - \sin \psi_1) \tag{5.2}$$

Solving these equations with $M(\psi_i) = M_p$ (i = 1...2), N_A = 0.0 and :

$$M_p = \frac{1}{4} f_{y,0} \cdot t_0^2 \cdot B_e \tag{5.3}$$

gives the following expression for the analytical strength of axially loaded uniplanar X-

joints $F_{1,y}$ (= 2F, due to symmetry) :

$$\frac{F_{1,y}}{f_{y,0} \cdot t_0^2 \cdot (\frac{B_e}{d_0})} = \frac{2}{(1-\beta)} \tag{5.4}$$

For $\beta = 1.0$, however, this simple approach leads to infinite solutions. Therefore, a more accurate approach is required, which is described in the next section.

5.1.5.2 Exact ring model approach

In order to obtain more accurate predictions of the analytical strength for large β values, the influences due to axial forces as well as shear forces are included.
In the assumed yield hinges, the axial forces are given by :

$$N(\psi_1) = N_A \cos\psi_1 - F\sin\psi_1 \tag{5.5}$$

$$N(\psi_2) = N_A \cos\frac{\pi}{2} - F\sin\frac{\pi}{2} \tag{5.6}$$

In the assumed yield hinges, the following expressions for the shear forces can be derived :

$$V(\psi_1) = N_A \sin\psi_1 + F\cos\psi_1 \tag{5.7}$$

$$V(\psi_2) = N_A \sin\frac{\pi}{2} + F\cos\frac{\pi}{2} \tag{5.8}$$

The approximated interaction formula between axial force, shear force and bending moment, based on the Von Mises yield criterion, for a rectangular cross-section according to the plasticity theory is given by Eq. 5.9.

$$\frac{M}{M_p} + \left[\frac{N}{N_p}\right]^2 + \left[\frac{V}{V_p}\right]^2 = 1.0 \tag{5.9}$$

with :

$$N_p = f_{y,0} \cdot t_0 \cdot B_e \tag{5.10}$$

50

$$V_p = \frac{1}{\sqrt{3}} f_{y,0} \cdot t_0 \cdot B_e \tag{5.11}$$

Substitution of Eqs. 5.1, 5.2 and Eqs. 5.5 to 5.8 in Eq. 5.9 for each of the two yield hinges, leads to the exact solution for the ultimate ring model strength $F_{1,y}$ of axially loaded uniplanar X-joints :

$$\frac{F_{1,y}}{f_{y,0} \cdot t_0^2 \cdot (\frac{B_e}{d_0})} = \frac{4}{(1-\beta) + \sqrt{(1-\beta)^2 + \frac{2-\beta^2}{\gamma^2}}} \tag{5.12}$$

5.1.6 Basic ultimate strength formula for axially loaded uniplanar X-joints

As mentioned in section 5.1.5, the expression derived from the analytical approach (Eq. 5.12) will form the basis for the ultimate strength equation. However, as can be observed in the exact solution (Eq. 5.12), the effective ring length B_e is still unknown. Based on regression analyses of the results of experiments or finite element analyses, an expression for the effective length B_e can be derived, which depends on β and 2γ. Subsequently, the expression derived for B_e has to be multiplied with Eq. 5.12 to obtain the ultimate strength equation for axially loaded uniplanar X-joints. Since this strategy leads to a complicated ultimate strength equation, one overall expression which includes both Eq. 5.12 and B_e/d_0, is proposed to serve as basis for the regression analyses.

Furthermore, as mentioned in 5.1.5, the forces F in the "ring model" approach, do not apply exactly at the saddle positions but at a distance which is somewhat smaller than d_1. Therefore, a regression constant R_4 is added to all β terms in the exact solution 5.12.
As a result, the following expression is proposed as a basis for the ultimate strength equation of axially loaded uniplanar X-joints.

$$\frac{F_{1,u}}{f_{y,0} \cdot t_0^2} = \frac{R_1 \gamma^{R_2\beta - R_3\beta^2}}{(1 - R_4\beta) + \sqrt{(1 - R_4\beta)^2 + \frac{2 - (R_4\beta)^2}{\gamma^2}}} \tag{5.13}$$

The regression constants R_i (i = 1...4) have to be determined by non-linear regression analyses of the FE results.

All FE results except the ultimate strength value for XA16, are used to calibrate the unknowns R_i (i = 1...4) of Eq. 5.13 (for the joints with $\beta \leq 0.73$, only the FE results which include modelling of the welds have been considered). Joint XA16 has been omitted from the regression analyses due to its high strength combined with a very small deformation

capacity. For safety reasons, the strength formula should underestimate the ultimate strength of this joint.

The final results of the regression analyses are presented in Eq. 5.14 and Table 5.3. Eq. 5.14 as well as the FE data points are shown in Fig. 5.6.

$$\frac{F_{1,u}}{f_{y,0} \cdot t_0^2} = \frac{8.7 \, \gamma^{0.5\beta - 0.5\beta^2}}{(1 - 0.9\beta) + \sqrt{(1 - 0.9\beta)^2 + \frac{2 - (0.9\beta)^2}{\gamma^2}}} \tag{5.14}$$
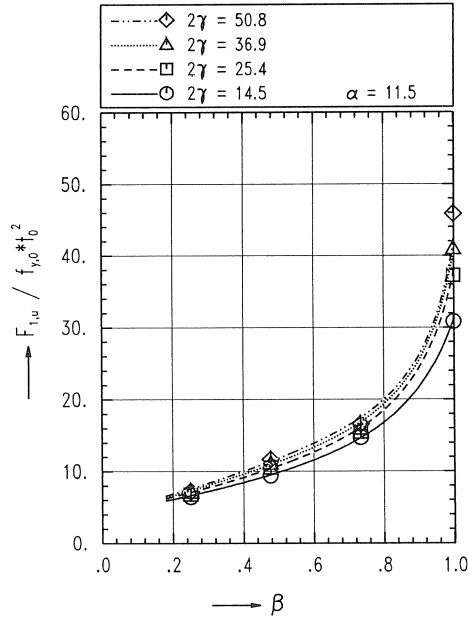
Fig. 5.6 : Ultimate strength of axially loaded uniplanar X-joints.

Good agreement exists between the ultimate strength formula and the data points, as can be observed from Table 5.3. Furthermore, it is shown that the ultimate strength of joint XA16 is 1.09 times the value predicted by Eq. 5.14.

Table 5.3 : Results of the regression analyses of axially loaded uniplanar X-joints (Eq. 5.14).

No. of data points	R^2 (%)	Mean	CoV.
15	99.82	0.984	2.84×10^{-2}

52

5.2 *Axially loaded uniplanar X-joints with variable chord lengths*

5.2.1 Introduction

In the past, many questions arose regarding the influence of the chord length on the strength of tubular joints. In order to investigate the influence of the chord length on the static strength of uniplanar X-joints, non-linear finite element analyses have been carried out on tubular X-joints, subjected to compression loading.

5.2.2 Research programme

The configuration and the dimensions of axially loaded X-joints are shown in Figs. 5.1 and 5.2. The research programme is summarized in Table 5.4. The study consists of a total of 16 finite element analyses on tubular X-joints subjected to compressive brace loading. Four α values (α = 3.0, 6.0, 11.5 and 18.0) have been considered for four β values (β = 0.25, 0.48, 0.73, 1.0). For the joints with β = 0.25 and 0.48, τ is taken as 0.5, for the other joints τ is set to 1.0. The nominal dimensions of the joints are given in Table 5.5.
The steel grade for all tubular members is S355 with f_y = 355 N/mm^2 and f_u = 510 N/mm^2.

Table 5.4 : Research programme of axially loaded X-joints with variable chord lengths.

	α			
	3.0	6.0	11.5	18.0
β = 0.25	XASC1	XASC2	XASC3	XASC4
β = 0.48	XASC5	XASC6	XASC7	XASC8
β = 0.73	XASC9	XASC10	XASC11	XASC12
β = 1.00	XASC13 *	XASC14 *	XASC15 *	XASC16 *

Remark :   * : modelled without a weld

5.2.3 Finite element analyses

The general characteristics of the FE analyses are summarized in chapters 2 and 3. The specific details of the FE analyses for uniplanar X-joints are as follows :

FE characteristics :
- the nominal dimensions of the joints, which are summarized in Table 5.5, are used to model the joints.
- one eighth of each joint has been modelled.
- eight noded thick shell elements are used to model the joints.

53

- the number of elements used to model the joints, depends on the α value. For $\alpha = 11.5$ the number of elements is about 220.
- no additional boundary conditions were needed to prevent rigid body movements. No restraints are applied to the chord ends.
- the load has been applied at the brace tip by displacement control.
- the geometry of the weld has been modelled in accordance with method 1 as described in section 4.1.2. For $\beta = 1.0$, no welds have been modelled.
- the material properties used for all tubular members are shown in Fig. 4.3 (S355). The Von Mises yield criterion and isotropic strain hardening have been used.

Table 5.5 : Nominal dimensions and numerical results of axially loaded X-joints with variable chord lengths.

| joint | Nominal dimensions | | | | | Numerical results | |
| | chord | | | brace | | | |
	d_0 mm	t_0 mm	l_0 mm	d_1 mm	t_1 mm	$F_{1,u}$ kN	$\dfrac{F_{1,u}}{f_{y,0} \cdot t_0^2}$
XASC1	406.4	16.0	610.	101.6	8.0	386.	4.25
XASC2	406.4	16.0	1219.	101.6	8.0	603.	6.63
XASC3	406.4	16.0	2342.	101.6	8.0	621.	6.84
XASC4	406.4	16.0	3658.	101.6	8.0	633.	6.97
XASC5	406.4	16.0	610.	193.7	8.0	532.	5.86
XASC6	406.4	16.0	1219.	193.7	8.0	873.	9.61
XASC7	406.4	16.0	2342.	193.7	8.0	959.	10.56
XASC8	406.4	16.0	3658.	193.7	8.0	1015.	11.17
XASC9	406.4	16.0	610.	298.5	16.0	904.	9.94
XASC10	406.4	16.0	1219.	298.5	16.0	1291.	14.21
XASC11	406.4	16.0	2342.	298.5	16.0	1406.	15.47
XASC12	406.4	16.0	3658.	298.5	16.0	1487.	16.37
XASC13	406.4	16.0	610.	406.4	16.0	2953.	32.49
XASC14	406.4	16.0	1219.	406.4	16.0	3272.	36.00
XASC15	406.4	16.0	2342.	406.4	16.0	3386.	37.26
XASC16	406.4	16.0	3658.	406.4	16.0	3456.	38.03
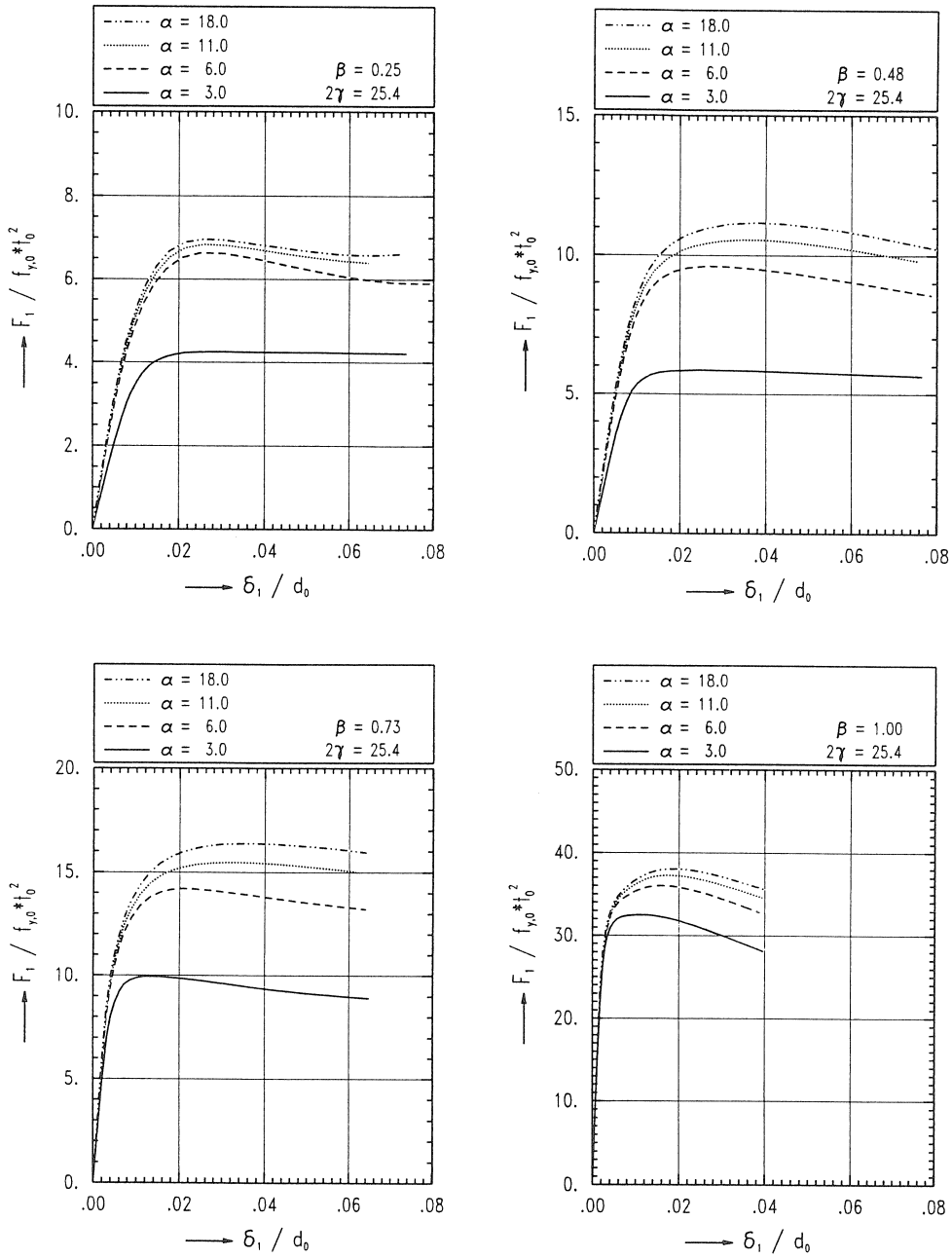
Fig. 5.7 : Numerical load-displacement curves of axially loaded uniplanar X-joints with variable chord lengths.

5.2.4 Numerical results

In Fig. 5.7, the load-displacement curves are separately given for each group of X-joints with the same β value and with variable chord lengths. The non-dimensionalized axial load $F_1/f_{y,0}.t_0^2$ has been plotted against the non-dimensionalized crown point displacement. The non-dimensionalized static strength values are given in Table 5.5.

In Fig. 5.9 the non-dimensionalized ultimate loads of the X-joints have been plotted as a function of α for each group of joints with the same β value.

Considering the load-deformation diagrams in Fig. 5.7 and the ultimate load versus α curves in Fig. 5.9, the following observations can be made.

For all β values, it appears that a decreasing value of α results in a decreasing value of the non-dimensionalized ultimate load. This effect is most pronounced for β values equal to 0.48 and 0.73.

For α values below 6.0, a significant drop in non-dimensional ultimate load (a drop up to 44 % for $\beta = 0.48$ and $\alpha = 3.0$, compared to the joint with $\alpha = 11.5$) is observed for all β values with the exception of $\beta = 1.0$. For $\beta = 1.0$, the chord ovalizing is much less than for other β values. Furthermore it can be observed that for α values above 11.5, the increase in ultimate load is small.

5.2.5 Basic ultimate strength formula for axially loaded uniplanar X-joints with variable chord lengths

In this section, an expression is derived which accounts for the chord length influence on the static strength of uniplanar X-joints. This chord length function has been related to the strength formula of uniplanar X-joints with $\alpha = 11.5$, as presented in section 5.1.6, which means that for the joints with $\alpha = 11.5$, the correction factor is 1.0.

The following expression has been derived to relate the strength of uniplanar X-joints with a chord length different from $\alpha = 11.5$ to the strength equation $F_{1,u}(\alpha = 11.5)$ for uniplanar X-joints with $\alpha = 11.5$:

$$g(\alpha) = \frac{F_{1,u}(\alpha)}{F_{1,u}(\alpha = 11.5)} \frac{11.5}{\alpha} \tag{5.15}$$

The function $F_{1,u}(\alpha)$ is the strength equation which includes the α effects.

In Fig. 5.8, the resulting data points have been presented as function of α. In this figure, it can be seen that for the joints with $\alpha \geq 6.0$, the influence of β is negligible.
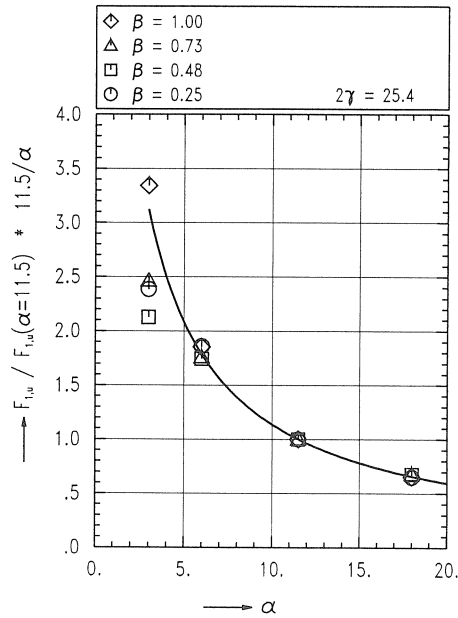
Fig. 5.8 : The function g(α) of axially loaded uniplanar X-joints.

The function $g(\alpha)$ is determined by means of regression analyses whereas the following expression is used as a basis for $g(\alpha)$:

$$g(\alpha) = \frac{R_1}{1 + R_2\,\alpha} \tag{5.16}$$

The regression constants R_1 and R_2 are obtained by performing regression analyses of the FE results. Only the uniplanar X-joints with $\alpha \geq 6.0$ have been included in the regression analyses, since for X-joints with α values smaller than 6.0, a pronounced β effect is shown which is not observed for the joints with $\alpha \geq 6.0$. Based on this FE database, the following values of the regression constants R_1 and R_2 and statistical quantities (Table 5.6) have been obtained :

$$g(\alpha) = \frac{12.5}{1 + \alpha} \tag{5.17}$$

This function $g(\alpha)$ is shown in Fig. 5.8.

Combining the results of Eqs. 5.15 and 5.17, gives the final expression of the strength of axially loaded X-joints for $\alpha \geq 6.0$:

57

$$F_{1,u}(\alpha) = f(\alpha) . F_{1,u}(\alpha = 11.5)$$ (5.18)

with the desired chord length function f(α) defined as :

$$f(\alpha) = g(\alpha)\frac{\alpha}{11.5} = \frac{12.5\,\alpha}{11.5\,(1+\alpha)}$$ (5.19)

The FE data points and the curves representing the basic strength equation are shown in Fig. 5.9.
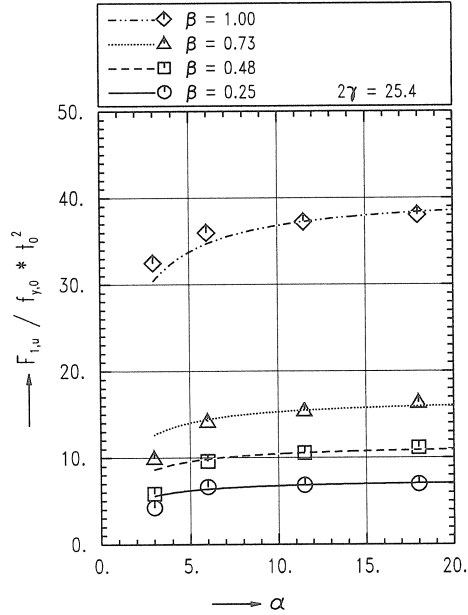
Fig. 5.9 : Ultimate strength of axially loaded uniplanar X-joints as a function of α.

It should be noted that the chord length function f(α) is based on a FE database which considers only one 2γ value (2γ = 25.4).

Table 5.6 : Results of the regression analyses of axially loaded uniplanar X-joints with variable chord lengths (Eq. 5.18).

No. of data points	R^2 (%)	Mean	CoV.
12	78.31	1.006	2.14×10^{-2}

58

6. Multiplanar XX-joints

6.1 *Axially loaded multiplanar XX-joints*

6.1.1 Introduction

In chapter 3, the results have been shown of the numerical simulations of the experiments which considered uniplanar X- and multiplanar XX-joints under different types of loading on the in-plane braces. Due to the good agreement between the experimental results and those obtained with numerical models, numerical parametric studies have been set up for axially loaded multiplanar XX-joints.

In this section, the results of the analyses on the axially loaded multiplanar XX-joints are presented in order to investigate the individual influences of the geometrical parameters β and 2γ and the load ratio J (= load on out-of-plane brace divided by the load on the in-plane brace). For a good comparison with the uniplanar behaviour, the corresponding uniplanar X-joints have been analyzed as well.

Furthermore, expressions have been derived for the analytical strength of multiplanar XX-joints, whereas several yield mechanisms can be observed. The transitions between the yield mechanisms are described in detail.

Finally, based on the FE results and the expressions derived from the analytical approach, strength formulae are established for axially loaded multiplanar XX-joints.

6.1.2 Research programme

The configuration of axially loaded multiplanar XX-joints is shown in Fig. 6.1, while the dimensions and the non-dimensional geometrical parameters are shown in Fig. 6.2.
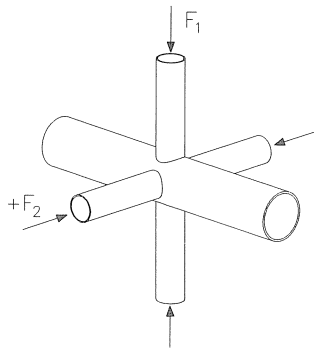
Fig. 6.1 : Configuration of axially loaded multiplanar XX-joints.
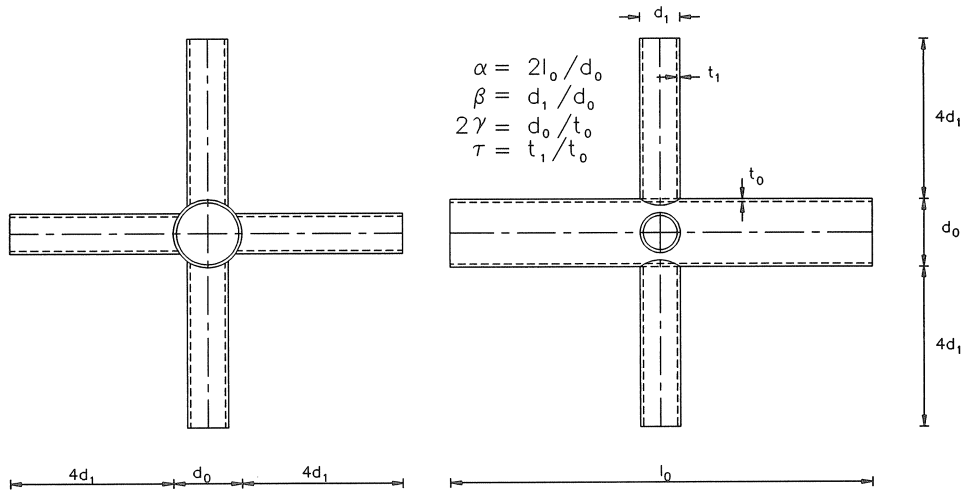
Fig. 6.2 : Dimensions and non-dimensional geometrical parameters of multiplanar XX-joints.

The research programme is summarized in Table 6.1. The study consists of a total of 52 finite element analyses on tubular X-joints subjected to compressive brace loading, while the corresponding uniplanar X-joints have been analyzed as well. Three β values and four 2γ values have been considered, while $d_0 = 406.4$ mm. For the joints with $\beta = 0.22$ and 0.41, τ is set to 0.63 and 0.79 respectively. For the other joints τ is taken as 1.0. For all joints, the chord length parameter α is set to 16.0. The nominal dimensions of the joints are given in Table 6.2.

The following load ratios J have been analyzed :
J = -0.6 : compression forces on the in-plane braces, tension forces on the out-of-plane braces.
J = 0.0 : unloaded out-of-plane braces.
J = 0.6 : this load ratio has been considered for the joints with $\beta = 0.60$ only.
J = 1.0 : all braces equally loaded in compression.

Note that negative forces represent tensile forces, while positive forces refer to compression.

The steel grade of all tubular members is S355 with $f_y = 355$ N/mm^2 and $f_u = 510$ N/mm^2. However, to prevent brace failure before joint failure, the yield strength of the braces of joint XXA1 has been increased to 690 N/mm^2

60

Table 6.1 : Research programme of axially loaded multiplanar XX-joints.

	2γ			
	14.5	25.4	36.9	50.8
$\beta = 0.22$	XXA1	XXA2	XXA3	XXA4
$\beta = 0.41$	XXA5	XXA6	XXA7	XXA8
$\beta = 0.60$	XXA9	XXA10	XXA11	XXA12

Table 6.2 : Nominal dimensions of axially loaded multiplanar XX-joints.

	Nominal dimensions				
	chord			braces	
joint	d_0 mm	t_0 mm	l_0 mm	d_1 mm	t_1 mm
XXA1	406.4	28.0	3251.	88.9	17.5
XXA2	406.4	16.0	3251.	88.9	10.0
XXA3	406.4	11.0	3251.	88.9	7.1
XXA4	406.4	8.0	3251.	88.9	5.0
XXA5	406.4	28.0	3251.	165.1	22.2
XXA6	406.4	16.0	3251.	165.1	12.5
XXA7	406.4	11.0	3251.	165.1	8.8
XXA8	406.4	8.0	3251.	165.1	6.3
XXA9	406.4	28.0	3251.	244.5	28.0
XXA10	406.4	16.0	3251.	244.5	16.0
XXA11	406.4	11.0	3251.	244.5	11.0
XXA12	406.4	8.0	3251.	244.5	8.0

6.1.3 Finite element analyses

The general characteristics of the FE analyses are summarized in chapters 2 and 3. The specific details of the FE analyses for multiplanar XX-joints are as follows :

FE characteristics :
- the nominal dimensions of the joints, which are summarized in Table 6.2, are used to model the joints.

61

- one eighth of each joint has been modelled.
- eight noded thick shell elements are used to model the joints.
- the number of elements used to model the joints is about 420. The FE mesh and the boundary conditions used for the XX-joints with $\beta = 0.60$, are shown in Fig. 3.1.
- no additional boundary conditions were needed to prevent rigid body movements.
- for the cases with load ratios of 0.0 and 1.0, the loads have been applied at each brace tip by displacement control. For the other load ratios, loads have been applied using the load control method in order to maintain a constant load ratio between the loads on the in-plane and the out-of-plane brace.
- the loads have been applied proportionally for each of the load ratios considered.
- the geometry of the weld has been modelled in accordance with method 2 as described in section 4.1.2.
- the material properties used for all tubular members are shown in Fig. 4.3 (S355). The Von Mises yield criterion and isotropic strain hardening have been used.

6.1.4 Numerical results

For each of the XX-joints considered, the load-displacement curves are separately given in Fig. 6.3. The non-dimensionalized axial load on the in-plane brace $F_1/f_{y,0}.t_0^2$ has been plotted against the non-dimensionalized displacement of the crown point of the in-plane brace. Yura's deformation limit has been presented for the joints where no maximum in load has been observed before Yura's deformation limit.

The (non-dimensionalized) static strength values are given in Table 6.3. In Fig. 6.8, the non-dimensionalized ultimate loads are presented in interaction contours for each group of XX-joints with the same β value. The numerically determined data points are reflected with regard to the line $F_1 = F_2$. For axially loaded multiplanar XX-joints, this is allowed due to symmetry in loading and geometry. The tension side of the interaction contour has not been determined since for joints loaded by tension, cracks occur in the experiments, which can not be simulated with the present numerical models.

For certain combinations of the parameters β, 2γ and load ratios J (i.e. low 2γ values in combination with high β values and J ratios between 0.6 and 1.0), it appears that the load on the in-plane brace exceeds the theoretical value of the punching shear capacity based on the chord yield stress $f_{y,0}$ according to :

$$V_{p.s.} = \pi.d_1.t_0.\frac{f_{y,0}}{\sqrt{3}} \qquad (6.1)$$

In practice, the "real" punching shear capacity becomes larger than $V_{p.s.}$ due to strain hardening. However, in the numerical analyses the exact punching shear strength cannot be determined since it is not possible to model the joint behaviour when cracks occur. The following conservative assumption is made for the ultimate punching shear capacity. Since for the steel grades commonly used, the ratio $f_{u,0}/f_{y,0}$ is larger than 1.2, the ultimate

Table 6.3 : Numerical results of the axially loaded uniplanar X- and multiplanar XX-joints.

| joint | Uniplanar X-joints | | Multiplanar XX-joints | | | | | | | |
| | | | J = -0.60 | | J = 0.0 | | J = 0.60 | | J = 1.0 | |
	$F_{1,u}$ kN	$\dfrac{F_{1,u}}{f_{y,0}\cdot t_0^2}$	$F_{1,u}$ kN	$\dfrac{F_{1,u}}{f_{y,0}\cdot t_0^2}$	$F_{1,u}$ kN	$\dfrac{F_{1,u}}{f_{y,0}\cdot t_0^2}$	$F_{1,u}$ kN	$\dfrac{F_{1,u}}{f_{y,0}\cdot t_0^2}$	$F_{1,u}$ kN	$\dfrac{F_{1,u}}{f_{y,0}\cdot t_0^2}$
XXA1	1669. *	6.00 *	1294. *	4.65 *	1670. *	6.00 *			1883. *	6.77 *
XXA2	589.	6.48	471. *	5.19 *	589.	6.48			632.	6.96
XXA3	289.	6.74	226. *	5.27 *	289.	6.73			317.	7.38
XXA4	153.	6.74	114. *	5.03 *	153.	6.75			174.	7.66
XXA5	2414.	8.68	1846.	6.63	2468.	8.87			**	**
XXA6	912.	10.04	680.	7.49	911.	10.02			1221.	13.44
XXA7	457.	10.63	342.	7.95	454.	10.57			600.	13.98
XXA8	247.	10.88	188.	8.26	246.	10.82			322.	14.19
XXA9	3215.	11.55	3008. *	10.81 *	3962.	14.24	**	**	**	**
XXA10	1195.	13.15	1083. *	11.91 *	1401.	15.41	2088.	22.97	2977.	32.76
XXA11	598.	13.93	526. *	12.25 *	679.	15.80	1036.	24.12	1496.	34.83
XXA12	326.	14.35	283. *	12.47 *	362.	15.92	546.	24.05	828.	36.43

*   : strength at Yura's deformation limit

** : omitted from the analyses since the ultimate capacity exceeds 1.2 times the theoretical punching shear capacity based on $f_{y,0}$
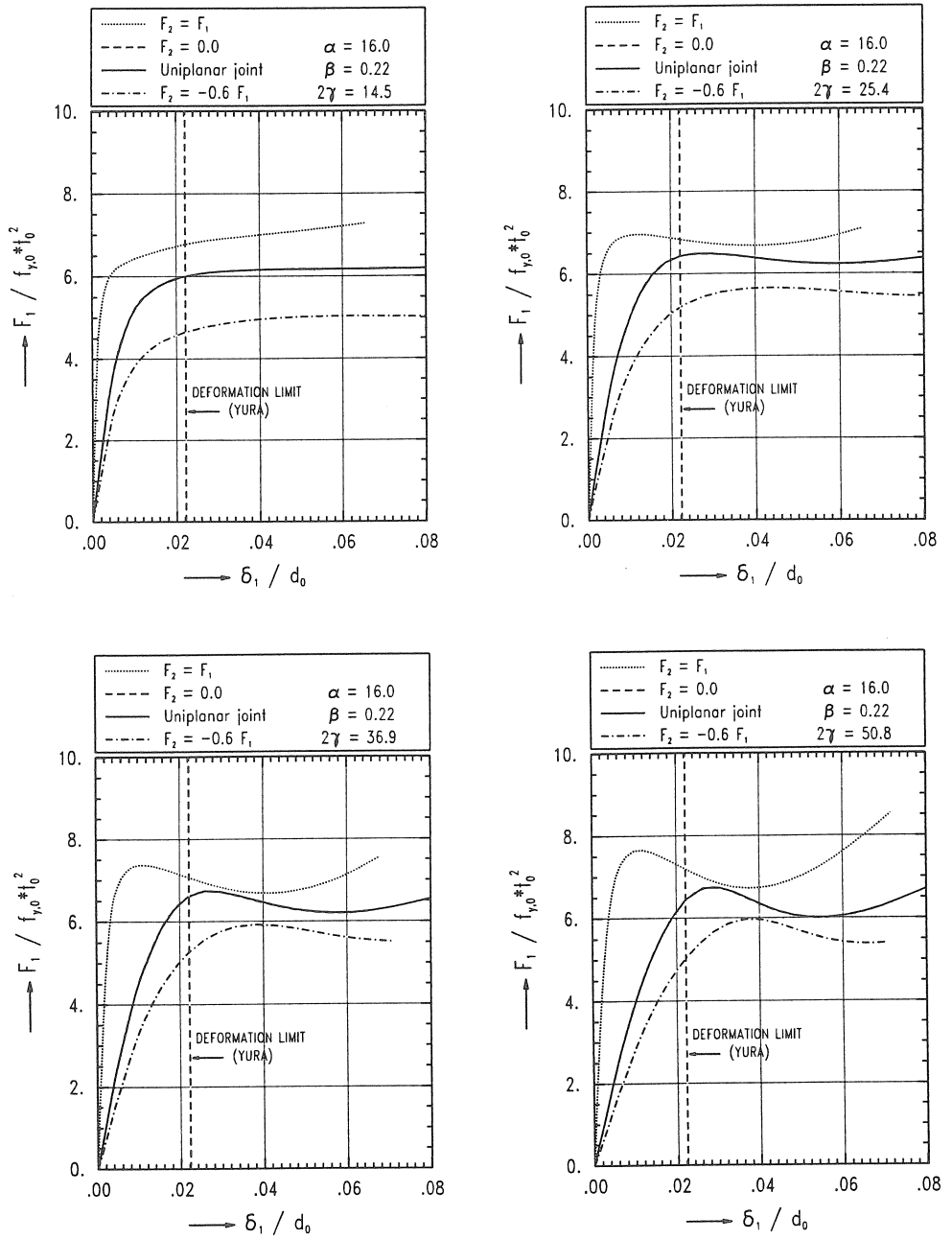
63

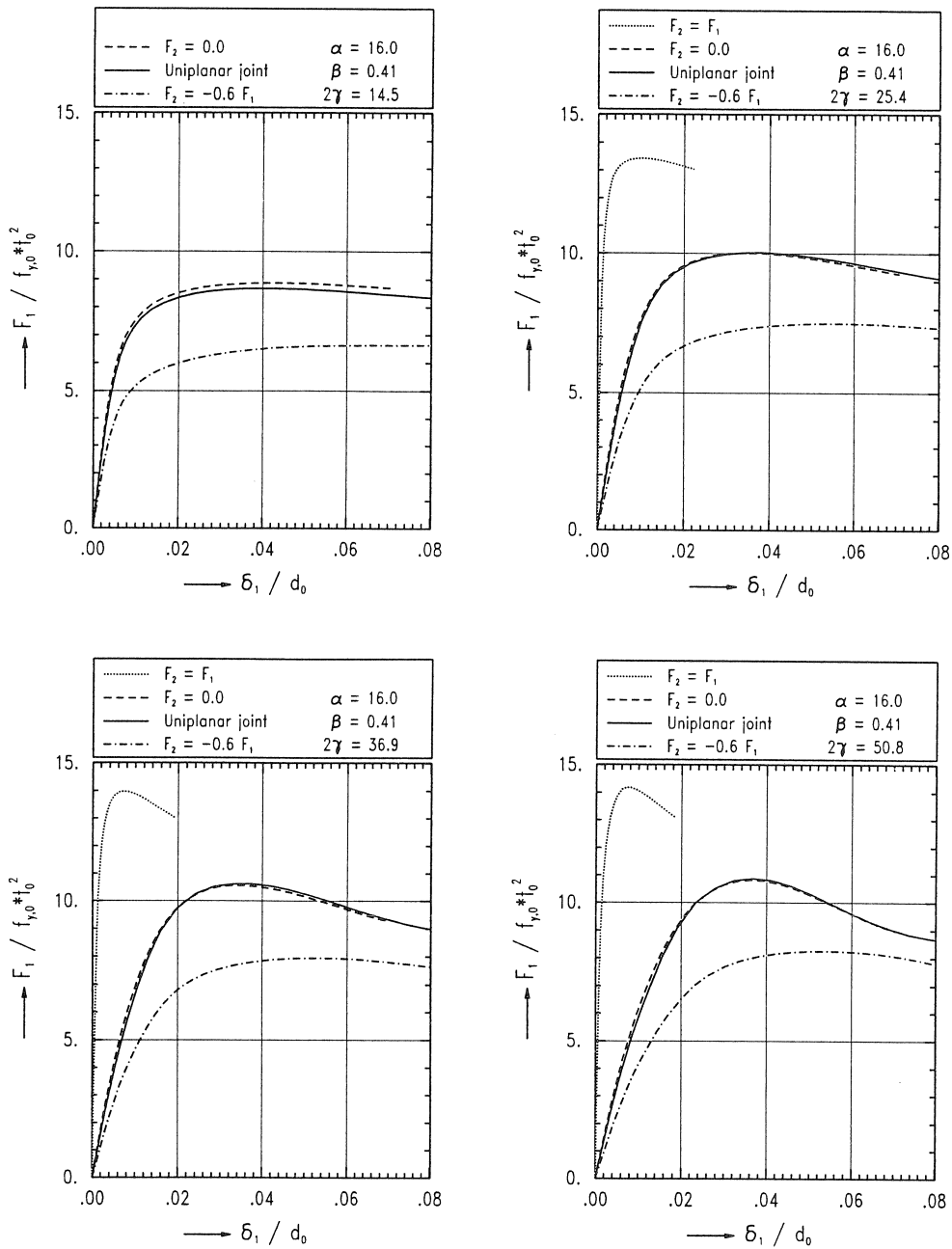Fig. 6.3 : Numerical load-displacement curves of axially loaded multiplanar XX-joints.

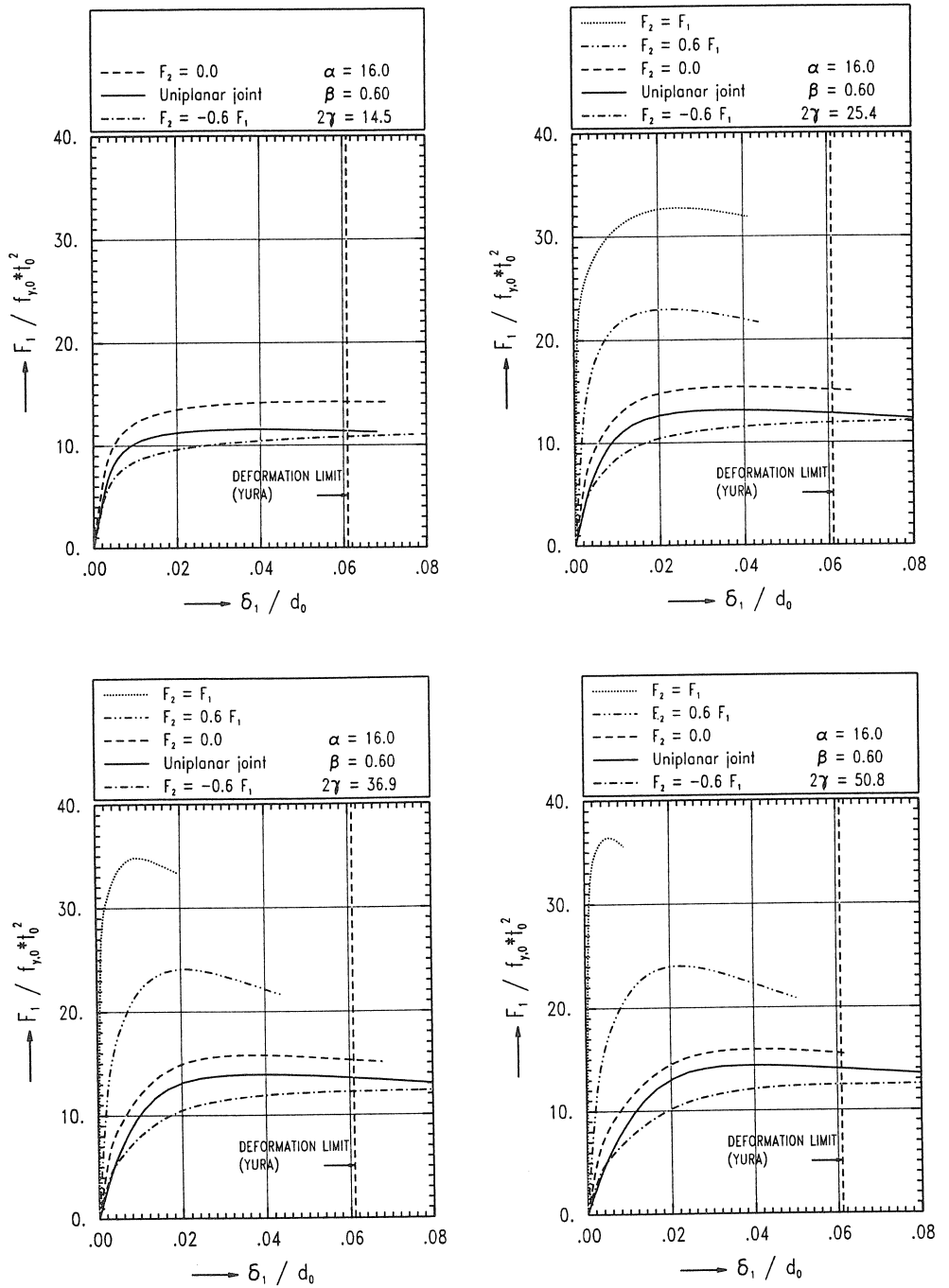Fig. 6.3 : Numerical load-displacement curves of axially loaded multiplanar XX-joints (continued).

Fig. 6.3 : Numerical load-displacement curves of axially loaded multiplanar XX-joints (continued).

punching shear capacity is set to 1.2 $V_{p.s.}$. This implies that the allowable punching shear capacity lies between the value obtained with Eq. 6.1 (based on $f_{y,0}$) and the value of Eq. 6.1 with $f_{u,0}$ instead of $f_{y,0}$. Numerical simulations which result in (ultimate) capacities larger than the ultimate punching shear capacity, are not incorporated in the load-deformation curves and are excluded from further analyses.

From the load-deformation diagrams in Fig. 6.3, the interaction contours in Fig. 6.8 and the numerical ultimate strengths summarized in Table 6.3, the following observations can be made.

The load-displacement behaviour of the joints with J = 0.0 and the behaviour of the corresponding uniplanar joints are almost equal for the joints with $\beta \leq 0.41$. For larger β values, the multiplanar joints with J = 0.0 behave somewhat stiffer and have ultimate capacities which are larger than the corresponding uniplanar joints.

In agreement with the behaviour found for axially loaded uniplanar X-joints, it appears that, for each group of joints with the same β value and the same J ratio, an increasing value of 2γ results in an increasing non-dimensionalized ultimate strength.

For all multiplanar XX-joints it is observed that, in case J varies from -1.0 to 1.0, an increasing value of the load ratio J results in an increasing (non-dimensional) ultimate load. This effect is most pronounced for the joints with $\beta = 0.60$.

For the group of XX-joints with equally loaded braces (J = 1.0) and β values of 0.41 and 0.60, the deformation capacity decreases very quickly for increasing values of 2γ. For the other joints, the deformation capacity is large.

6.1.5 Analytical approach for axially loaded multiplanar XX-joints : ring model

In this section, formulae are derived which describe the analytical strength of axially loaded multiplanar XX-joints under different load ratios. Yield contours are presented in order to show the influence of the load ratio J.

In contradiction to uniplanar X-joints, several failure modes (= yield mechanisms) can be distinguished for multiplanar XX-joints depending on the load ratio J, β and 2γ. In Fig. 6.4, an example of the different yield contours, including the transition between the contours is given for a multiplanar XX-joint with $\beta_1 = \beta_2 = 0.41$ and $2\gamma = 14.5$. Two failure mechanisms and the exact yield contour can be observed. In the following sections, each of the three parts of the yield contour is discussed in detail.

6.1.5.1 Ring model approach for multiplanar XX-joints - mechanism I

The ring model which describes failure mechanism I, is shown in Fig. 6.5 (only one quarter of the chord cross section has been modelled). Mechanism I is characterized by the

67
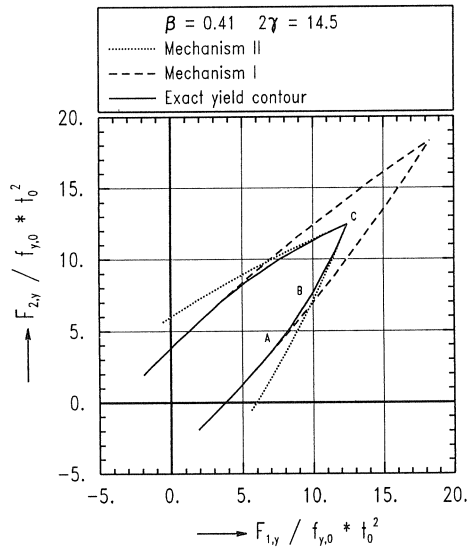
Fig. 6.4 : Example of an analytically determined yield contour for an axially loaded multiplanar XX-joint with $\beta_1 = \beta_2 = 0.41$ and $2\gamma = 14.5$.
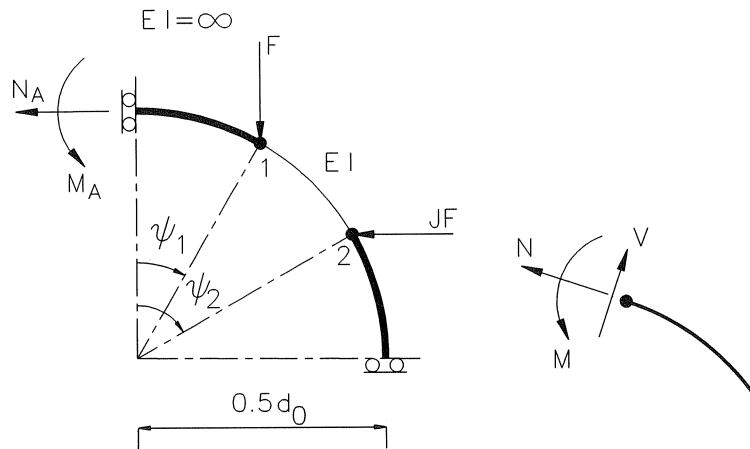
Fig. 6.5 : Analytical "ring model" approach for axially loaded multiplanar XX-joints - mechanism I.

development of two yield hinges, while the signs of the bending moments in the two yield hinges are opposite:
- point 1 : the saddle point of the in-plane brace ($\psi_1 = \arcsin \beta_1$)
- point 2 : the saddle point of the out-of-plane brace ($\psi_2 = \arccos \beta_2$)

68

The axial force on the in-plane brace (= F_1) is represented by the force F. The load on the out-of-plane brace (= F_2) has been set to JF.

Although the simplest derivation of the ring model strength formulae can be obtained by incorporating bending moments only (see section 5.1.5), in this section, the influences due to the axial and shear forces are included.

The following expressions hold for the bending moments in the assumed yield hinges 1 and 2, with N_A = -JF :

$$-M(\psi_1) = M_A - JF\frac{d_0}{2}(1-\cos\psi_1) \tag{6.2}$$

$$+M(\psi_2) = M_A - JF\frac{d_0}{2}(1-\cos\psi_2) + F\frac{d_0}{2}(\sin\psi_2 - \sin\psi_1) \tag{6.3}$$

In the assumed yield hinges, the axial forces are given by :

$$N(\psi_1) = -JF\cos\psi_1 - F\sin\psi_1 \tag{6.4}$$

$$N(\psi_2) = -JF\cos\psi_2 - F\sin\psi_2 \tag{6.5}$$

In the assumed yield hinges, the following expressions for the shear forces can be derived :

$$V(\psi_1) = -JF\sin\psi_1 + F\cos\psi_1 \tag{6.6}$$

$$V(\psi_2) = -JF\sin\psi_2 + F\cos\psi_2 \tag{6.7}$$

The interaction formula between axial force, shear force and bending moment, based on the Von Mises yield criterion, for a rectangular cross-section according to the plasticity theory is approximated by Eq. 6.8 (see also section 5.1.5).

$$\frac{M}{M_p} + \left[\frac{N}{N_p}\right]^2 + \left[\frac{V}{V_p}\right]^2 = 1.0 \tag{6.8}$$

Substituting Eqs. 6.2 to 6.7 in Eq. 6.8 for each of the two yield hinges and solving the set of two equations, results in the exact solution of the unknowns M_A and the analytical yield strengths $F_{1,y}$ (= 2F due to symmetry) of axially loaded multiplanar XX-joints.

69

$$\frac{F_{1,y}}{f_{y,0} \cdot t_0^2 \cdot (\frac{B_e}{d_0})} = \frac{4}{f(\beta_1,\beta_2,J) + \sqrt{f(\beta_1,\beta_2,J)^2 + \frac{g(\beta_1,\beta_2,J)}{2\gamma^2}}} \tag{6.9}$$

with :

$$f(\beta_1,\beta_2,J) = \sqrt{(1-\beta_2^2)} - \beta_1 + J(\beta_2 - \sqrt{1-\beta_1^2}) \tag{6.10}$$

$$g(\beta_1,\beta_2,J) = (1+3J^2)(\beta_1^2+1-\beta_2^2) + (3+J^2)(1-\beta_1^2+\beta_2^2)$$
$$- 4J(\beta_1\sqrt{1-\beta_1^2} + \beta_2\sqrt{1-\beta_2^2}) \tag{6.11}$$

In Fig. 6.4, the dashed line represents the yield contour for failure mechanism I for a multiplanar XX-joint with $\beta_1 = \beta_2 = 0.41$ and $2\gamma = 14.5$.

6.1.5.2 Ring model approach for multiplanar XX-joints - mechanism II

One quarter of the ring model which describes failure mechanism II, is shown in Fig. 6.6. Similar to mechanism I, mechanism II is characterized by the development of two yield hinges with opposite signs of the bending moments :
- point 1 : in the saddle point of the in-plane brace ($\psi_1 = \arcsin \beta_1$)
- point 3 : for $\beta_1 = \beta_2$, point 3 lies exactly between the saddle points of the in- and out-of plane brace ($\psi_3 = \pi/4$). The out-of-plane force F_2 still acts in the saddle point of the out-of-plane brace.

The following expressions hold for the bending moments in the assumed yield hinges 1 and 3 ($N_A = -JF$) :

$$-M(\psi_1) = M_A - JF\frac{d_0}{2}(1-\cos\psi_1) \tag{6.12}$$

$$+M(\psi_3) = M_A - JF\frac{d_0}{2}(1-\cos\psi_3) + F\frac{d_0}{2}(\sin\psi_3 - \sin\psi_1) \tag{6.13}$$

In the assumed yield hinges, the axial forces are given by :

$$N(\psi_1) = -JF\cos\psi_1 - F\sin\psi_1 \tag{6.14}$$

$$N(\psi_3) = -JF\cos\psi_3 - F\sin\psi_3 \tag{6.15}$$

In the assumed yield hinges, the following expressions for the shear forces can be derived.

70
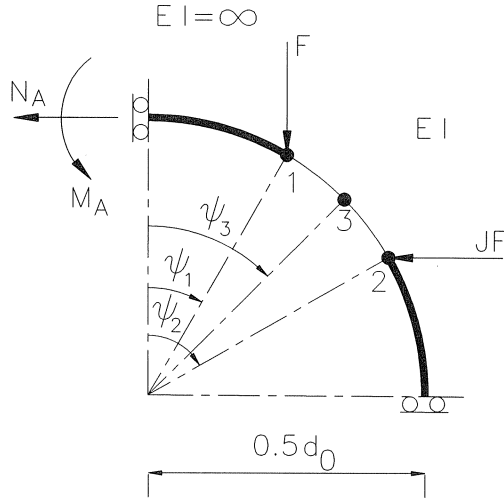
Fig. 6.6 : Analytical "ring model" approach for axially loaded multiplanar XX-joints
- mechanism II.

$$V(\psi_1) = -JF\sin\psi_1 + F\cos\psi_1 \tag{6.16}$$

$$V(\psi_3) = -JF\sin\psi_3 + F\cos\psi_3 \tag{6.17}$$

Substituting Eqs. 6.12 to 6.17 in Eq. 6.8 for each of the two yield hinges, followed by solving this set of equations, results in the exact solution of the unknowns M_A and the analytical strength $F_{1,y}$ for failure mode II.

$$\frac{F_{1,y}}{f_{y,0} \cdot t_0^2 \cdot (\frac{B_e}{d_0})} = \frac{4}{f(\beta_1,\beta_2,J) + \sqrt{f(\beta_1,\beta_2,J)^2 + \frac{g(\beta_1,\beta_2,J)}{2\gamma^2}}} \tag{6.18}$$

with :

$$f(\beta_1,\beta_2,J) = (\frac{1}{2}\sqrt{2} - \beta_1) + J(\frac{1}{2}\sqrt{2} - \sqrt{1-\beta_1^2}) \tag{6.19}$$

$$g(\beta_1,\beta_2,J) = (1+3J^2)(\beta_1^2 + \frac{1}{2}) + (3+J^2)(1\frac{1}{2} - \beta_1^2) - 4J(\beta_1\sqrt{1-\beta_1^2} + \frac{1}{2}) \tag{6.20}$$

In Fig. 6.4, the dotted line represents the yield contour for failure mode II for a multiplanar XX-joint with $\beta_1 = \beta_2 = 0.41$, $2\gamma = 14.5$.

71

Special attention should be given to the solution for J = 1. This point is situated at the diagonal $F_1 = F_2$ of the interaction contour. For this load ratio, three yield hinges are observed in the ring model. Yield hinges occur in point 1 (the saddle point of the in-plane brace) and in point 3 (exactly between yield hinges 1 and 2). However, also in point 2 a yield hinges appears. In contradiction to mechanism I, the signs of the bending moment in the yield hinges 1 and 2 are equal for this case. The sign of the bending moment in yield hinge 3 is still opposite to the bending moments in the yield hinges 1 and 2.

6.1.5.3 Ring model approach for multiplanar XX-joints - exact yield contour

In Fig. 6.4, the solid line represents the exact yield contour for the multiplanar XX-joint with $\beta_1 = \beta_2 = 0.41$ and $2\gamma = 14.5$. Although only one set of β and 2γ values is considered in this example, the following observations can be made for increasing J values, which are also valid for XX-joints with different β and 2γ values :

- for negative and small positive J ratios, the exact interaction contour is equal to the contour for mechanism I and represented by Eqs. 6.9 to 6.11.

- for increasing J ratios, the following transition takes place from mechanism I to II. At the moment, the exact solution leaves the contour for failure mode I (point A in the contour), the yield hinge in location 2 leaves location 2, and shifts in the direction of location 3 whereas the absolute value of the bending moment in location 2 decreases (point B in the yield contour). A further increase in J results in a further shift of the yield hinge towards location 3. As soon as J is equal to 1, the yield hinge reaches location 3 (point C in the yield contour). At the same time, the absolute value of the bending moment in location 2 again reaches its maximum, but is opposite from sign.

The analytical derivation of this transition part between mechanisms I and II can be described as follows :

Replacing all β_2 terms in Eq. 6.9 with $\beta_3 = \cos \psi_3$ results in an expression which describes the analytical strength of multiplanar XX-joints with a yield hinge located in point 3 with ψ_3 ($\psi_3 \leq \psi_2$) while the force still acts in point 2. Subsequently, this equation is minimized with respect to β_3 in order to determine the location of yield hinge 3 according to :

$$\frac{d F_{y,1}}{d \beta_3} = 0 \qquad (6.21)$$

Solving this equation leads to the following relationship :

$$J = \frac{\beta_3}{\sqrt{1 - \beta_3^2}} \qquad (6.22)$$

which results in the following location of yield hinge 3 :

72

$$\psi_3 = \arccos \beta_3 \qquad \text{for } J \leq \frac{\beta_3}{\sqrt{1-\beta_3^2}}$$

$$\psi_3 = \arccos\left(\frac{J}{\sqrt{1+J^2}}\right) \qquad \text{for } J \geq \frac{\beta_3}{\sqrt{1-\beta_3^2}} \tag{6.23}$$

Substituting the value of $\beta_3 = \cos \psi_3$ in Eq. 6.9 for β_2, leads to the strengths values $F_{1,y}$ for the transition part of the yield contour.

- for $J = 1$, the exact interaction contour is equal to the interaction contour for mechanism II and given by Eq. 6.18. However, this is only one point (on the diagonal) of the interaction contour for failure mode II.
- the locations where the dashed lines cross the dotted lines do not have any physical meaning.

6.1.6 Basic ultimate strength formulae for axially loaded multiplanar XX-joints

The ultimate strength of axially loaded multiplanar XX-joints is described by two relationships. First, a strength equation is established for the multiplanar XX-joints with $J = 0.0$, i.e. the joints with unloaded out-of-plane braces. Secondly, the influence of the load ratio J on the strength of multiplanar XX-joints is included by a function $f(\beta, J)$.

6.1.6.1 Basic ultimate strength formula for the multiplanar XX-joints with $J = 0.0$

Similar to the strategy for uniplanar X-joints, one overall expression which includes the B_e/d_0 ratio, is proposed as a basis for the ultimate strength equation for the XX-joints with $J = 0.0$.

After substitution of $J = 0.0$ and $\beta = \beta_1 = \beta_2$ in the analytical "ring model" solution 6.9, a regression constant R_4 is added to the β terms to account for the "real" positions of the forces, which is in agreement with the strategy for axially loaded uniplanar X-joints.
As a result, the following expression is proposed as a basis for the ultimate strength equation of axially loaded multiplanar XX-joints with $J = 0.0$.

$$\frac{F_{1,u}}{f_{y,0} \cdot t_0^2} = \frac{R_1 \gamma^{R_2 \beta - R_3 \beta^2}}{\sqrt{1-(R_4\beta)^2} - R_4\beta + \sqrt{(\sqrt{1-(R_4\beta)^2} - R_4\beta)^2 + \frac{2}{\gamma^2}}} \tag{6.24}$$

The regression constants R_i (i = 1...4) have to be determined by non-linear regression

analyses on the FE results. All FE results of the axially loaded multiplanar XX-joints with $J = 0.0$, are used to calibrate the unknowns R_i (i = 1...4) of Eq. 6.24.

The final results of the regression analyses are presented in Eq. 6.25 and Table 6.4 (first row).

$$\frac{F_{1,u}}{f_{y,0} \cdot t_0^2} = \frac{8.0 \; \gamma^{0.7\beta - \beta^2}}{\sqrt{1 - (0.9\beta)^2} - 0.9\beta + \sqrt{(\sqrt{1 - (0.9\beta)^2} - 0.9\beta)^2 + \frac{2}{\gamma^2}}} \tag{6.25}$$

Eq. 6.25 as well as the FE data points are shown in Fig. 6.7.

As can be observed from Table 6.4 and Fig. 6.7, Eq. 6.25 describes the strength of the multiplanar XX-joints with $J = 0.0$ very well.
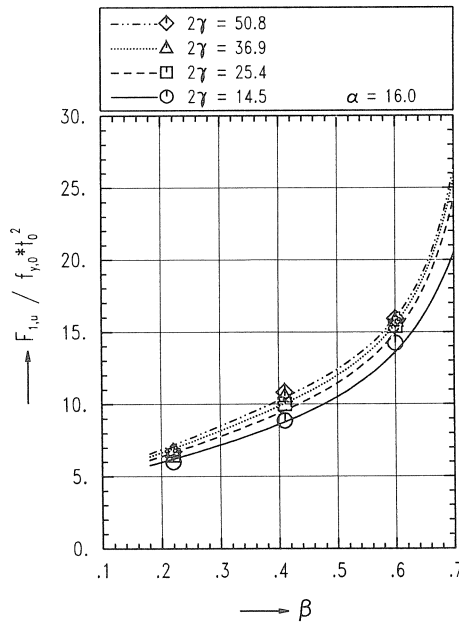
Fig. 6.7 : Ultimate capacity of axially loaded multiplanar XX-joints with $J = 0.0$.

Table 6.4 : Results of the regression analyses of axially loaded multiplanar XX-joints.

	No. of data points	R^2 (%)	Mean	CoV.
$J = 0.0$ (Eq. 6.25)	12	99.03	1.007	3.73×10^{-2}
$-1.0 \leq J \leq 1.0$ (Eq. 6.27)	37	99.53	1.006	2.48×10^{-2}
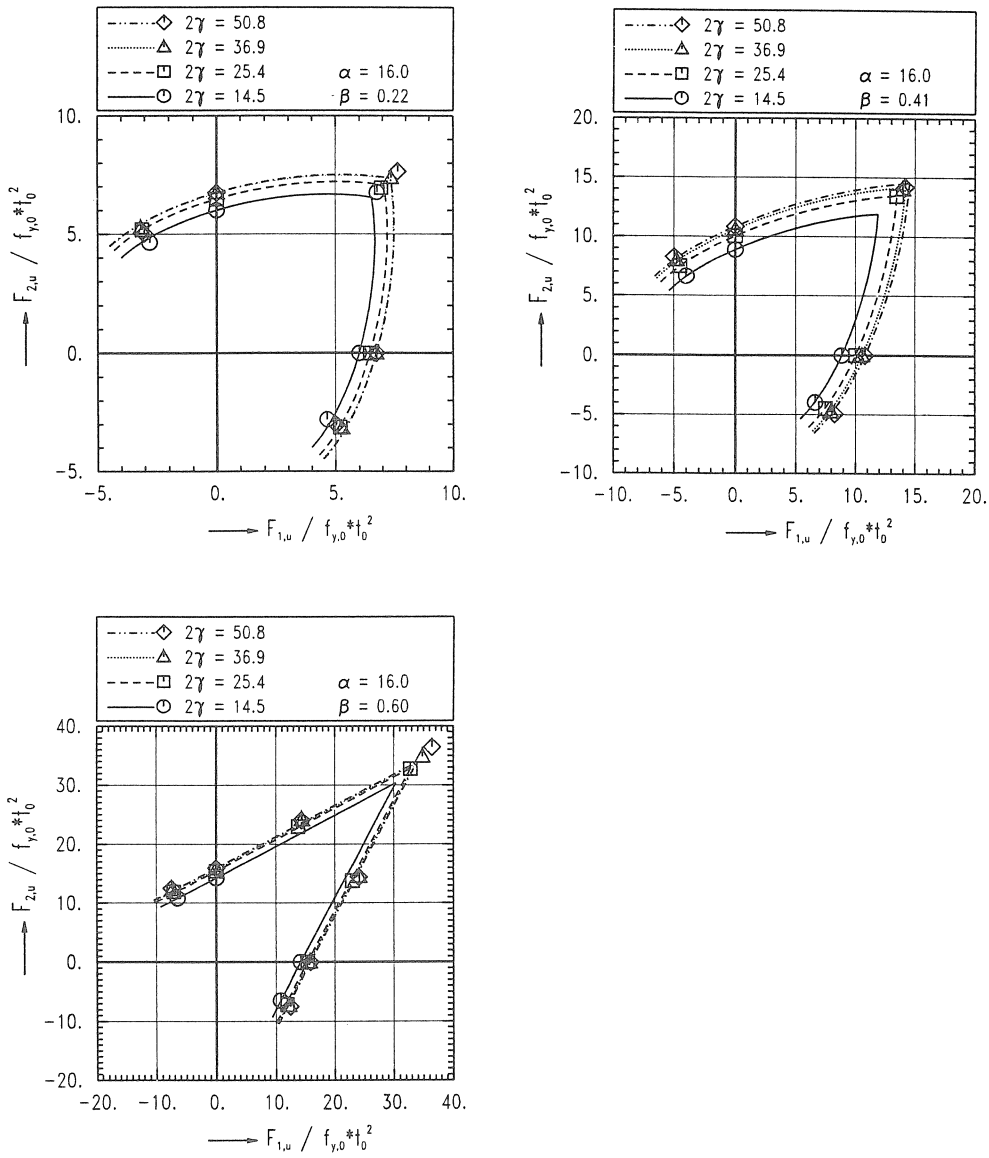
Fig. 6.8 : Ultimate capacity contours of axially loaded multiplanar XX-joints.

6.1.6.2 Basic ultimate strength formula for the multiplanar XX-joints with variable load ratios

As shown in the analytical strength equations derived in the "ring model" approach, it appears that the interaction effects due to different load ratios are described by complicated

75

expressions which include linear and quadratic terms of β and the load ratio J (Eqs. 6.9 to 6.11). Due to the complexity of these equations, the following expression which includes linear and quadratic terms of β and J, is used as a basis to describe the load interaction effects, whereas $F_{1,u}(J = 0.0)$ describes the ultimate capacity of the multiplanar XX-joints with J = 0.0 (Eq. 6.25) :

$$F_{1,u}(J) = \frac{F_{1,u}(J=0.0)}{1 - ((R_1 + R_2\beta + R_3\beta^2)J + (R_4 + R_5\beta + R_6\beta^2)J^2)} \tag{6.26}$$

Based on regression analyses which includes the FE data points summarized in Table 6.3, the following equations are obtained for the ultimate strengths of axially loaded multiplanar XX-joints :

$$F_{1,u}(J) = \frac{F_{1,u}(J=0.0)}{1 - (1.6\beta - 1.2\beta^2)J + (1.5\beta - 2.5\beta^2)J^2} \tag{6.27}$$

$$F_{2,u} = JF_{1,u}$$

The statistical values which result from the regression analyses are summarized in Table 6.4 (second row).

The FE data points and the load contours (described by Eq. 6.27) are presented in Fig. 6.8, for each group of XX-joints with the same β value.

6.2 *Axially loaded multiplanar XX-joints with variable chord lengths*

### 6.2.1 Introduction

As mentioned in section 1.4.2, many uncertainties exist about the influence of the chord length on the strength of tubular joints. In section 5.2, the chord length influence has been determined for axially loaded uniplanar X-joints.

For multiplanar XX-joints, an additional parameter i.e. the load ratio J between the in-plane and out-of-plane force has to be taken into account. In order to investigate the influence of the chord length on the static strength of axially loaded multiplanar XX-joints for various load ratios, non-linear finite element analyses have been carried out.

6.2.2 Research programme

The research programme is summarized in Table 6.5. The configuration of axially loaded multiplanar XX-joints is shown in Figs. 6.1 and 6.2. The study consists of a total of 44

76

finite element analyses on multiplanar tubular XX-joints subjected to compressive brace loading. Four α values (α = 3.0, 6.0, 12.0 and 16.0) have been considered for three β values (β = 0.22, 0.41, 0.60). The value of d_0 is equal to 406.4 mm. Furthermore, for β = 0.60, two values of 2γ have been analyzed to determine if the 2γ value has influence on the static behaviour for varying chord lengths (for 2γ = 50.8 only one load ratio J has been considered). The nominal dimensions of the joints are given in Table 6.6.

Table 6.5 : Research programme of axially loaded multiplanar XX-joints with variable chord lengths.

		α			
		3.0	6.0	12.0	16.0
β = 0.22	2γ = 25.4	XXAS1	XXAS2	XXAS3	XXAS4
β = 0.41	2γ = 25.4	XXAS5	XXAS6	XXAS7	XXAS8
β = 0.60	2γ = 25.4	XXAS9	XXAS10	XXAS11	XXAS12
	2γ = 50.8	XXAS13	XXAS14	XXAS15	XXAS16

For all joints, three load ratios J have been analyzed (-0.6, 0.0 1.0). For the joints with β = 0.60, an additional load ratio has been considered (0.6).
The steel grade for all tubular members is S355 with f_y = 355 N/mm^2 and f_u = 510 N/mm^2.

6.2.3 Finite element analyses

The general characteristics of the FE analyses are summarized in chapters 2 and 3. The specific details of the FE analyses for multiplanar XX-joints are as follows :

FE characteristics :
- the nominal dimensions of the joints, which are summarized in Table 6.6, are used to model the joints.
- one eighth of each joint has been modelled.
- eight noded thick shell elements are used to model the joints.
- the number of elements used to model the joints, depends on the α value. For α = 16.0, the number of elements is about 420. The FE mesh and boundary conditions used for axially loaded multiplanar XX-joints with α = 12.0 and β = 0.60 are shown in Fig. 3.1.
- no additional boundary conditions were needed to prevent rigid body movements. No restraints are applied to the chord ends.
- the load has been applied at the brace tip by displacement control for the joints with load ratio J = 0.0 and 1.0. For the other load ratios, loads have been applied using the load controlled method.

- the axial loads have been applied proportionally.
- the geometry of the weld has been modelled in accordance with method 2 as described in section 4.1.2.
- the material properties used for all tubular members are shown in Fig. 4.3 (S355). The Von Mises yield criterion and isotropic strain hardening have been used.

Table 6.6 : Nominal dimensions of the multiplanar XX-joints with variable chord lengths.

| | Nominal dimensions | | | | |
| | chord | | | braces | |
joint	d_0 mm	t_0 mm	l_0 mm	d_1 mm	t_1 mm
XXAS1	406.4	16.0	610.	88.9	10.0
XXAS2	406.4	16.0	1219.	88.9	10.0
XXAS3	406.4	16.0	2438.	88.9	10.0
XXAS4	406.4	16.0	3251.	88.9	10.0
XXAS5	406.4	16.0	610.	165.1	12.5
XXAS6	406.4	16.0	1219.	165.1	12.5
XXAS7	406.4	16.0	2438.	165.1	12.5
XXAS8	406.4	16.0	3251.	165.1	12.5
XXAS9	406.4	16.0	610.	244.5	16.0
XXAS10	406.4	16.0	1219.	244.5	16.0
XXAS11	406.4	16.0	2438.	244.5	16.0
XXAS12	406.4	16.0	3251.	244.5	16.0
XXAS13	406.4	8.0	610.	244.5	8.0
XXAS14	406.4	8.0	1219.	244.5	8.0
XXAS15	406.4	8.0	2438.	244.5	8.0
XXAS16	406.4	8.0	3251.	244.5	8.0

6.2.4 Numerical results

In Fig. 6.9, the load-displacement curves are separately given for each group of XX-joints with the same load ratio J and variable chord length. The non-dimensionalized axial load

$F_1/f_{y,0}.t_0^2$ on the in-plane brace has been plotted against the non-dimensionalized crown point displacement of the in-plane brace.

Table 6.7 : Numerical results of the axially loaded multiplanar XX-joints with variable chord lengths.

joint	Load ratio J							
	-0.60		0.0		0.60		1.0	
	$F_{1,u}$ kN	(1)	$F_{1,u}$ kN	(1)	$F_{1,u}$ kN	(1)	$F_{1,u}$ kN	(1)
XXAS1	249. *	2.74 *	380.	4.18			626.	6.88
XXAS2	426. *	4.69 *	565.	6.22			632.	6.96
XXAS3	458. *	5.04 *	583.	6.41			632.	6.96
XXAS4	471. *	5.19 *	589.	6.48			632.	6.96
XXAS5	371. *	4.08 *	531.	5.85			1204.	13.24
XXAS6	576.	6.33	813.	8.94			1221.	13.43
XXAS7	651.	7.17	883.	9.71			1221.	13.43
XXAS8	680.	7.49	911.	10.02			1221.	13.44
XXAS9	810. *	8.92 *	1055. *	11.61 *	1685.	18.54	2931.	32.25
XXAS10	981. *	10.80 *	1288.	14.17	2005.	22.06	2977.	32.76
XXAS11	1055. *	11.60 *	1369.	15.06	2062.	22.69	2977.	32.76
XXAS12	1083. *	11.91 *	1401.	15.41	2088.	22.97	2977.	32.76
XXAS13			265. *	11.66 *				
XXAS14			327.	14.39				
XXAS15			353.	15.53				
XXAS16			362.	15.92				

Remarks :

(1) : $\dfrac{F_{1,u}}{f_{y,0}.t_0^2}$

*   : strength at Yura's deformation limit
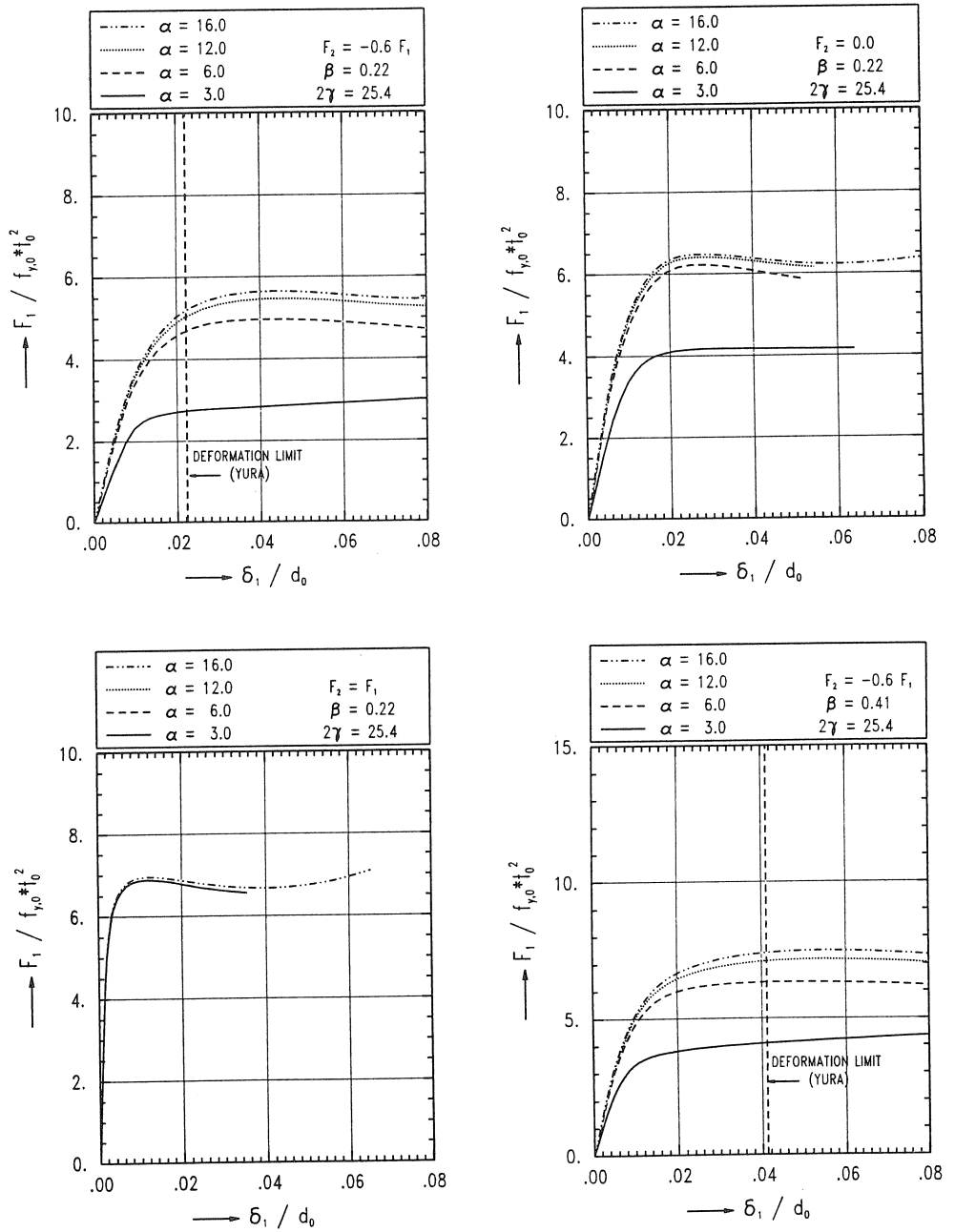
Fig. 6.9 : Numerical load-displacement curves of axially loaded multiplanar XX-joints with variable chord lengths.
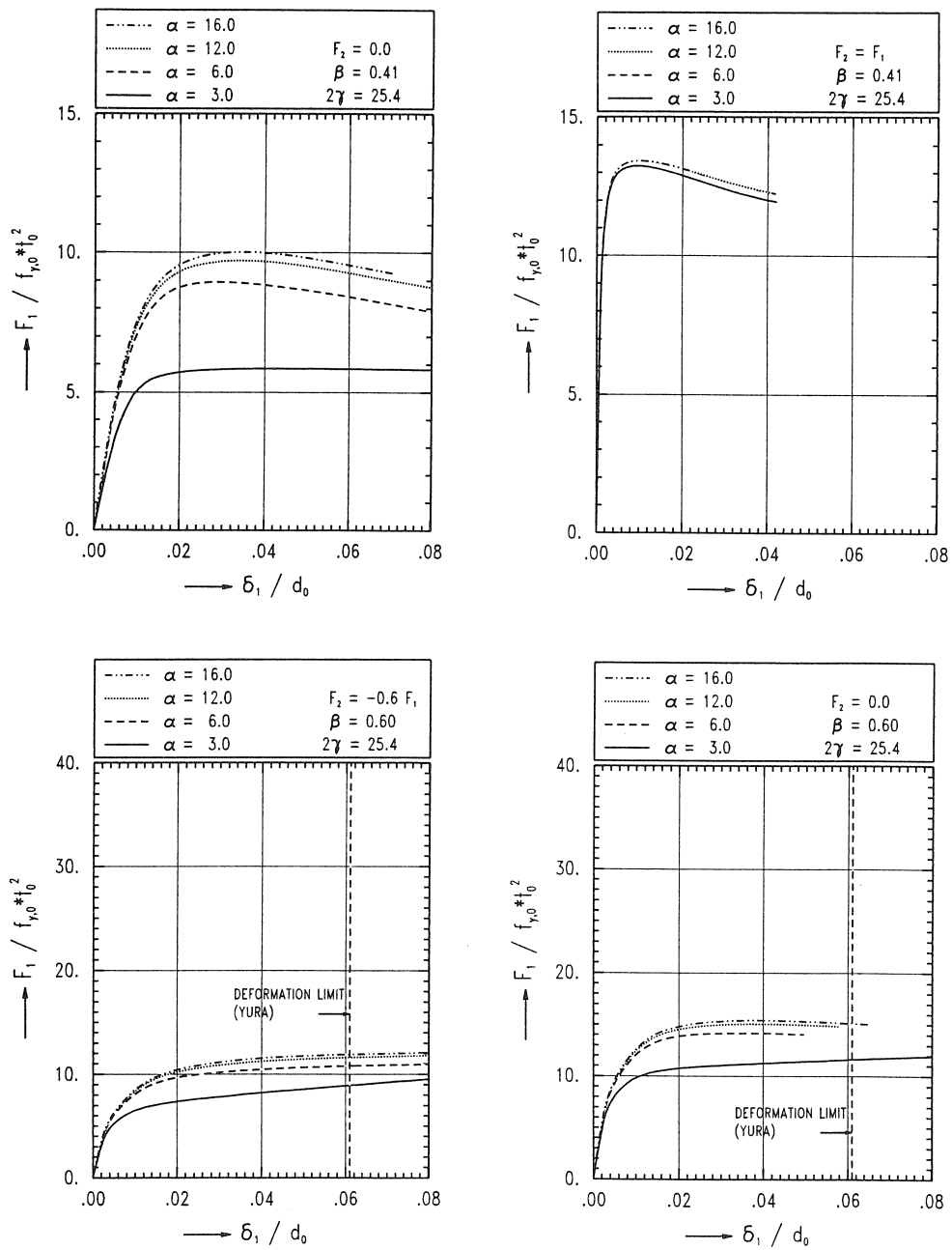
Fig. 6.9 : Numerical load-displacement curves of axially loaded multiplanar XX-joints with variable chord lengths (continued).
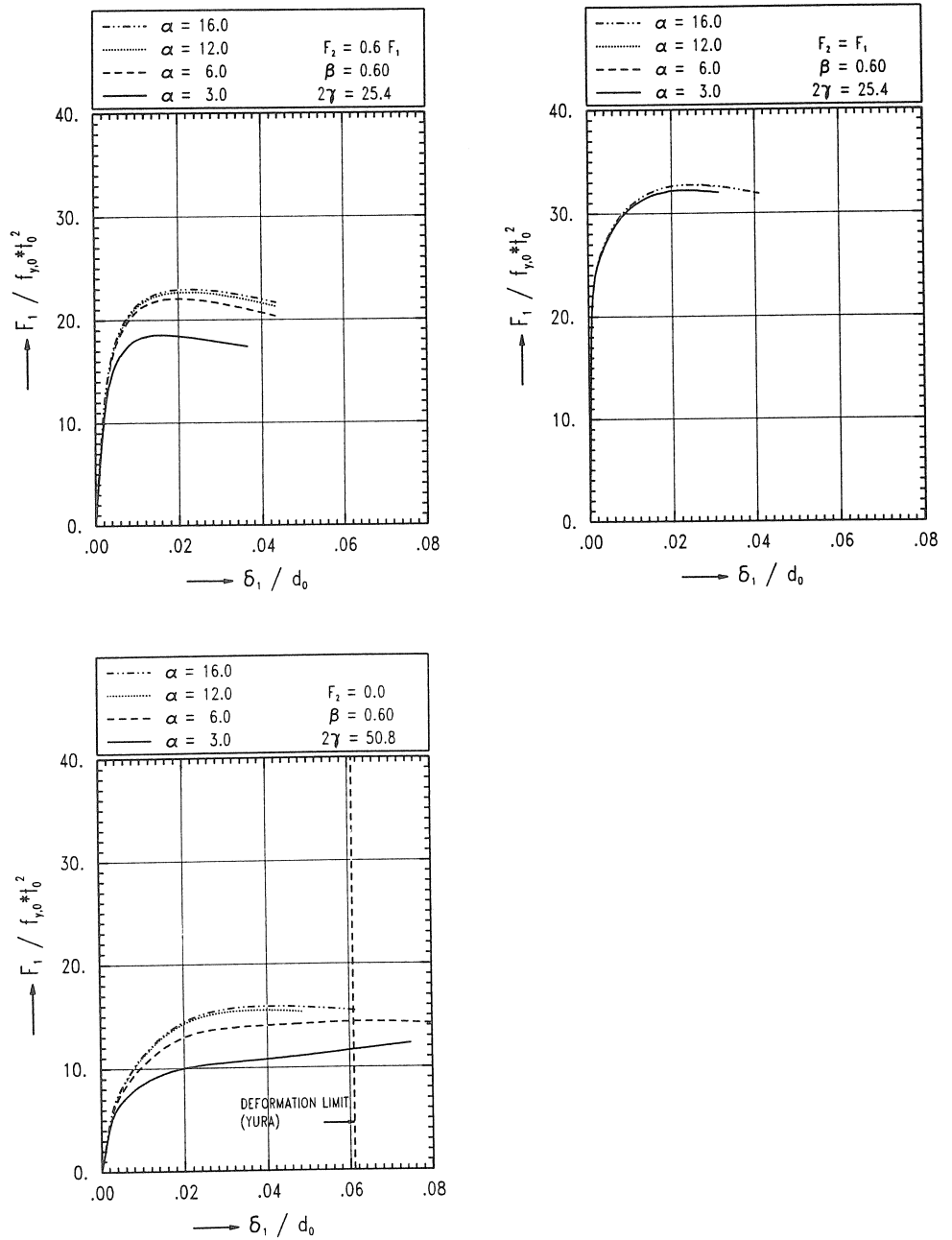
Fig. 6.9 : Numerical load-displacement curves of axially loaded multiplanar XX-joints with variable chord lengths (continued).

82

Yura's deformation limit has been plotted in the figures which consider joints for which no maximum in load has been observed before Yura's deformation limit. The non-dimensionalized static strength values are given in Table 6.7. In Fig. 6.11, for each XX-joint, the non-dimensionalized ultimate loads of the joints with variable chord lengths have been plotted as a function of α for various load ratios.

Considering the load-deformation diagrams in Fig. 6.9 and the ultimate load versus α curves in Fig. 6.11, the following observations can be made.

In agreement with uniplanar X-joints, for all β values it appears that a decreasing value of α results in a decreasing value of the non-dimensionalized ultimate load. This effect is most pronounced for the joints with a load ratio of -0.6, due to the largest chord ovalizing for this load ratio. For the joints with J = 1.0, the chord ovalizing is very small, resulting in a negligible decrease in strength for decreasing chord lengths.
For all joints with load ratios J unequal to 1.0, a significant drop in non-dimensional ultimate load is observed if α becomes smaller than 6.0.

6.2.5 Basic ultimate strength formula for axially loaded multiplanar XX-joints with variable chord lengths

In this section, an expression is derived for the chord length influence on the static strength of axially loaded multiplanar XX-joints. This chord length function is related to the strength of axially loaded multiplanar XX-joints with $\alpha = 16.0$, presented in section 6.1, which means that for joints with $\alpha = 16.0$, the correction factor is 1.0.

In line with the analyses for axially loaded uniplanar X-joints, the strength of each XX-joint has been divided by the chord length parameter α. Subsequently, for each joint, this ratio has been divided by the corresponding ratio of the same XX-joint with $\alpha = 16.0$:

$$g(\alpha, J) = \frac{F_{1,u}(\alpha)/\alpha}{F_{1,u}(\alpha = 16.0)/16.0} = \frac{F_{1,u}(\alpha)}{F_{1,u}(\alpha = 16.0)} \cdot \frac{16.0}{\alpha} \qquad (6.28)$$

in which $F_{1,u}(\alpha = 16.0)$ is the strength equation based on multiplanar XX-joints with $\alpha = 16.0$. The function $F_{1,u}(\alpha)$ is the strength equation which includes the α effects.

The resulting data points are shown in Fig. 6.10. As can be observed from this figure, the load ratio J plays an important role for the smaller α values.

Furthermore, from the two figures shown for the joints with $\beta = 0.6$ (for $2\gamma = 25.4$ and $2\gamma = 50.8$ respectively), it can be seen that the resulting data points for each of the joints with J = 0.0 lie almost at the same position, thus implying that the 2γ value of the joints has no influence on the joint behaviour for variable chord lengths.

The function $g(\alpha, J)$ is determined on the basis of regression analyses. The following expression has been proposed for $g(\alpha, J)$:
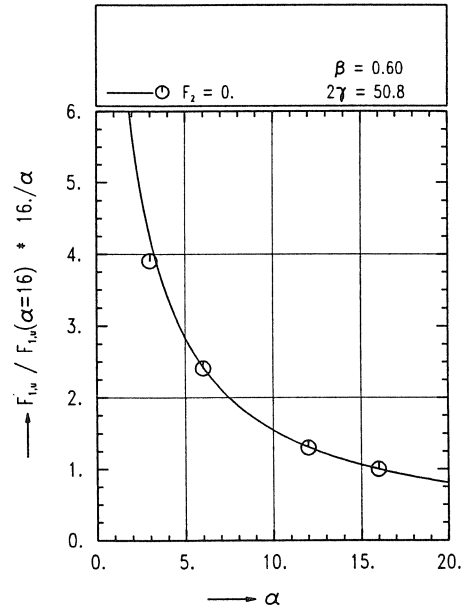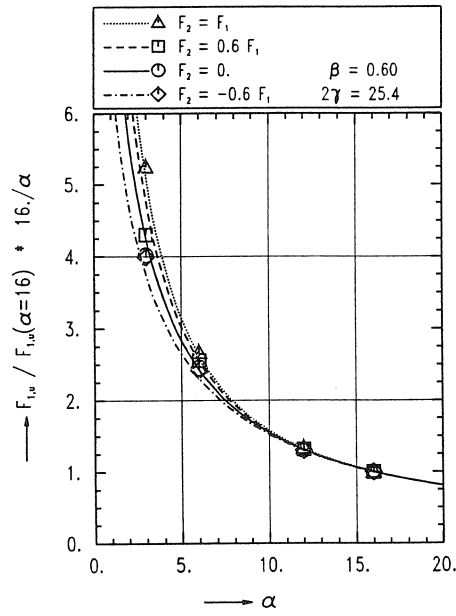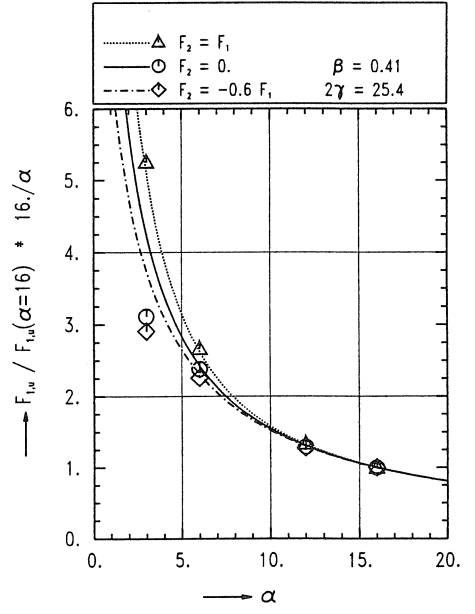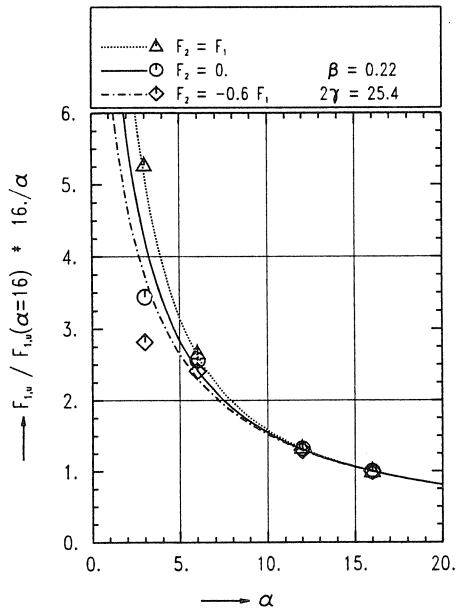
Fig. 6.10 : The function g(α) of axially loaded multiplanar XX-joints.

84

$$g(\alpha, J) = \frac{R_1}{1 + R_2 \alpha} \cdot (1 + R_3 J e^{R_4 \alpha}) \qquad (6.29)$$

The term which includes J, incorporates the decreasing influence of J for increasing α values (see Fig. 6.10).

The regression constants R_i (i = 1...4) are obtained by performing regression analyses of the FE results. Only the multiplanar XX-joints with $\alpha \geq 6.0$ have been included in the regression analyses, since for the joints with $\alpha < 6.0$ a pronounced influence of β is observed which does not occur for the joints with $\alpha \geq 6.0$.

Based on the strengths of these joints, the following values of the regression constants R_i (i = 1...4) and statistical quantities (Table 6.8) have been obtained :

$$g(\alpha, J) = \frac{17.0}{1 + \alpha} \cdot (1 + 0.5 J e^{-0.3\alpha}) \qquad (6.30)$$

In Fig. 6.10, this function $g(\alpha, J)$ is shown for each load ratio J considered.
Combining the results of Eqs. 6.28 and 6.30 gives the final, general expression for the strength of axially loaded multiplanar XX-joints for $\alpha \geq 6.0$:

$$F_{1,u}(\alpha) = f(\alpha, J) \cdot F_{1,u}(\alpha = 16.0) \qquad (6.31)$$

with the chord length function $f(\alpha, J)$ defined as :

$$f(\alpha, J) = g(\alpha, J) \frac{\alpha}{16.0} = \frac{17.0\alpha}{16.0\,(1+\alpha)} \cdot (1 + 0.5 J e^{-0.3\alpha}) \qquad (6.32)$$

For the joints with $\alpha = 16.0$, it is observed that $f(\alpha, J) = 1.0$ (the term with J has become almost 0.0, due to the negative exponent).

The FE data points and the curves representing the proposed strength equation are shown in Fig. 6.11 for each group of XX-joints with the same β value. Although $f(\alpha, J)$ has been determined by including the data points with $\alpha \geq 6.0$ only, the curves have been presented for $\alpha \geq 3.0$, to show the tendencies for smaller α values. It is observed that for the lower α and β values the ultimate capacity equation overestimates the actual strength.

Table 6.8 : Results of the regression analyses of axially loaded multiplanar XX-joints with variable chord lengths (Eq. 6.31).

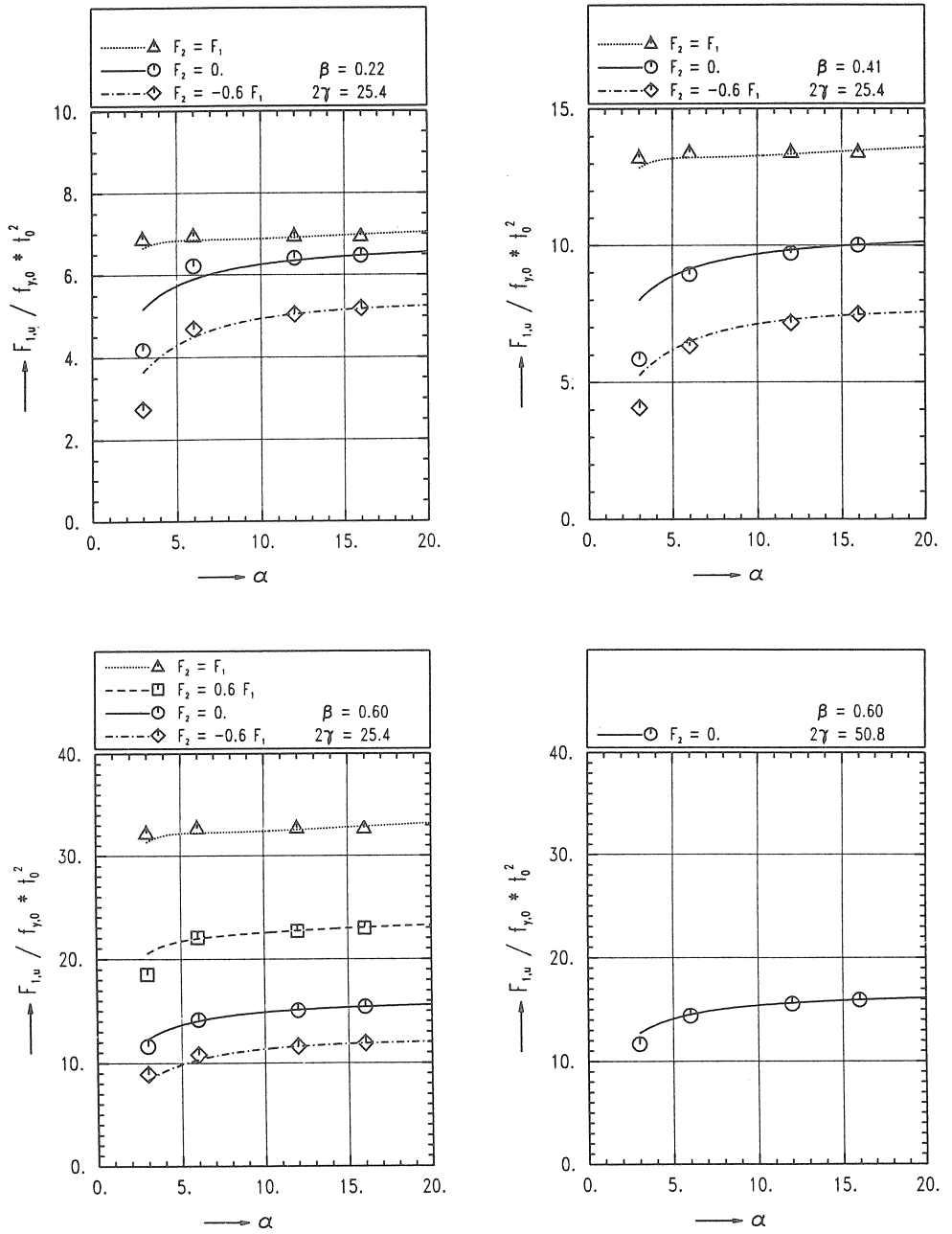| No. of data points	R^2 (%)	Mean	CoV.
33	99.96	1.003	1.54 $\times 10^{-2}$

Fig. 6.11 : Ultimate capacity of axially loaded multiplanar XX-joints with variable chord lengths.

7.   Simplification of the basic strength formulae

The basic ultimate strength derived in the previous sections for the axially loaded uniplanar X- and multiplanar XX-joints may be too complicated to be used for design purposes. Therefore, simplifications of these expressions may be required. Although simplification of the ultimate strength equations is not incorporated in the present research work, the following general remarks are made.

In line with the strategy used to simplify Kurobane's (mean) strength equations for uniplanar joints followed by evaluation to design rules, a term by term analysis can be made i.e. each term of the strength equation is considered separately and simplified to a form resulting in approximately the same value as obtained from the original term. In this way, the original form of the formulae which resulted from analytically derived formulae, remains unchanged. A disadvantage, however, is that the number of included terms, which is considerably for some formulae, does not change either.

A more rigorous way to simplify the strength equations is to consider the influence on the strength of two or more terms and to replace these terms by one simple approximate expression. In this way, the number of terms included in the equations, decreases.

The most rigorous way to come to simplified equations is to consider the general form of the equations. Almost all strength equations derived in the previous sections, consider a quotient, where the denominator only depends on β and γ.

For example, the following equation (5.14) has been derived as a basis for the ultimate strength of axially loaded uniplanar X-joints.

$$\frac{F_{1,u}}{f_{y,0} \cdot t_0^2} = \frac{8.7 \; \gamma^{0.5\beta - 0.5\beta^2}}{(1 - 0.9\beta) + \sqrt{(1 - 0.9\beta)^2 + \frac{2 - (0.9\beta)^2}{\gamma^2}}} \qquad (5.14)$$

After simplification of the denominator, the following expression has been obtained :

$$\frac{F_{1,u}}{f_{y,0} \cdot t_0^2} = \frac{R_1 \; \gamma^{R_2\beta - R_3\beta^2}}{1 - R_4\beta + R_5 \frac{\beta}{\gamma}} \qquad (7.1)$$

The regression constants R_i (i = 1...5) have to be determined by performing regression analyses on the available data (see section 5.1.6).

As a result, the following equation has been obtained :

$$\frac{F_{1,u}}{f_{y,0} \cdot t_0^2} = \frac{4.3 \; \gamma^{0.5\beta - 0.5\beta^2}}{1 - 0.9\beta + 0.24\dfrac{\beta}{\gamma}} \tag{7.2}$$

The statistical values resulting from the regression analysis are summarized in Table 7.1. The FE data points as well as Eq. 7.2 are shown in Fig. 7.1. Although the simplification is very rough, the simplified formula predicts the strength of the X-joints almost as accurate as the unmodified form.
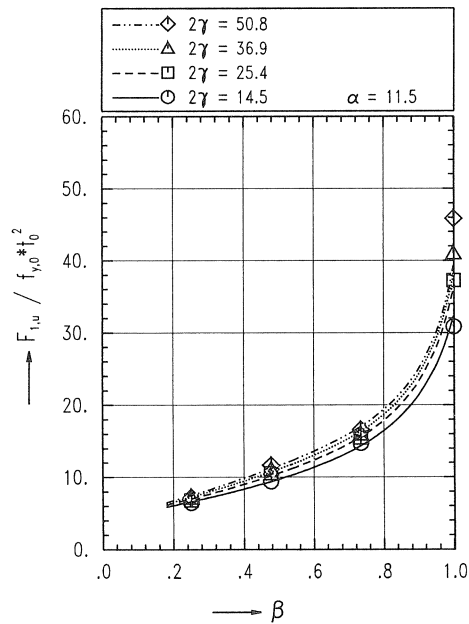
Fig. 7.1 : Ultimate strength of axially loaded uniplanar X-joints - simplified equation.

A disadvantage of this method, which considers very rough simplifications, is that for some terms (e.g. the β/γ term in the denominator), there is not a direct relation any more with the original, analytically derived, strength equation.

Table 7.1 : Results of the regression analyses of axially loaded uniplanar X-joints - simplified equation (Eq. 7.2).

No. of data points	R^2 (%)	Mean	CoV.
15	99.25	1.003	3.59×10^{-2}

8. Conclusions

This section reports the conclusions of the experimental and numerical research into the static behaviour of uniplanar and multiplanar X-joints.

The conclusions of the numerical calibration and the numerical parameter studies are presented separately. The following subdivision has been made :

- 8.1 Numerical calibration
- 8.2 Numerical parametric studies

8.1 *Numerical calibration*

Based on the results of 12 finite element analyses on uniplanar X- and multiplanar XX-joints with the set of geometrical parameters : $\alpha = 12.0$, $\beta = 0.6$, $2\gamma = 40$ and $\tau = 1.0$, the following conclusions can be drawn :

- the numerically determined load-displacement and moment-rotation curves and the numerically determined values of the defined "ultimate load" are in good agreement with the experimental values. The numerically determined values of the defined ultimate load are between 0.94 and 1.14 of the experimentally determined values.

- since material cracking is not modelled, the differences between the numerically and experimentally determined ultimate loads are largest for the joints loaded by out-of-plane bending, where at failure large cracks were observed in the experimental specimens.

- for the joints considered (especially in case of small gaps between the braces), it is necessary to model the welds in the numerical analyses. Shell elements are used to model the welds, giving accurate solutions.

8.2 *Numerical parametric studies*
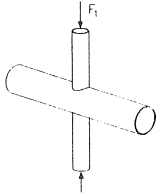
Due to the good agreement between the experimentally and numerically determined load-displacement behaviour, extensive numerical parametric studies have been carried out. In this section, the final results of these numerical analyses are summarized by presenting the ultimate strength equations which have been derived.

The presented strength formulae are based on the numerical results combined with analytically developed strength formulae. However, as mentioned in chapter 7, some equations may require further simplification before inclusion in design codes.

8.2.1 Uniplanar X-joints

8.2.1.1 Uniplanar X-joints with $\alpha = 11.5$

Based on numerical and analytical analyses of axially loaded uniplanar X-joints with unrestrained chord ends and $\alpha = 11.5$, the following strength equation is proposed :

<table>
<tr>
<td></td>
<td>Axially loaded uniplanar X-joints :</td>
</tr>
<tr>
<td colspan="2">

$$\frac{F_{1,u}}{f_{y,0} \cdot t_0^2} = \frac{8.7 \, \gamma^{0.5\beta - 0.5\beta^2}}{(1 - 0.9\beta) + \sqrt{(1 - 0.9\beta)^2 + \dfrac{2 - (0.9\beta)^2}{\gamma^2}}} \qquad (5.14)$$

</td>
</tr>
<tr>
<td colspan="2">

valid for : $\alpha = 11.5$

$\qquad\quad 0.25 \leq \beta \leq 1.0$

$\qquad\quad 14.5 \leq 2\gamma \leq 50.8$

</td>
</tr>
</table>

Remarks :
- for safety reasons i.e. due to the high strength combined with the small deformation capacity, the strength equation underpredicts the strength of the joints with $\beta = 1.0$ and $2\gamma = 50.8$.

8.2.1.2 Axially loaded uniplanar X-joints with variable chord lengths

For axially loaded uniplanar X-joints with different values of the chord length, the strength $F_{1,u}(\alpha)$ can be determined in relation with the strength $F_{1,u}(\alpha = 11.5)$ for uniplanar X-joints with $\alpha = 11.5$ according to :

<table>
<tr>
<td>

</td>
<td>Axially loaded uniplanar X-joints with variable chord lengths :</td>
</tr>
<tr>
<td colspan="2">

$$F_{1,u}(\alpha) = f(\alpha) . F_{1,u}(\alpha = 11.5) \hspace{3cm} (5.18)$$

with the chord length function $f(\alpha)$ defined as :

$$f(\alpha) = \frac{12.5\,\alpha}{11.5\,(1+\alpha)} \hspace{3cm} (5.19)$$

</td>
</tr>
<tr>
<td colspan="2">

valid for : $6.0 \leq \alpha \leq 18.0$
$\quad\quad\quad\quad 0.25 \leq \beta \leq 1.0$
$\quad\quad\quad\quad 2\gamma = 25.4$

</td>
</tr>
</table>

Remarks :
- the function $f(\alpha)$ is based on the results of numerical analyses on X-joints with completely released chord ends. As a result, the function $f(\alpha)$ describes an increase in strength for increasing values of the chord length. For uniplanar X-joints where end plates have been fixed to the chord ends, an opposite trend is expected.

91

8.2.2 Multiplanar XX-joints

8.2.2.1 Axially loaded multiplanar XX-joints with $\alpha = 16.0$

For axially loaded multiplanar XX-joints with $\alpha = 16.0$ and load ratios J between -0.6 and 1.0, the following strength expressions have been derived :
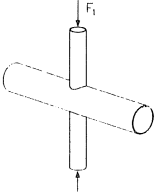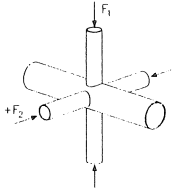
<table>
<tr>
<td></td>
<td colspan="2">Axially loaded multiplanar XX-joints :</td>
</tr>
<tr>
<td colspan="3" align="center">J = 0.0 :</td>
</tr>
<tr>
<td colspan="2">$$\frac{F_{1,u}}{f_{y,0} \cdot t_0^2} = \frac{8.0 \; \gamma^{0.7\beta - \beta^2}}{\sqrt{1 - (0.9\beta)^2} - 0.9\beta + \sqrt{(\sqrt{1 - (0.9\beta)^2} - 0.9\beta)^2 + \dfrac{2}{\gamma^2}}}$$</td>
<td>(6.25)</td>
</tr>
<tr>
<td colspan="3" align="center">$-0.6 \leq J \leq 1.0$:</td>
</tr>
<tr>
<td colspan="2">$$F_{1,u}(J) = \frac{F_{1,u}(J=0.0)}{1 - (1.6\beta - 1.2\beta^2)J + (1.5\beta - 2.5\beta^2)J^2}$$

$$F_{2,u} = J F_{1,u}$$</td>
<td>(6.27)</td>
</tr>
<tr>
<td colspan="3">valid for : $\alpha = 16.0$
            $0.22 \leq \beta \leq 0.60$
            $14.5 \leq 2\gamma \leq 50.8$</td>
</tr>
</table>

Remarks :
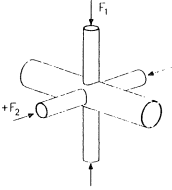- in principle, the basic analytical strength formulae for axially loaded multiplanar XX-joints have been derived in a similar way as for uniplanar joints.
  However, after application of the general expression to uniplanar X-joints, the multiplanar features disappear. Therefore, the ultimate strength equation used for axially loaded uniplanar X-joints can not be directly related any more to the ultimate strength

equation used for axially loaded multiplanar XX-joints with J = 0.0 (i.e. with unloaded out-of-plane braces). Nevertheless, it can be observed that for both formulae, the same correction factor (0.9) should be applied to the β terms.
- the strength equation which accounts for the load interaction effects, underestimates the strength of the multiplanar XX-joints with J= 1.0, β = 0.60 and high 2γ values, due to the small deformation capacity, which is in line with the assumptions for uniplanar X-joints with β = 1.0 and high 2γ values.

8.2.2.2 Axially loaded multiplanar XX-joints with variable chord lengths

Eq. 6.25 which describes the strength of axially loaded multiplanar XX-joints with J = 0.0 has been based on the results of numerical simulations of XX-joints with α = 16.0. For different values of the chord length, a correction should be applied to the strength equation. This correction function f(α, J) is expressed by :

<table>
<tr>
<td>

</td>
<td>
Axially loaded multiplanar XX-joints with variable chord lengths :
</td>
</tr>
<tr>
<td colspan="2">

$$F_{1,u}(\alpha) = f(\alpha,J).F_{1,u}(\alpha = 16.0) \qquad (6.31)$$

with the chord length function f(α, J) defined as :

$$f(\alpha,J) = \frac{17.0\alpha}{16.0\,(1+\alpha)}.(1+0.5Je^{-0.3\alpha}) \qquad (6.32)$$

</td>
</tr>
<tr>
<td colspan="2">

valid for : $6.0 \leq \alpha \leq 16.0$
$\qquad\quad 0.22 \leq \beta \leq 0.60$
$\qquad\quad 2\gamma = 25.4$
$\qquad\quad -0.60 \leq J \leq 1.0$

</td>
</tr>
</table>

Remarks :
- although not clear at first sight, there is a close relation with the function f(α) presented for axially loaded uniplanar X-joints. Namely, the denominators of both functions contain the α value of the X-joints to which each of the correction functions have been related (α = 11.5 for uniplanar X-joints and α = 16.0 for multiplanar XX-joints) while the nominators of both functions include a term α + 1, which is equal to 12.5 for uniplanar X-joints and 17.0 for multiplanar XX-joints. In this way, the values of both correction

functions are 1.0 for the joints to which the correction functions have been related.
- for α values below 16.0, the correction function $f(\alpha, J)$ provides values less than 1.0. For decreasing α values, the strength decreases less for large load ratios (but ≤ 1.0) than for smaller load ratios, due to the smaller chord ovalisation.
- it has been observed that the correction function $f(\alpha, J)$ does not depend on the 2γ value.

9. Notation
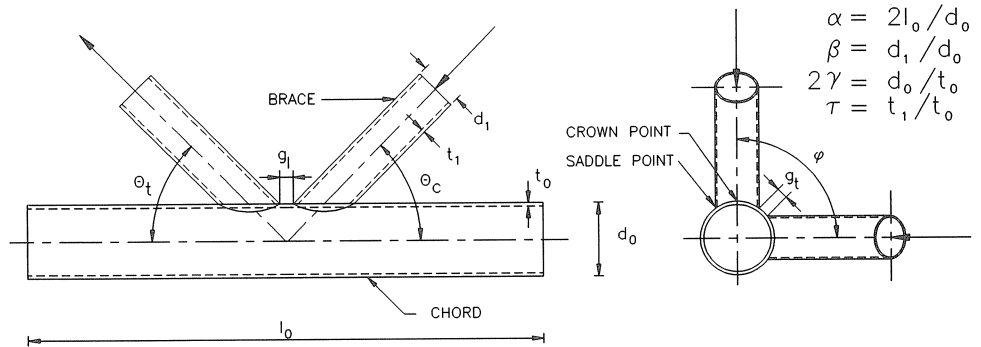
indices i	:	0 : chord ; 1 : in-plane brace ; 2 : out-of-plane brace
a	:	constant used in the Ramberg-Osgood relationship
B_e	:	effective chord length
CoV.	:	coefficient of variation
d_0	:	outer diameter of the chord
d_1	:	outer diameter of the brace
f_y	:	yield stress
$f_{y,0}$	:	yield stress of the chord member
$f_{y,0,L}$	:	(measured) yield stress of the chord member in longitudinal direction
f_u	:	ultimate tensile stress
$f_{u,0}$	:	ultimate tensile stress of the chord member
$f_{u,0,L}$	:	(measured) ultimate tensile stress of the chord member in longitudinal direction
g_l	:	in-plane (= longitudinal) gap between the braces
g_t	:	out-of-plane (= transverse) gap between the braces
l_0	:	length of the chord
u_j	:	j = x, y or z : displacement in X, Y or Z-direction (used to describe boundary conditions)
t_0	:	wall thickness of the chord
t_1	:	wall thickness of the brace
F	:	axial force on the in-plane brace (ring model approach)
F_i	:	axial force on member i (i = 1...2)
$F_{i,y}$	:	axial force on member i which leads to failure in the ring model

94

	:	approach (i = 1...2)
$F_{i,u}$	:	ultimate axial force on member i (i = 1...2)
$F_{u,up}$	:	ultimate strength of a uniplanar X-joint determined with Kurobane's strength formula, (negative forces refer to tension, positive forces to compression)
J	:	load ratio applied on the out-of-plane braces and the in-plane braces
M_p	:	full plastic moment capacity
$M_{1,Yura,test}$	:	experimentally determined bending moment on the in-plane brace at Yura's deformation limit
$M_{1,Yura,num}$	:	numerically determined bending moment on the in-plane brace at Yura's deformation limit
$M_{i,ipb}$	:	in-plane bending moment on member i (i = 1...2)
$M_{i,u,ipb}$	:	ultimate in-plane bending moment on member i (i = 1...2)
$M_{i,opb}$	:	out-of-plane bending moment on member i (i = 1...2)
$M_{i,u,opb}$	:	ultimate out-of-plane bending moment on member i (i = 1...2)
N	:	constant used in the Ramberg-Osgood relationship
N_p	:	plastic yield capacity
V_p	:	plastic shear yield capacity
$V_{p.s}$	:	punching shear capacity
R_j	:	regression constant j
R^2	:	correlation coefficient in regression analyses
α	:	chord length parameter $2.l_0/d_0$
β	:	diameter ratio d_1/d_0
δ_i	:	relative vertical displacement of the crown point of member i (i = 1..2)
2γ	:	chord diameter to thickness ratio d_0/t_0
ε	:	true strain
ε_0	:	reference strain used in the Ramberg-Osgood relationship
σ	:	true stress
σ_0	:	reference stress used in the Ramberg-Osgood relationship
ϕ	:	out-of-plane angle between the planes in which the braces are located
ϕ_i	:	rotation of member i (i = 1..2)
ϕ_j	:	j = x, y or z : rotation about the X, Y or Z-axis (used to describe boundary conditions)
ψ_j	:	angle indicating the position of yield hinge j in the ring model approach
θ_c	:	angle between the compression brace and the chord
θ_t	:	angle between the tension brace and the chord
τ	:	brace wall to chord wall thickness ratio t_1/t_0

10. References

American Petroleum Institute (1991), "Recommended Practice for Planning, Designing and Constructing Fixed Offshore Platforms." API RP2A, 19th Edition.
American Welding Society, Structural Welding Code (1992), AWS D1.1-92.
Borst R. de (1991a), "Computational Methods in Non-Linear Solid Mechanics.

Part 1 : Geometrical Non-Linearity and Solution Techniques." T.U. Delft Report 25-2-90-5-04, TNO-IBBC Report BI-90-069, Delft, The Netherlands.

Borst R. de (1991b), "Computational Methods in Non-Linear Solid Mechanics. Part 2 : Physical Non-Linearity." T.U. Delft Report 25-2-91-2-06, TNO-IBBC Report BI-91-043, Delft, The Netherlands.

Eurocode 3 (1992), "Design of Steel Structures, Part 1: General Rules and Rules for Buildings." + Appendices.

Kurobane Y., Makino Y., Mitsui Y. (1980), "Re-Analysis of Ultimate Strength Data for Truss Connections in Circular Hollow Sections.", Kumamoto University, Kumamoto, Japan, IIW Doc. XV-461-80.

Mäkeläinen P.K., Puthli R.S.(1988), "Semi-Analytical Models for the Static Behaviour of T and DT Tubular Joints." International Conference on Behaviour of Offshore Structures (BOSS), Trondheim, Norway, pp. 1285-1300.

MARC Analysis Research Corporation (1990a), "User Information Manual." Vol. A, Revision K4, Palo Alto, U.S.A.

MARC Analysis Research Corporation (1990b), "MARC Element Library." Vol. B, Revision K4, Palo Alto, U.S.A.

Marshall P.W. (1991), "Design of Welded Tubular Connections - Basis and Use of AWS Code Provisions.", Elsevier Science Publisher's Ltd., Madison Square, New York, U.S.A.

Paul J.C (1992), "The Ultimate Behaviour of Multiplanar TT-and KK-Joints Made of Circular Hollow Sections." Doctoral Dissertation, Kumamoto University, Kumamoto, Japan.

Ramberg W., Osgood W.R. (1943), Techn. Note No. 902, NACA, pp. 268-290.

SDRC (1990), "I-DEAS Finite Element Modelling User's Guide." Structural Dynamics Research Corporation, Ohio, U.S.A.

Togo T. (1967), "Experimental Study on Mechanical Behaviour of Tubular Joints." Doctoral Dissertation, Osaka University, Osaka, Japan (in Japanese).

Vegte G.J. van der, Koning C.H.M. de, Puthli R.S., Wardenier J. (1990), "Static Behaviour of Multiplanar Welded Joints in Circular Hollow Sections." Stevin Report 25.6.90.13/A1/11.03, TNO-IBBC Report BI-90-106/63.5.3860, Rev. Feb. 1991, Delft, The Netherlands.

Vegte G.J. van der, Koning C.H.M. de, Puthli R.S., Wardenier J. (1991), "The Static Strength and Stiffness of Multiplanar Tubular Steel X-Joints." Internat. Journal Offshore and Polar Eng., ISOPE, Vol. 1, No. 1, pp. 42-52.

Vegte G.J. van der (1995), "The Static Strength of Uniplanar and Multiplanar Tubular T- and X-Joints." Doctoral Dissertation, Delft University of Technology, Delft University Press, The Netherlands.

Wardenier J. (1982), "Hollow Section Joints." Delft University Press, Delft, The Netherlands.

Yura J.A., Zettlemoyer N., Edwards I.F. (1980), "Ultimate Capacity Equations for Tubular Joints." Proceedings Offshore Technology Conference, Paper OTC 3690, Houston, U.S.A.